

**Structural Characterization of the Oxygen Reactive Hemoglobins
from the clam *Lucina pectinata***

by

Rafael A. Estremera-Andújar

A dissertation submitted in partial fulfillment of the requirements for the degree of

DOCTOR IN PHILOSOPHY
in
APPLIED CHEMISTRY
(Biophysics)

UNIVERSITY OF PUERTO RICO
MAYAGÜEZ CAMPUS
2014

Approved by:

Samuel P. Hernández-Rivera, Ph.D.
Member, Graduate Committee

Date

Carmen L. Cadilla-Vázquez, Ph.D.
Member, Graduate Committee

Date

Juan Manuel García-Ruiz, Ph.D.
Member, Graduate Committee

Date

Juan López-Garriga, Ph.D.
President, Graduate Committee

Date

Magda Latorre-Esteves, Ph.D.
Representative of Graduate Studies

Date

Aidalú Joubert-Castro, Ph.D.
Chairperson, Chemistry Department

Date

ABSTRACT

Hemoglobins comprise a challenging area of study within biochemical research. They play an important physiological role in organisms, like oxygen transport and storage. Three hemoglobins were discovered in the ctenidia tissue of the *Lucina pectinata* bivalve mollusk. Hemoglobin I (HbI) is classified as sulfide reactive, while hemoglobin II (HbII), hemoglobin III (HbIII), and the HbII-III complex are unreactive towards H₂S. The functional aspects of these oxygen carrier proteins can be explained by a series of contributing factors. The distal heme pocket composition of the heterodimer of HbII-III complex and the homodimer of HbIII and HbII contains TyrB10 and GlnE7, which are common in other hemoglobins of non-vertebrate organisms. These residues contribute to the ligand stabilization and dissociation by a hydrogen bond network with the heme-ligand moiety. The heme pocket size, the hydrogen bonding network, and the orientation of the heme-oxygen complex of the HbII-III complex and that of HbII act together to confer stability to the protein. At pH 7, the crystallographic structure of HbII (2OLP) shows a dimer, where oxygen is tightly anchored to the heme group through hydrogen bonds with TyrB10 and GlnE7. At pH 5, the crystallographic structure of HbII-III complex (3PT7) shows a heterodimeric structure with the same behavior of the homodimer HbII. The mechanism used by these hemoglobins, their function, ligand selection, and stabilization remains partially unknown. This study contributes to the better understanding of this mechanism. Crystals of the Oxy complex of HbII-III were grown at different pH values (4 to 8) using the capillary counterdiffusion (CCD) technique to elucidate the crystallographic structure and to determine conformational changes of the conformations of the TyrB10 and GlnE7 residues; as well as the structural scenarios induced by pH changes. Good prismatic ruby-red crystals were obtained at all pH values with precipitant agents, such as sodium formate and

ammonium sulfate. The crystallographic structures of the Oxy heterodimers complexes of HbII-III have been compared with the Oxy homodimers complexes of HbII, at pH 4 to 8, to determine structural changes, differences in the distal site, the peripheral side groups, and the planarity of the heme pocket. The HbIII component was isolated and purified from the complex of HbII-III with a new protocol. The purity of the HbIII component was confirmed with MS/MS spectrometry. Crystallization conditions for the Oxy and Cyano complexes for HbIII were obtained. X-ray data sets were acquired using synchrotron radiation to a maximum resolution of 2.65, 2.24, 1.86 and 1.85 Å for pH 4, 6, 7 and pH 8, respectively. All obtained crystals were isomorphous, belonging to the $P4_22_12$ space group. The crystallographic data suggests that pH is a driving force for a conformational change in the HbII-III complex protein structure, specifically in the distal region of the heme group. These changes can promote the rearrangement of the TyrB10 and GlnE11 residues, with or without a hydrogen bond network, with the oxygen ligand in the heme pocket of HbII-III complex at pH values mentioned above. The results indicate a conformational equilibrium between an open and a closed conformational model at the heme pocket for the Oxy complex of HbII-III.

RESUMEN

Las hemoglobinas comprenden un área de reto en los estudios dentro de las investigaciones en el área de la bioquímica. Estas juegan un papel fisiológico importante en los organismos, tales como el transporte y almacenamiento de oxígeno. Tres hemoglobinas fueron descubiertas en los tejidos del ctenidio del molusco bivalvo en *Lucina pectinata*. Hemoglobina I (HbI), se clasifica como reactiva a sulfuro de hidrógeno (H_2S), donde, la hemoglobina II (HbII), la hemoglobina III (HbIII) y el complejo de hemoglobina HbII-III no son reactivas hacia H_2S . Los aspectos de la función de estas proteínas que transportan oxígeno pueden explicarse por un conjunto de factores contribuyentes. La composición del bolsillo distal del grupo hemo para el heterodímero del complejo HbII-III y del homodímero de HbIII y HbII contienen TyrB10 y GlnE7, los cuales aparecen comúnmente en otros tipos de hemoglobinas de organismos invertebrados. Dichos residuos contribuyen a la estabilización y disociación del ligando por una red de puentes de hidrógeno en el centro activo. El tamaño del grupo hemo, la red de puentes de hidrógeno y la orientación del complejo oxígeno-hemo del complejo HbII-III y HbII actúan juntos para proveer estabilidad a la proteína. A pH 7, la estructura cristalográfica de HbII (2OLP) muestra un dímero, donde el oxígeno está anclado fuertemente al grupo hemo a través de puentes de hidrógeno con TyrB10 y GlnE7. A pH 5 la estructura cristalográfica del complejo HbII-III (3PT7) muestra una estructura heterodimérica con el mismo comportamiento del homodímero HbII. El mecanismo que utilizan estas proteínas, su función, la selección del ligando y la estabilización del mismo no se conocen con certeza. Este estudio contribuye a entender mejor este mecanismo. Se crecieron cristales del complejo Oxi-HbII-III a diferentes valores de pH (4 a 8) utilizando la técnica de contradifusión capilar (CDC) para elucidar la estructura cristalográfica y determinar cambios conformacionales en los residuos de TyrB10 y

GlnE7, así como los escenarios estructurales inducidos por cambios en pH. Se obtuvieron cristales prismáticos de color rojo a todos los pH, utilizando formato de sodio y sulfato de amonio como agentes precipitantes. Se comparó la estructura cristalográfica del complejo Oxi del heterodímero HbII-III con el homodímero HbII, a pH 4 a 8, para determinar cambios estructurales, diferencias en el sitio distal, los grupos periferales y la planaridad del bolsillo del grupo hemo. El componente de HbIII fue aislado y purificado del complejo HbII-III con un nuevo protocolo. La pureza de HbIII se confirmó a través de espectrometría de masa MS/MS. Se obtuvieron condiciones de cristalización para los complejos Oxi y Ciano de HbIII. Los datos de rayos X fueron adquiridos utilizando radiación de sincrotrón a una resolución máxima de 2.65, 2.24, 1.86 y 1.85 Å para los pH de 4, 6, 7 y 8, respectivamente. Todos los cristales obtenidos fueron isomorfos, pertenecientes al grupo espacial P4₂2₁2. Estos datos cristalográficos sugieren que el pH es la fuerza motriz para el cambio conformacional en la estructura del complejo de HbII-III, específicamente en la región distal del grupo hemo. Estos cambios promueven el rearrreglo de la TyrB10 y GlnE11, con o sin la red de puentes de hidrógeno, con el ligando de oxígeno en el grupo hemo del complejo HbII-III a los valores de pH mencionados previamente. Los resultados indican un equilibrio conformacional entre el modelo conformacional abierto/cerrado en el hemo del complejo Oxi-HbII-III.

*Copyright® Rafael A. Estremera-Andújar
2014*

Este trabajo lo dedico a toda mi familia que durante estos años siempre han estado apoyándome y dándome el ánimo necesario para alcanzar la meta trazada. A mis padres, Antonio Estremera Soto y a mi madre Elsa Andújar Rodríguez que nunca dudaron y siempre estuvieron a mi lado incondicionalmente no importando la distancia que nos separase durante mis años de internado allende a los mares en la madre patria España. Gracias mil, los amo a todos con todas las fuerzas de mi corazón. DIOS quiero darte las gracias pues sin tu amor y fortaleza nunca hubiese terminado lo que Tú me permitiste comenzar y a su vez terminar.

ACKNOWLEDGEMENTS

Quisiera agradecer a mi comité graduado por su apoyo en este proceso, Dr. Samuel Hernández-Rivera, Dra. Carmen Cadilla-Vázquez, Dr. Juan Manuel García-Ruiz y a mi director de tesis, el Dr. Juan López Garriga por contribuir con este proceso.

Esta investigación fue subvencionada en parte por la Fundación Nacional de Ciencias (National Science Foundation) (NSF-MCB-0544250, 0843608, JLG), Institutos Nacionales de la Salud (National Institutes of Health) (NIH-NIGMS MBRS-SCORE 2-S06GM08103-34; MIRT5TW00096, RISER2SGM088023 y 2G12-RR003051), National Institute on Minority Health and Health Disparities (8G12-MD007600), la Universidad de Puerto Rico en Mayagüez y la Universidad de Puerto Rico en Aguadilla. Fondos del gobierno de Andalucía, España, No. RMN1344, el proyecto OptiCryst del “IVth Framework of the European Commission” y el proyecto de la Factoría de Cristalización Consolide-Ingenio colaboraron en la financiación de este trabajo de investigación.

Agradezco también al Laboratorio de Estudios Cristalográficos en Granada, España, parte del Consejo Superior de Investigaciones Científicas y a todo su personal, el cual me permitió el desarrollo profesional en el área de la cristalización y la cristalografía de moléculas biológicas. Gracias al Dr. José A. Gavira por aportar de manera significativa al desarrollo de esta tesis. A su vez deseo agradecer a las facilidades del European Synchrotron Radiation Facilities (ESRF) y a la líneas BM16 y BM14U. Reconozco al Sr. Edwin O. Lazo del Brookhaven National Laboratory por su contribución en resolver las estructuras cristalográficas presentadas en este trabajo doctoral y a la Dra. Ruth Pietri por su ayuda para con este trabajo de tesis.

Quiero agradecer a toda mi familia por su apoyo a través de estos años de ardua investigación científica para lograr alcanzar la meta comenzada. Agradezco a los miembros del

laboratorio de investigación, los cuales de una u otra forma aportaron en este esfuerzo y al Dr. José M. Planas Rivera por su ayuda incondicional con la corrección en este trabajo escrito.

En adición deseo agradecer de lo más profundo de mi corazón a mis dos grande amigos y “compinches”: Dr. Carlos R. Ruiz Martínez a al Dr. Carlos A. Nieves Marrero, con los cuales he logrado alcanzar muchas metas durante todos estos años. Me brindaron su apoyo y su ayuda incondicional. ¡Gracias! no hay palabras que describan la gratitud que siento hacia ustedes. Esta tesis también es vuestra, mis queridos amigos.

TABLE OF CONTENTS

TABLE OF CONTENTS.....	x
LIST OF TABLES.....	xii
LIST OF FIGURES.....	xiv
LIST OF ABBREVIATIONS.....	xviii
1. INTRODUCTION.....	1
1.0. Research justification.....	1
1.1. Previous work.....	9
2. OBJECTIVES.....	19
2.1. To isolate and purify HbIII from the HbII-III complex.....	19
2.2. To design a crystallization methodology to obtain crystals for the Oxy and Cyano complexes of HbIII.....	19
2.3. To develop a pH dependence crystallization experiment for the Oxy complex of HbII-III as a pH function of 4 to 9.....	19
2.4. To develop an X-ray methodology to elucidate structural models of the Oxy and Cyano complexes of HbIII and the complex of Oxy-HbII-III as a pH function 4 to 8.	19
2.5. To perform a comparative analysis between the crystallographic structures of the Oxy homodimer of HbII with the Oxy heterodimer of HbII-III complex within a pH range from 4 to 8.....	20
3. METHODOLOGY.....	21
3.1. Extraction, isolation and purification of <i>Lucina pectinata</i> hemoglobins.....	21
3.2. Preparation of crystallization samples of <i>Lucina pectinata</i> HbII-III and HbIII.....	24
3.3. Preparation the Cyano-HbIII from <i>Lucina pectinata</i>	25
3.4. Crystallization screening techniques.....	25
3.4.1. Vapor diffusion method-hanging drop technique.....	25
3.4.2. Capillary counterdiffusion technique.....	26
3.5. Structure solution and refinement.....	28
3.5.1. X-ray diffraction and crystal mounting.....	28
3.5.2. X-ray data acquisition and structure refinement and resolution.....	29
4. RESULTS AND DISCUSSION.....	31
4.1. Isolation and purification of hemoglobins from <i>L. pectinata</i>	31
4.1.1. Purification of <i>HbII and HbIII with Ion Exchange Chromatography (IEC)</i>	32
4.1.2. Spectroscopic confirmation of the Cyano and Oxy complex for HbIII.....	35
4.2. Crystallization of the hemoglobins from <i>L. pectinata</i>	37
4.2.1. Crystallization conditions for Oxy-HbIII and Cyano-HbIII.....	37
4.2.2. Crystallization conditions for Oxy-HbII-III complex at different pH.....	39
4.3. Crystallographic results for the Oxy complex of HbII-III at pH 4 to 8.....	43
4.3.1. Structural model finding for primary structure for Oxy-HbII-III complex.....	45
4.3.2. Secondary and tertiary structure for Oxy-HbII-III complex.....	47
4.3.3. Tertiary structure of Oxy- HbII-III complex at different pH.....	58
4.3.4. Heme pocket analysis for Oxy-HbII-III complex at different pH.....	62
4.4. Crystallographic structure comparison between the Oxy heterodimer of HbII-III complex with the Oxy homodimer of HbII at different pH from 4 to 8.....	71

4.4.1. Secondary structure distribution between the homodimer of Oxy-HbII and the heterodimer of Oxy-HbII-III complex at pH 4 to 8.....	71
4.4.2. Tertiary structure comparison between the homodimer of Oxy-HbII and the heterodimer of Oxy-HbII-III complex at pH 4 to 8; protein-protein interaction.....	76
4.4.3. Heme pocket analysis between the Oxy proteins HbII-III complex and HbII....	79
5. CONCLUSIONS AND FUTURE WORK.....	90
5.1. Conclusions.....	90
5.2. Future Work.....	92
REFERENCES.....	93

LIST OF TABLES

<i>Table</i>	<i>Descriptions</i>	<i>Page</i>
4.1	Proteins identified by MS/MS.	34
4.2	Crystallization conditions for Oxy-HbIII and Cyano-HbIII.	38
4.3	Crystallization conditions for Oxy-HbII-III complex.	40
4.4	Summary of X-ray data collection, statistics and refinements results for Oxy-HbII-III complex crystals precipitated with sodium formate and ammonium sulfate at different pH values. Statistical values for the highest resolution shell for crystal growth are given in parentheses in the Resolution range row. Values in parentheses belong to the highest resolution shell.	44
4.5	Amino acid sequence of HbIII, according to Huckenhull-Jhonson, Rivera and Ruiz-Martínez.	46
4.6	Secondary structure distribution for <i>Lucina pectinata</i> Oxy-HbII-III complex using the STRIDE web server (Hening and Frishman, 2004).	51
4.7	Summary of total number of helices for the Oxy-HbII-III complex.	52
4.8	Different types of turns for the Oxy-HbII-III complex.	52
4.9	Summary of the different coils and turns for the Oxy-HbII-III complex.	53
4.10	LigPlot+ interactions between chain A and B for the Oxy-HbII-III complex at pH 4 to 8 and Cyano-HbII-III complex at pH 5.	58
4.11	Residues found in the protein-protein interaction between dimers of the Oxy-HbII-III complex. All interactions were obtained using LigPlot+ program version 1.4.5 (Laskowski and Swindells, 2011).	61
4.12	Area and volume of the protein-protein interaction for the Oxy-HbII-III complex.	62
4.13	Summary of the stereochemistry of the 2- and 4-vinyl groups for the Oxy-HbII-III complex at a pH range of 4 to 8.	64
4.14	Bond angles between O1-O2-Fe in the heme pocket of the Oxy-HbII-III complex.	65
4.15	Heme contacts in the Oxy-HbII-III complex at different pH values.	66
4.16	Area and volume of the heme pockets A and B for the Oxy-HbII-III complex.	71
4.17	Secondary structure distribution for chain A of the Oxy dimers of HbII and the HbII-III complex in <i>Lucina pectinata</i> , using STRIDE web server (Hening and Frishman, 2004).	73

4.18	Secondary structure distribution for chain B of the Oxy dimers of HbII and the HbII-III complex <i>Lucina pectinata</i> , using STRIDE web server (Hening and Frishman, 2004).	74
4.19	Summary of the helices for Oxy-HbII and the Oxy-HbII-III complex.	75
4.20	Summary of the different types of turns for the Oxy dimers of HbII and the HbII-III complex.	75
4.21	Summary of the different coils and turns for Oxy-HbII and the Oxy-HbII-III complex.	76
4.22	Residues found in the protein-protein interaction between the homodimer of Oxy-HbII. All interactions were obtained using LigPlot+ program version 1.4.5 (Laskowski and Swindells, 2011).	77
4.23	Total amount of residues participating in protein-protein interactions for Oxy-HbII and the Oxy-HbII-III complex at pH 4 to 8.	78
4.24	Interactions between chain A and B for Oxy-HbII and Oxy-HbII-III complex.	78
4.25	Area and volume from protein-protein interaction for Oxy-HbII and the Oxy-HbII-III complex.	79
4.26	Total amount of water molecules found in the crystallographic structure of Oxy-HbII and Oxy-HbII-III complex at pH 4 to 8.	79
4.27	Comparison between the 2- and 4-vinyl group conformations in the dimers of Oxy-HbII and the Oxy-HbII-III complex at pH range of 4 to 8.	80
4.28	Distance for Fe and oxygen ligand in HbII and the HbII-III complex.	82
4.29	Bond angle between O1-O2-Fe in the heme pocket for HbII and the HbII-III complex.	82
4.30	Distance for the distal site of the Oxy dimers of HbII and the HbII-III complex.	84
4.31	Distance for the proximal site of the Oxy dimers of HbII and the HbII-III complex.	86
4.32	Area and volume of the heme pocket A and B for Oxy-HbII and the Oxy-HbII-III complex.	87

LIST OF FIGURES

<i>Figure</i>	<i>Description</i>	<i>Page</i>
1.0	Heme pocket for HbII at pH 4. Heme A is shown on the left, heme B with a water molecule as a ligand is shown on the right.	7
1.1	Structure of the Oxy-HbII-III complex of <i>L. pectinata</i> at pH 5. (Ruiz-Martínez 2011, 3PT7)	13
1.2	The open and closed conformation proposed for the HbII distal environment.	16
3.1	The <i>Lucina pectinata</i> clam.	21
3.2	XK 16/70 column with strong anion exchange Q Sepharose High Performance (QHP).	22
3.3	Vapor diffusion experiment using the hanging drop method.	26
3.4	Schematic diagram for the Granada Crystallization Box (GCB2™).	27
3.5	Crystal collection and mounting.	28
3.6	Schematic illustration for a protein crystallographic structure.	30
4.1	SEC chromatogram of the crude extract from the clam <i>L. pectinata</i> .	31
4.2	IEC for the HbII-III complex with HiPrep 16/10 QFF column.	32
4.3	IEC for HbIII to confirm the purity of the protein.	33
4.4	IEC for the HbII-III complex with QHP matrix using a XK 16/70 column.	34
4.4.1	Peptide sequence identified with MS/MS spectrometry, sample 1	35
4.4.2	Peptide sequence identified with MS/MS spectrometry, sample 2	35
4.5	UV-Vis spectrum for Oxy-HbIII.	36
4.6	UV-Vis spectrum for Cyano-HbIII.	36
4.7	a) Crystal for Cyano-HbIII at pH 5 with precipitant agent of sodium formate and b) Oxy-HbIII at pH 4 with precipitant agent of ammonium sulfate.	38
4.8	UV-Vis spectrum for the Oxy-HbII-III complex.	39
4.9	Crystals for Oxy-HbII-III complex at pH 8 with different precipitant agents. a) sodium formate and b) ammonium sulfate.	40

4.10	X-ray diffraction frames for the Oxy-HbII-III complex, (a) at pH 6 with a resolution of 2.24 Å obtained at 100 K; and (b) at pH 7 with a resolution of 1.86 Å obtained at 100 K.	44
4.11	Ramachandran plots for the Oxy-HbII-III complex at pH a) 4, b) 6, c) 7, and d) 8. Each plot was produced by the MolProbity 4.0 web server program.	49
4.12	Crystallographic structure for Oxy-HbII-III complex without the heme group. Chain A (left) and chain B (right) at pH a) 4, b) 5, c) 6, d) 7 and e) 8. Each helix, A to H, are identified by colors: red, blue, light blue, yellow, cyan, orange, wheat, cyan-deep teal, and deep salmon, respectively. The coils are green and the turns are violet.	53
4.13	STRIDE web server output for secondary structure comparison of Oxy-HbII-III complex at pH 4 to 8. The red color indicates an alpha helix, blue, 3_{10} helix and yellow, turn or coil.	55
4.14	Crystallographic structures of the Oxy-HbII-III complexes overlapping using PyMOL at pH 4 (green), pH 5 (red), pH 6 (yellow), pH 7 (magenta), and pH 8 (cyan).	56
4.15	RMSD plot for the overlapping of chain A with chain B for the Oxy-HbII-III complex at pH 4 and 8.	57
4.15.1	Residues found in the protein-protein interaction between dimers of the Oxy-HbII-III complex at pH 4 using LigPlot+ program	59
4.15.2	Gln and Lys residues interaction between chains A (HbII, left) and chain B (HbIII, right) at pH 7	60
4.16	Heme A of the HbII-III complex at pH 4.	63
4.17	Heme A (left) and heme B (right) of the Oxy-HbII-III complex at pH 4 (green), pH 5 (cyan), pH 6 (violet), pH 7 (grey-white) and pH 8 (dark salmon) which show the stereochemistry of the 2- and 4-vinyl groups.	64
4.18	Crystallographic structure of the heme A (left) with oxygen ligand and heme B (right) for the HbII-III complex at pH 6 (magenta), 7 (yellow) and 8 (orange).	65
4.19	Heme A (left) and B (right) with the oxygen ligand at pH 5 (cyan), 6 (magenta) and 7 (yellow).	65
4.20	Overlapping Heme A (left) and heme B (right) of the Oxy-HbII-III complex at pH 4 (green) and pH 8 (dark salmon).	67

4.21	Heme groups and the residues for chain A (left) and B (right) at pH 5 (cyan) and 6 (purple) for the complex HbII-III.	68
4.22	Heme A (left) and heme B (right) for the HbII-III complex at pH 6 (magenta), pH 7 (yellow) and pH 8 (orange). The heme A and B at pH 8 show the absence of an oxygen ligand. The Tyr(B10) shows different distances as a function of pH, being closer to Fe at pH 8.	69
4.23	Crystallographic structures of heme A (left) and heme B (right) with a water molecule (proximal site) and the residues for HbII-III complex at pH 4 (green) and pH 8 (orange).	70
4.23.1	Residues found in the protein-protein interaction of HbII-II (green) and HbII-III (magenta) at pH 8.	77
4.24	Heme A (left) of the HbII (green) overlapping with heme A of the Oxy-HbII-III complex (cyan) at pH 4. Heme B (right) of the HbII (green) overlapping with heme B of the Oxy-HbII-III complex (cyan) at pH 4.	80
4.25	Heme A (left) of the HbII (green) overlapping with heme A of the Oxy-HbII-III complex (cyan) at pH 4. Heme B (right) of the HbII (green) overlapping with heme B of the Oxy-HbII-III complex (cyan) at pH 4, top view.	81
4.26	Heme A (left) of the HbII (green) overlapping with heme A of the Oxy-HbII-III complex (cyan) at pH 8. Heme B (right) of the HbII (green) overlapping with heme B of the Oxy-HbII-III complex (cyan) at pH 8.	81
4.27	Heme A (left) of the HbII (green) overlapping with residues of the heme A of the Oxy-HbII-III complex (cyan) at pH 5. Heme B (right) of the HbII (green) overlapping with residues of the heme B of the Oxy-HbII-III complex (cyan) at pH 5.	83
4.28	Heme A (left) of the HbII (green) overlapping with residues of the heme A of the Oxy-HbII-III complex (cyan) at pH 6. Heme B (right) of the HbII (green) overlapping with residues of the heme B of the Oxy-HbII-III complex (cyan) at pH 6.	83
4.29	Heme A (left) of the HbII (green) overlapping with residues of the heme A of the Oxy-HbII-III complex (cyan) at pH 7. Heme B (right) of the HbII (green) overlapping with residues of the heme B of the Oxy-HbII-III complex (cyan) at pH 7.	84
4.30	Heme A (left) of the HbII (green) overlapping with residues of the heme A of the Oxy-HbII-III complex (cyan) at pH 8. Heme B (right) of the HbII (green) overlapping with residues of the heme B of the Oxy-HbII-III complex (cyan) at pH 8.	85

4.31	Heme A (left) of the HbII (green) overlapping with residues of the heme A of the Oxy-HbII-III complex (cyan) at pH 4. Heme B (right) of the HbII (green) overlapping with residues of the heme B of the Oxy-HbII-III complex (cyan) at pH 4.	86
4.32	Structure overlapping of Oxy-HbII (red) and the Oxy-HbII-III complex (cyan) at pH 4; chain A on the left side and chain B on the right side.	88
4.33	Structure overlapping of Oxy-HbII (red) and the Oxy-HbII-III complex (cyan) at pH 5; chain A on the left side and chain B on the right side.	88
4.34	Structure overlapping of Oxy-HbII (red) and the Oxy-HbII-III complex (cyan) at pH 6; chain A on the left side and chain B on the right side.	89
4.35	Structure overlapping of Oxy-HbII (red) and the Oxy-HbII-III complex (cyan) at pH 7; chain A on the left side and chain B on the right side.	89
4.36	Structure overlapping of Oxy-HbII (red) and the Oxy-HbII-III complex (cyan) at pH 8; chain A on the left side and chain B on the right side.	89

LIST OF ABBREVIATIONS

%	percentage
α	Alpha
Ψ	Psi
β	Beta
Φ, ϕ	Phi
μL	microliters
μm	micrometer
#	number
$^{\circ}$	degrees
24-PRECIP-KIT	24 Precipitants for Screening by Capillary Counterdiffusion
3D	Tridimension or tridimensional
KIT-AS-49	Kit by capillary counterdiffusion, ammonium sulphate at pH 4 to 9
KIT-SF-49	Kit by capillary counterdiffusion, sodium formate at pH 4 to 9
\AA	Angstrom
aa	Amino acid
<i>A. suum</i>	<i>Ascaris suum</i>
\AA^2	Square angstrom (area)
\AA^3	Cubic Angstrom (volume)
Ala	Alanine
all-RMSD	All atoms root mean square deviation
Arg	Arginine
<i>AscarisHb</i> or <i>HbAs</i>	Hemoglobin from <i>Ascaris suum</i>
Asn	Asparagine
Asp	Aspartic acid
BLAST	Basic Local Alingnement Search Tool
C	Carbon, or Temperature unit (Celsius)
CcP	Cytochrome c peroxidase
$\text{C}\alpha$	Alpha carbon
CASTp	Computed Atlas of Surface Topography of proteins

CCD	Capillary counterdiffusion
CDC	Contradifusión capilar
CCP4	Collaborative Computational Project No. 4
cDNA	Complementary deoxyribonucleic acid
CN	Cyanide
CNS	Crystallography and NMR system
CO	Carbon monoxide
COOT	Crystallographic Object-Oriented Toolkit
Cys	Cysteine
Da	Dalton
DTT	Dithiothreitol
EDTA	Ethylenediaminetetraacetic acid
et al.	And others
ESRF	European Synchrotron Radiation Facilities
EPR	Electron Paramagnetic Resonance
Fe	Iron
Fe ^{IV}	Ferryl ion
FPLC	Fast Protein (Performance) Liquid Chromatography (Chromatographer)
GCB2	Granada crystallization box two
GCB–D	Granada Crystallization Box–Domino Crystallization Kit
GE	General Electric healthcare life science
Gln	Glutamine
Glu	Glutamic acid
Gly	Glycine
GN	Gene number
H	Hydrogen or proton
H ₂ S	Hydrogen sulfide
H ₂ O ₂	Hydrogen peroxide
Hb	Hemoglobin
HbIISi	Hemoglobin II from <i>Scapharca inaequalvis</i>
HbISi	Hemoglobin I from <i>Scapharca inaequalvis</i>

HbI	Hemoglobin I from <i>Lucina pectinata</i>
HbII	Hemoglobin II from <i>Lucina pectinata</i>
HbIII	Hemoglobin III from <i>Lucina pectinata</i>
HbII-III	Hemoglobin II-III from <i>Lucina pectinata</i>
HCl	Hydrochloric acid
HD	Hanging drop
HDVD	Hanging drop vapor diffusion
HEPES	4-(2-hydroxyethyl)-1-piperazineethanesulfonic acid
His	Histidine
IEC	Ion exchange chromatography
IR	Infrared
K	Potassium, or Temperature unit (Kelvin), or kinetic constant
k	Kilo (SI unit), or kinetic constant
K ₃ Fe(CN) ₆	Potassium ferricyanide
kDa	Kilodalton
k _{off} or K _D	Dissociation constant (kinetics)
k _{on}	Association constant (kinetics)
Leu	Leucine
Lys	Lysine
<i>L. pectinata</i>	<i>Lucina pectinata</i>
M	Molar (concentration)
Mb	Myoglobin
metMb	Met myoglobin
Met	Methionine
mg/mL	milligrams per milliliters
mL	milliliters
mL/min	milliliters per minutes
mm	millimeter
mM	milimolar
Mol	molecule
M ⁻¹ s ⁻¹	Inverse molarity multiply by inverse seconds

m-RMSD	Main chain root mean square deviation
MS/MS	Tandem Mass Spectrometry
MW	Molecular weight
N	Nitrogen
N ^o	number
N/A	not applicable
NaCl	Sodium chloride
NaCN	Sodium cyanide
NaH ₂ PO ₄	Sodium dihydrogen phosphate
NaOH	Sodium hydroxide
NCBI	<i>National Center for Biotechnology Information</i>
-N ⁺ (CH ₃) ₃	Trimethylammonium cation
NMR	Nuclear magnetic resonance
nm	Nanometer
N ^o	number
NO	Nitrogen monoxide
O, Oxy, O ₂	Oxygen
OS	organism
P	Primitive (no additional symmetry)
p ₅₀	Half-saturation pressure, dioxygen affinities
P450st	Cytochrome P450 from the thermoacidophilic crenarchaeon <i>Sulfolobus tokodaii strai 7</i>
p-Cys	Cystein rich protein
PDB	Protein Data Bank
PDBsum	Protein Data Bank summary (a web-base database)
PEG	Polyethylene glycol
PE	Protein Existence
pH	Quantitative measure of the acidity or basicity
Phe	Phenylalanine
PHENIX	Python-based Hierarchical Environment for Integrated Xtallography
PISA	Protein interfaces, surfaces and assemblies

PROCHEC	Programs to check the stereochemical quality of protein structures
PyMOL	molecular visualization system
QFF	Q Sepharose Fast Flow
QHP	Q Sepharose High Performance
rTHB1	Recombinant truncate hemoglonine 1
RCBS	Research collaborator for structural bioinformatics
REFMAC5	Program for the refinement of macromolecular structures
R_{factor}	Residual factor
R_{free}	Free-residual factor
RMS	Root mean square
RMSD	Root mean square deviation
rpm	Revolutions per minute
RR	Resonance Raman
S	sulfur
s^{-1}	per second
SAXS	Small angle X-ray scattering
SEC	Size Exclusion Chromatography
Ser	Serine
SFCHECK	Program for assessing the agreement between an atomic model and X-ray data
STRIDE	Interactive interface to the secondary structure assignment
SV	Sequence Version
SWMb	Sperm whale myoglobin
TEA	Triethanolamine
Thr	Threonine
TLS	Translation/Libration/Screw
trHb	truncated Hemoglobin
Tris	2-amino-2-hydroxymethyl-propane-1,3-diol
Tyr	Tyrosine
UV	Ultraviolet
v/v	volume/volume (concentration unit)

VHb	<i>Vitreoscilla</i> hemoglobin
Val	Valine
Vis	Visible
VDX	VDX plate for hanging drop experiment
W, H ₂ O	Water
WAXS	Wide angle X-ray scattering
Ym-10	Cellulose membrane 10 kDa

1. INTRODUCTION

Hemoglobins comprise a challenging area of study within biochemical research. They play an important physiological role in organisms, such as oxygen transport and storage (Trent III et al., 2001; Nieves-Marrero 2011). These studies provide a broad research framework that result in the correlation of protein structure with their function and the understanding of the ligand carrier mechanisms. Hemoglobins are widely distributed in different organisms in nature. Knowledge of the processes of carrying and storing diatomic ligands (O₂, CO and others) is the basis to the understanding of the function of these hemoglobins. In order to understand the ligand binding dynamics and ligand dissociation mechanisms, and to relate them with the protein's function, it is necessary to establish the specific amino acid interactions within prosthetic groups, the shape of the structural cavities in proteins; the interactions between globin chains; interactions with water molecules (how many), and other important aspects that occur in the ligand stabilization and release mechanisms (Patrizi et al., 2014; Lapini et al., 2012; Marcelli et al., 2012; Feis et al., 2007; Bustamante et al., 2014).

The clam *Lucina pectinata*, as a model organism of a non-vertebrate system in which hemoglobins function, has been well studied. Our research is focused on the elucidation of the crystallographic structures of the Oxy-HbII-III complex as function of pH; and the Oxy and Cyano complexes of HbIII. These findings will provide a better understanding of the protein's action mechanism and will demonstrate the role of pH as a driving force in the oxygen release mechanism.

1.0 Research justification

Our target hemoglobins were discovered inside the ctenidia tissue of the *Lucina pectinata* bivalve mollusk (Read, 1965). This clam is collected in the tropical coasts of Puerto Rico at La

Parguera (Navarro et. al., 1996). The hemoglobins found inside the ctenidia tissue are: hemoglobin I (HbI), hemoglobin II (HbII), and hemoglobin III (HbIII). The HbI is a sulfide reactive hemoglobin, while HbII, HbIII and the protein complex HbII-III are oxygen carrier proteins (Kraus and Wittenberg, 1990; Ruiz-Martínez, 2011). Structurally, hemoglobin I is a monomer at all concentration. Hemoglobin II was isolated as a tetramer at high concentrations and hemoglobin III exists as a dimer at all tested concentrations (Kraus and Wittenberg, 1990). Our organism, the clam *Lucina pectinata*, lives in a sulfide rich ecosystem inside the mangrove's mud. However, inside the clam, the hemoglobins, HbII, HbIII and HbII-III complex, remain oxygenated in the presence of hydrogen sulfide (Kraus and Wittenberg, 1990). Hemoglobins play a role in oxygen and H₂S transport and its symbiotic relation with the bacteria found inside the clam (Kraus and Wittenberg, 1990).

Hemoglobin II, hemoglobin III and the hemoglobin II-III complex have the same amino acid composition around the distal pocket (Hockenhull-Johnson et al., 1993; Gavira et al., 2008; Ruiz-Martínez, 2011). Also, the composition of HbII and HbIII has 94 identical residues, including the distal and proximal amino acid residues in the heme pocket, proximal histidine (His) at position F8, and the distal site: phenylalanine (Phe) at position E11, glutamine (Gln) at position E7, and tyrosine (Tyr) at position B10 (Hockenhull-Jonson et. al., 1991 and 1993). Moreover, the electron parametric resonance (EPR) spectra of HbII and HbIII began the discussion which related the tyrosinate group as distal ligand to the heme iron pocket of the clam (Kraus et. al., 1990). This study suggests that tyrosinate may act as a distal heme ligand in the alkaline form of hemoglobin HbII and HbIII in the ferrous form (Kraus and Wittenberg, 1990). Furthermore, it was thought that the leucine (Leu) CD4 and the phenylalanine (Phe) B14 could facilitate the movement of TyrB10 into the distal part of the heme pocket for hemoglobins HbII

and HbIII (Hockenhull-Jonson et al., 1993). These structural similarities between the HbII and HbIII open the possibility to conduct comparative studies of the heme pocket residues effect on the ligand selection and stabilization, and the protein folding arrangements.

The discussion of the ligand control in protein reactivity has been the main approach of several investigations. Some research findings have divided ligand control into two broad categories: i) proximal control and ii) distal control, which plays the main role, based on the architecture of the heme ligand binding site (Peterson et al., 1997). The fundamental effect of the distal residues is defined by the interaction between the iron-bound ligand environment, as well as the ligand ambient immediately after dissociation and just prior to binding the ligand (Peterson et al., 1997). Additionally, the amino acid residues in positions B10 and E7 have been identified to play an important role in modulating the ligand reactivity (Peterson et al., 1997; Gibson et al., 1992; Springer et al., 1994). In this regard, relevant biophysical experimental measurements in solution present the structural similarities between HbII and HbIII. These similarities have been demonstrated molecularly and kinetically, finding the amino acid composition of each protein (Hockenhull-Johnson et al., 1991 and 1993; Torres-Mercado et al., 2003) and obtaining their O₂ and CO kinetic constants (Kraus and Wittenberg, 1990). A computational modeling representation of the heme pocket was employed to visualize the effect in the ligand stabilization of GlnE7 and TyrB10 residues. This visualization contributes to determine the evolution of the structural interpretation based on the physico-chemical parameters previously reported for the oxygen carrier proteins. The kinetic parameters ($k_{\text{off}} = 0.075 \text{ s}^{-1}$ for HbIII and $k_{\text{off}} = 0.11 \text{ s}^{-1}$ for HbII) are similar, but this does not mean that HbIII and HbII have the same patterns of oxygen or carbon monoxide unbinding. Despite all scientific efforts, the hypothesis proposed to explain the relationship between the ligand release mechanism and the

structure and function of the protein remains unclear. For this reason, the X-ray structures of HbIII and HbII-III complex, can be used as a model to establish a coherent explanation of the ligand selections, stabilization, and dissociation mechanism. There is a need to confirm if tyrosine B10 in HbIII really acts like ligand binding at heme site in a way that is similar to that proposed for HbII and HbII-III complex (Nieves-Marrero, 2011; Ruiz-Martínez, 2011).

Previous ligand reaction studies with O₂, CO, NO, CN, and H₂O₂ in HbI and HbII have been used to generate a model regarding the ligand selection and stabilization at the heme pocket. This study proposes an explanation of the HbII heme pocket residues behavior when the heme iron interacts with the H₂O₂ (De Jesús-Bonilla et al., 2006). Further analysis is required in order to establish a relationship between pH and the TyrB10 and the ferryl compound (Fe^{IV}=O). The formation of the ferryl compound is an important aspect in the radical catalytic cycle and the degradation processes of some hemoglobins (De Jesús-Bonilla et al., 2006). Based on this, the oxidation state of the heme iron affects the pocket conformation where the ferryl compound is generated. For this reason, it is necessary to clarify the effect of the iron oxidation state in the heme pocket size and volume. To achieve this, a comparative study using different ligands (oxygen and cyanide) for HbIII and a pH dependence experiment for HbII-III complex is required. To gain more knowledge of the mechanism of ligand selection and stabilization, oxygen will be used as a ligand to help us establish the control factors at distal behavior in the ferrous scenario, and cyanide as a ligand will be used to study the ferric behavior scenario. The cyanide ligand has provided an excellent way to perform oxidation state measurements in the heme ferric state, even if the cyanide binds tightly to the iron atom in Fe(III) in Hbs (Vu et al., 2004). The cyanide anion forms a low-spin ferric complex (Cerda et al., 1999; Helbing et al., 2004) that allows the establishment of a correlation between the heme pocket conformations and

the heme oxidation state adopted by the iron, which in turn affects the perturbation in the protein folding. The X-ray structure models for Oxy and Cyano complexes for HbIII, will establish significant structural similarities and differences to contribute in the ligand selection and stabilization model. Crystallographic structure for the Oxy complex of HbII-III as a function of pH could be an important contribution towards the understanding of the mechanism for dissociation and stabilization of the oxygen ligand.

The structural findings of our comparative study between the Oxy and Cyano forms of HbIII; and the pH effect on Oxy heterodimers of the HbII-III complex, and homodimer of HbII are fundamental to confirm the structural adaptation of TyrB10 in the proposed model of **open** and **closed** conformation of the heme pocket. This model proposes that the TyrB10 swings away from the iron atom in the **open** conformation, while in the **closed** conformation it is at a favorable distance in order to interact directly with the heme iron, and not through a hydrogen bonding network with the bound ligand (Pietri et al., 2005). This suggests that the HbII heme pocket does not allow the entrance of a water molecule while a ligand is bound to the iron, but is flexible enough to adopt various conformational states that may accelerate or reduce the reaction rate with the ligands. The flexibility of the distal residues in the heme pocket of HbII may maintain the GluE7 away from the heme binding center, giving the TyrB10 a conformational freedom so as to control ligand reactivity. The freedom of movement ascribed to TyrB10 may destabilize the bound oxygen, releasing it to the symbiont or the host. We can apply this conformational model to other hemoglobins, in which the dissociation of the oxygen ligand is slow (Pietri et al., 2005) as well as to the component of HbIII and for the complex of HbII-III. More X-rays structural models are needed to support the above suggestion. Our complete comparative study, based on X-ray structural models for HbIII and HbII-III complex, will

address this need. Our findings could establish a structural explanation of TyrB10 as control residue in the ligand stabilization. Also, our pH study could show the distal control effect in the Oxy HbII-III complex.

To understand the hemoglobins, it is important to perform crystallization and crystallographic experiments. The crystallographic study of the hemoglobin found in the blood of the clam *Scapharca inaequivalvis* reveals that the PheF4 residue in HbIISi (*Scapharca inaequivalvis* hemoglobin II), presents two alternate conformations where these residues have a central role in regulating oxygen affinity (Ronda et al., 2013). The crystallographic structure for HbI X-ray was elucidated years ago (Rizzi et al., 1994 and 1996). Similarly, the Oxy complex for the component of HbII was solved by Gavira and co-workers (Gavira et al., 2008); the crystallographic structure of HbII as a function of pH (4, 5, 8 and 9) was solved by Nieves-Marrero (Nieves-Marrero, 2011); and the crystallographic structure of Oxy and Cyano complexes for HbII-III was solved by Ruiz-Martínez (Ruiz-Martínez, 2011). However, as of yet the Oxy and Cyano complexes for the HbIII component remain unsolved.

To further obtain data about a relevant structural model of the HbIII component with different ligands, it is necessary to obtain certain facts about the proteins and address the following issues: i) confirmation of the amino acid sequences with the HbIII X-ray structural model, ii) determination of the volume and size of the HbIII pocket when the heme iron is in its ferrous or ferric state, iii) evaluation of the heme planarity as a function the ligand (O₂, CN) perturbation, iv) elucidation of the residues involved in the heme pocket ligand reactivity control, v) determination of the pH effect in the proteins folding and in the heme pocket residues and vi) evaluation of the pH effect in the protein-protein contact residues inside the dimer.

The study of the effect of pH variation (from 4 to 8) on the crystallographic structure of the HbII-III complex would show how the protein structure is affected. Residues at distal position have been found to be affected when the pH changes in the Oxy complex of HbII-III. Similarly, the secondary and tertiary structure of the hemoglobins is affected when the pH changes. Nieves-Marrero presented the pH effect on the crystallographic structure at pH 4 to 9 for the Oxy homodimer of HbII (Nieves-Marrero, 2011). This study showed that the crystallographic structure at pH 4 does not have an oxygen ligand in the heme pocket, whereas the crystallographic structure at pH 5 to 9 proved to remain oxygenated (Figure 1.0).

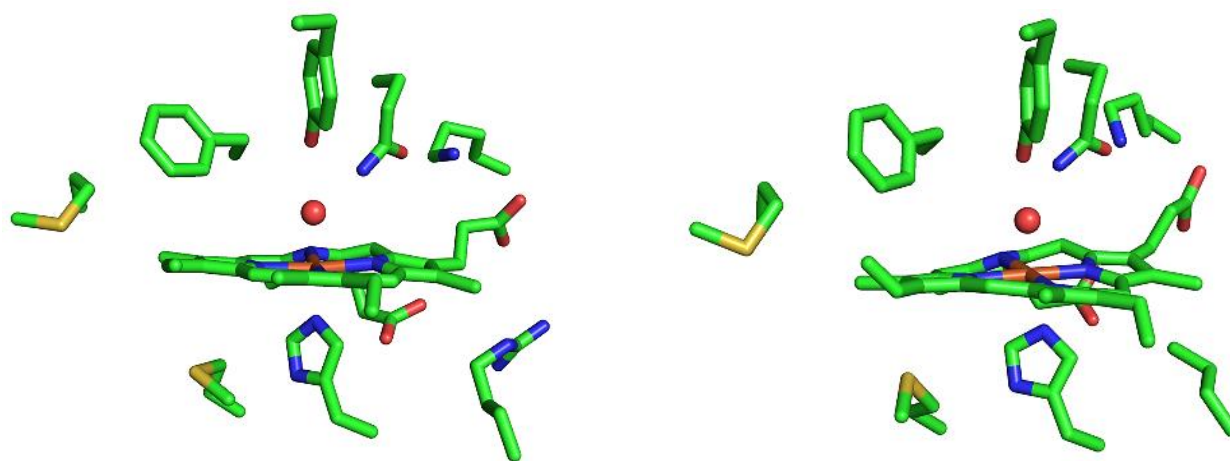


Figure 1.0. Heme pocket for HbII at pH 4. Heme A is shown on the left, heme B with a water molecule as a ligand is shown on the right.

Pietri and co-workers reported different structural properties of Oxy-HbII at pH 4, 5, 8 and 9, with various techniques. They found that acidic conditions facilitate the release of the oxygen ligand in HbII through changes in the microenvironment around the heme group and the orientation of the peripheral amino acids (Pietri et al., 2014). The orientation of the 2-vinyl group changes from twisted out (out-of-plane) to in-plane. This is very important for the oxygen release process (Pietri et al., 2014).

The stereochemistry of the 2- and 4-vinyl groups in the porphyrin ring modify the electron density and the reactivity of the ligand (Reid et al., 1986; Lee et al., 1991). At slightly acidic conditions, the orientation of the 2-vinyl group changes the electron density from the heme iron. This causes destabilization of the interaction between the iron and the oxygen ligand facilitating the oxygen release (Pietri et al., 2014). The TyrB10 moves away from the heme and the water molecule located at the dimer interface undergoes relocation (Pietri et al., 2014). This suggests that the related motion of the 2-vinyl, the TyrB10 and the water molecule under slightly acidic conditions allow the oxygen dissociation from the dimer of HbII.

How can the pH change the environment inside the clam *Lucina pectinata*? The results reported by Pietri and co-workers established that when H₂S is present, the pH of a solution of Oxy-HbII decreases from pH 5 to nearly pH 4, and the oxygen ligand is not bound to the heme pocket iron (Pietri et al., 2014). This data suggests the hypothesis that H₂S regulates the oxygen dissociation from HbII in the tissue of the clam *L. pectinata*. It is possible that the decrease in pH occurs because the concentration of H₂S in the mangrove soils where the clam lives is ~1.0 mM (Pietri et al., 2014; Laurent et al., 2009).

In the clam *Lucina pectinata*, the HbI binds H₂S and transports it to the gills, the concentration of H₂S increases in this tissue and then the H₂S is liberated, affecting the environment which causes a pH decrease. After that, the oxygen ligand is released from HbII to the clam (Pietri et al., 2014). Pietri and co-workers demonstrated the slow oxygen ligand dissociation, and they attributed it to the distal amino acid interaction occurring between TyrB10 and GlunE7 and the ligand with a strong hydrogen bonding network, and also to the small size of the heme cavity (Pietri et al., 2014). In spite of all this data, more research is needed in order to present a clearer picture of the oxygen release mechanism.

1.1. Previous work

The lamellibranch *Phacoides pectinatus* (*Lucina pectinata*) is a bivalve mollusk that inhabits in the sulfide rich coastal sediments of Puerto Rico and houses chemoautotrophic symbiont bacteria (Read, 1965; Torres-Mercado et al., 2003). Studies have demonstrated that its dark-red ctenidia contains three hemoglobins: hemoglobin I (HbI), hemoglobin II (HbII) and hemoglobin III (HbIII); and a cystein rich protein (p-Cys) of different structures and functions (Read, 1965). HbI is a monomeric sulfide-reactive hemoglobin that reacts with H₂S to form ferric sulfide species (Kraus and Wittenberg, 1990). The HbII, HbIII and the complex HbII-III are the oxygen reactive hemoglobins. These kind of hemoglobins remain oxygenated in presence of H₂S and have very similar amino acid composition, but differ markedly from HbI (Kraus and Wittenberg, 1990). The hemoglobins HbII and HbIII have a tetramer and dimeric structure, respectively, at high concentration (Kraus and Wittenberg, 1990). A dimeric structure from crystallographic data for HbII was reported by Gavira and co-workers, and Ruiz-Martínez reported a new crystallographic structure for HbII-III Oxy and Cyano complexes and found an heterodimeric interaction (Gavira et al., 2008; Ruiz-Martínez, 2011).

Sequence analysis were determined and their functional characterization for HbII and HbIII were carried out (Kraus and Wittenberg, 1990). For HbII, the Edman degradation results revealed that it consists of 150 amino acid residues with a calculated molecular weight of 17,476 Da (Hockenhuil-Johnson et al., 1991). Torres-Mercado and co-workers obtained the coding region of the full-length HbII cDNA with 151 amino acid sequence and the molecular weight including the heme group as well as the acetylated N-terminal residues is 17,654.07 Da (Torres-Mercado et. al., 2003). The differences in molecular weight and amino acid composition reported is due to the additional aspartic acid found in the cDNA derive amino acid sequence of

HbII. Edman degradation of HbIII shows that it has 152 amino acids, including heme and terminal N-acetyl serine with a molecular weight of 18,068 Da (Hockenhull-Johnson et al., 1993). Rivera and co-workers (Rivera et al., 2008), using a cDNA clone, characterized the hemoglobin HbIII from *Lucina pectinata*, a 152 amino acid sequence. The partial cDNA clone from Rivera's lab matches the *Lucina pectinata* HbIII amino sequence reported in the NCBI protein database (GenBank accession no. P41262) with only a single amino acid difference (Asn72Asp; AsnE12Asp). An amino acid homology analysis between HbII and HbIII reveals 94 identical residues in common including the Phe at position CD1, the proximal His at position F8, and the distal Gln and Tyr at position E7 and B10, respectively (Rivera et al., 2008).

The crystallographic studies of the hemoglobins from the clam *L. pectinata* started with the hemoglobin HbI. This was the first X-ray structure solved and related with its function in the clam *L. pectinata* (Rizzi et al., 1994). A crystallographic study of HbII made by Gavira and co-workers, established the crystallographic structure for the oxy homodimer from HbII (Gavira et al., 2008). Ruiz-Martínez reported a crystallographic structure for the Oxy and Cyano heterodimer of HbII-III complexes (Ruiz-Martínez, 2011). The methodology employed for the Oxy homodimer of HbII can be used as a reference to perform a parallel procedure to study the oxygenated HbII-III complex and the Oxy and Cyano complex of HbIII. The methodology employed to study the pH dependence of the Oxy HbII can be used, as well, as a model to study the heterodimer of Oxy-HbII-III complex at different pH from 4 to 8 (Nieves-Marrero, 2011). All of the *Lucina pectinata* hemoglobins have been characterized using several spectroscopic and molecular techniques, offering unique structural information to correlate it with their functional properties.

The biochemical properties of HbI, HbII and HbII-III complex were confirmed by X-ray crystallography studies. Casale and co-workers reported the crystallization condition for the HbI-Oxy and the preliminary crystallographic data at 2.0 Å resolution (Casale et al., 1991). Rizzi and co-workers reported the crystal structure for the aquo-met HbI at 1.5 Å resolutions and the structural model for HbI was solved employing the molecular replacement technique (Rizzi et al., 1994). This structural model proposes that the heme distal pocket of HbI has residues of GlnE7, PheB10, PheE11 and PheCD1 (Rizzi et al., 1994). These three phenylalanine residues in a distal site (B10, E11 and CD1) are described as a “Phe-cage” (Rizzi et al., 1994 and 1996). The composition reported by Rizzi was validated by cDNA derivate amino acid sequence by Antonmmattei-Pérez and co-workers (Antonmmattei-Pérez et al., 1999). Rizzi suggested that the H₂S ligand in HbI was stabilized by hydrogen bonding with the carbonyl group of the GlnE7. The “Phe-cage” is essential in the stabilization and release of the ligand inside the heme pocket (Rizzi et al., 1994 and 1996). This structural model was used to establish the structural bases for a functional explanation of the sulfide reactive hemoglobin inside the invertebrate organism. Bolognesi and co-workers developed a comparative X-ray study of HbI-CN and sperm whale myoglobin (SWMb) (Bolognesi et al., 1999). The experiment on HbI-CN and SWMb-CN, showed the structural evidence for the ligand orientation inside the heme pocket and described the functionality of the “Phe-cage” residues.

Oxy HbII at pH 7 was crystallized and analyzed. Gavira and co-workers crystallized the Oxy HbII using capillary counterdiffusion crystallization technique (Gavira et al., 2006). Nieves-Marrero and Ruiz-Martínez crystallized the homodimer Oxy-HbII and the Oxy and Cyano heterodimer complexes of HbII-III with the capillary counterdiffusion crystallization (CCD) technique (Nieves-Marrero et al., 2010; Ruiz-Martínez et al., 2009) Also, Torres-

Mercado and co-workers performed the cDNA amino acid sequences of HbII, revealing a unique amino acid composition in the heme pocket. This heme pocket has the following residues: GlnE7, TyrB10, PheCD1 and PheE11 (Torres-Mercado et al., 2003). The distal residues GlnE7 and TyrB10 in HbII are similar compared with several truncate hemoglobins (trHb) heme pocket (Samuni et al., 2003; Ouellet et al., 2003). The trHb has a kinetics behavior similar to HbII since they exhibit high affinity and slow dissociation rate for oxygen. This slow oxygen dissociation rate in trHb as well as in HbII is a consequence of a strong hydrogen bond network between the GlnE7, TyrB10 and the bound ligand (Ouellet et al., 2002; Pietri et al., 2005).

Ruiz-Martínez crystalized and reported a new crystallographic structure of the Oxy and Cyano complexes of HbII-III with a PDB number of 3PT7 and 3PT8, respectively (Ruiz-Martínez et al., 2009 and 2011). They established the predominant role in the ligand stabilization and selection mechanism where the TyrB10 and GlnE7 in the distal side are involved. An important interaction reported by Ruiz-Martínez is the heme stabilization by two hydrogen bond networks, one at the distal side, LysF3 and the propionate 6 for the heme group, and the other by the proximal site between ArgF11 with HisF8 and water molecule (Ruiz-Martínez, 2011). One important finding was that the folding of HbII-III complex was stabilized by water molecules between chains and the major non-bonding contacts. When the volume for the heme pockets with different oxidation state is compared, the Oxy complex for chain A (HbII) is larger than the heme pocket of chain B (HbIII). In the Cyano complex, the volume behavior was reversed: chain A was smaller than chain B (Ruiz-Martínez, 2011). The kinetics study provided evidence that HbIII component has a predominant role in the decrease of association constant due to the presence of HbIII instead HbII, when compared to the homodimer of HbII (the second order constant k_{on} for the HbII-Oxy complex was $5.00 \times 10^6 \text{ M}^{-1}\text{s}^{-1}$ and for the Oxy-

HbII-III complex was $0.661 \times 10^6 \text{ M}^{-1}\text{s}^{-1}$). Ruiz-Martínez presented the hypothesis that the heterodimer of HbII-III complex is the functional oxygen carrier protein in *Lucina pectinata* (Ruiz-Martínez, 2011). Figure 1.1 shows the complete dimeric assembly for Oxy-HbII-III complex with a PDB number of 3PT7, reported by Ruiz-Martínez at pH 5 and evidences the interaction between both chains.

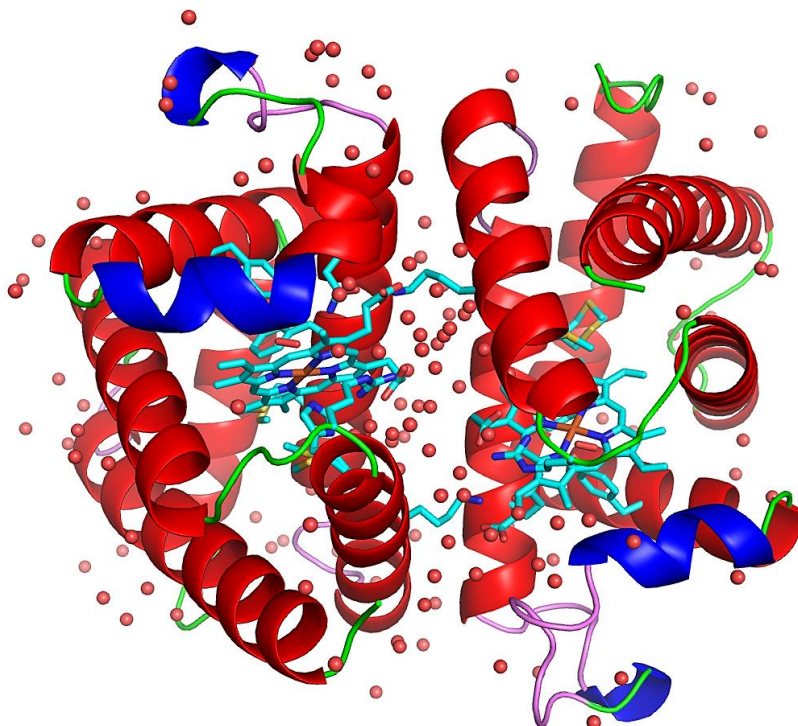


Figure 1.1. Structure of the Oxy-HbII-III complex of *L. pectinata* at pH 5. (Ruiz-Martínez 2011, 3PT7)

Studies correlating the hemoglobins oxygen release mechanism of the non-vertebrate organisms with the pH dependence are scarce. The pH effect as oxygen activation control factor in the ligand selection and discrimination is still open to discussion. The p_{50} (half-saturation pressure, dioxygen affinities) studies showed the pH effect in the reactive behaviors of several proteins from the *Chironomus thummi* and the *Dicrocoelium dentriticum* organisms (Gersonde et al., 1972; Smit et al., 1986). Saroff established that relevant pH discussions relate with the oxygen affinity and release correlated with the residues at the position B10 and E7 (Saroff,

2004). Saroff, Bolognesi and co-workers established the correlation of hydrogen bond interactions with the oxygen and protons of the ionisable groups (Bolognesi et al., 1997; Saroff, 2004). The effect of pH in the oxy homo dimer of HbII is an excellent model to support this research effort (Nieves-Marrero, 2011). The HbII shows variations in the secondary structure as a function of pH, such as: different distribution of the alpha helix and the 3_{10} helix. The interactions at the dimers interface were modified by the effect of the pH. The stabilization of the dimer between the heme group and the peripheral propionate with the Lys92 are a significant contribution by this amino acid. Nieves-Marrero suggested that the TyrB10 and GlnE7 are involved in the mechanism of the dissociation of the oxygen in the heme group as a function of pH (Nieves-Marrero, 2011). This study showed that when the pH decreased from 9 to 5, the oxygen bond with the iron became weaker, from 1.8 Å to 2.0 Å.

The structure deposited in the RCSB PDB for the Oxy complex of HbII at pH 4, 5, 7, 8 and 9 (3PI4, 3PI3, 2OLP, 2PI2 and 3PI1) presented a homodimer for the heme protein of Oxy-HbII at each pH. The structural analysis presents a dimer interface interaction between helix E and F from both dimers. This interaction is commonly found in cooperative invertebrate hemoglobins (Royer et al., 2001 and 2005; Pietri et al., 2014). Gavira and co-workers presented the homodimer complex of Oxy HbII at pH7 (Gavira et al., 2008). They reported a dimer interface surface of 846 Å², but the Oxy HbII at pH 4 had an average area of 823 Å² and 852 Å² for pH 9 (Nieves-Marrero, 2011). When analyzing the interface area, it decreases as function of pH, showing a direct proportionality between pH and the interface surface. The same behavior was shown by water molecules as a function of pH (Pietri et al., 2014; Nieves-Marrero, 2011). There is a rearrangement of this water molecule as a function of pH; in agreement with the Rhonda and co-workers results showing a cluster of water molecules between the dimeric

interface of their E and F helix in the hemoglobins HbI and HbII of *Scapharca inaequivalvis* (Ronda et al., 2013). This supports Pietri's idea that the water cluster is implicated in the cooperative mechanism (Pietri et al., 2014). The crystallographic structures of the Oxy homodimer for the component of HbII at different pH values (4, 5, 8 and 9) were used to demonstrate the oxygen release from the homodimer of HbII (Nieves-Marrero, 2011). At pH 5, the HbII dimer presented the movement of the 2-vinyl group, the TyrB10 residue and the water cluster at the dimer interfaces was found to play an important role for the oxygen release (Pietri et al., 2014). The orientation of the 2-vinyl group in the porphyrin ring in HbII suggested that the oxygen dissociation was affected by the pH. They established the following hypothesis: HbI transports the ligand H₂S to the gills, following the release of H₂S; then, the ligand decreases the pH in the gills and induces oxygen release from HbII (Pietri et al., 2014).

At pH 7, the hemoglobin HbII has the high affinity state and the structure is less tight, so it allows the oxygen binding. Based on these observations, the cooperative subunits interactions in Oxy-HbII are observed at ~20% of oxygen saturation (Bonaventura et al., 2010), but above 50% of saturation, the cooperative behavior is no longer operative, where the TyrB10 and GluE7 anchor the oxygen ligand in a closer conformation that added affinity for the oxygen in this state (Bonaventura et al., 2010).

Previous research suggests that HbII and HbIII may act as a terminal oxidase (Kraus and Wittenberg, 1990). This was partially supported by the association (k_{on}) and dissociation (k_{off}) constant measured for both proteins (Kraus and Wittenberg, 1990). The values reported by Kraus and Wittenberg for HbIII are the following $k_{on} = 0.29 \times 10^{-6} \text{ M}^{-1}\text{s}^{-1}$ and the $k_{off} = 0.08 \text{ s}^{-1}$, and for HbII the $k_{on} = 0.39 \times 10^{-6} \text{ M}^{-1}\text{s}^{-1}$ and $k_{off} = 0.11 \text{ s}^{-1}$. These results suggest differences in configuration of the HbIII and HbII distal heme pocket that may affect the different ligand

dynamics processes. Kraus and Wittenberg implicated that the tyrosinate directly bonded in the distal position to the ferric heme at alkaline pH (Kraus and Wittenberg, 1990). To elucidate the functional properties of HbII, biophysical studies were performed based on the pH behavior of the heme pocket residues, specifically the TyrB10. These studies suggest the possible existence of two conformations inside the pocket: the **open** and **closed** conformations. These conformations have shown certain interactions between the TyrB10, the ligand, and the heme iron (Peterson et al., 1997; Pietri et al 2005). Other spectroscopic studies have indicated that discrimination and stabilization of ligands appears to be dictated by the unusual distal heme pocket environment (Pietri et al., 2006). Resonance Raman (RR) and Infrared (IR) studies, suggest that, under physiological conditions, the distal heme pocket of HbII can adopt two structural conformations with respect to the tyrosine residue at the B10 position. The **open** conformation, when the TyrB10 swings away from the iron atom, and the **closed** conformation when it is closer. In the close conformation, it has a favorable distance to interact directly with the ligand, or weakly with the iron atom. Figure 1.2 shows the **open** and **closed** conformational models of the HbII heme distal environment (Peterson et al., 1997; Pietri et al., 2005).

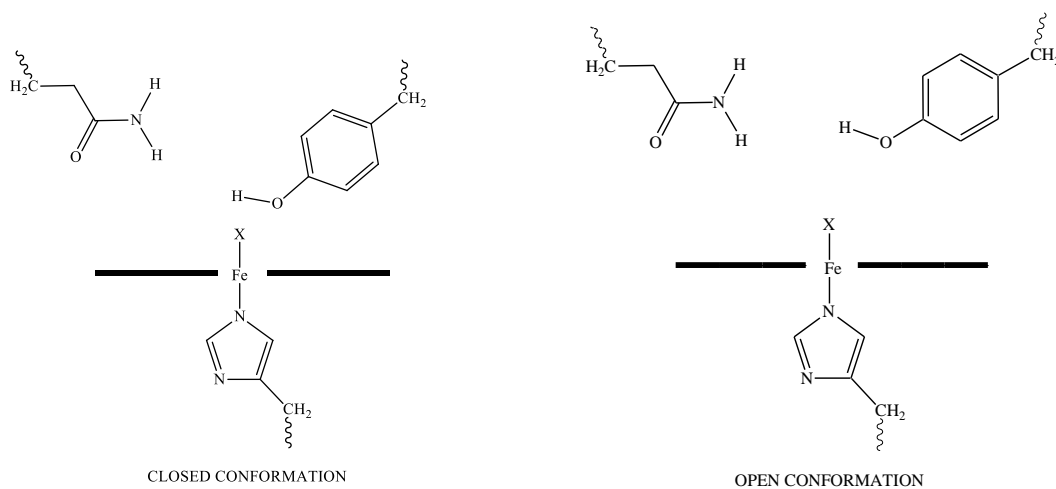


Figure 1.2. The open and closed conformation proposed for the HbII distal environment.

Doyle and co-workers studied the crystallization and crystallographic conditions for HbIII (Doyle et al., 1994). Hanging drop vapor diffusion (HDVD) technique was employed at a controlled temperature of 295K. The precipitating agent used to obtain the HbIII crystals was 15% PEG 8000 and 500 mM lithium sulfate (Doyle et al., 1994). The protein solution crystallized contained 1.1 mM of HbIII, 0.05 mM EDTA and phosphate buffer, pH 7.5. The crystal shape was tetragonal with dimension of 0.35 X 0.2 X 0.10 mm. Also, the crystallographic data established a P4₂2₁2 space group, with unit cell constants of a = b = 76.8 Å, c = 153.6 Å. HbIII and HbII have similarities in the amino acid sequence of eight helices, which give the following homology: 75% A, 75% B, 71% C, 29% D, 80% E, 82% F, 44% G and 50% H (Doyle et al., 1994). The crystallographic comparison between these two hemoglobins, based on their folding, is not yet possible because the structural model of HbIII remains unsolved.

Ramos-Santana and López-Garriga (Ramos-Santana and López-Garriga et al., 2012) studied the peripheral side groups of the heme pocket from the Cyano complex of HbI from *L. pectinata*. These peripheral groups of 6 and 7-propionate, have simply been considered as anchors of the heme to the protein matrix (Ramos-Santana and López-Garriga, 2012; Schneider et al., 2007). The hydrogen bonding with the residues in the distal site from the heme pocket with the ligand and the hydrogen bond network between 6 and 7-propionate group, and the mechanism of the dissociation and stabilization remains unclear (Ramos-Santana and López-Garriga et al., 2012). They suggested that the proximal network modulated by the His98 trans-effect, affecting the rate of dissociation of the oxygen ligand and the distal network, TyrB10 and GlnE7 on the heme pocket, is responsible for the slow dissociation of the oxygen ligand in HbII from *L. pectinata* and similar at the hemoglobin in *Ascaris suum* (Peterson et al., 1997; Gavira et al., 2008; Ramos-Santana and López-Garriga, 2012).

The findings above show the necessity to determine the structural models of the following hemoglobins complexes: Oxy-HbII-III at pH 4 to 8, to contribute with a better insight of the oxygen release mechanism for non-vertebrate organisms. The findings of HbIII in combination with the pH effects study of the Oxy heterodimer of HbII-III complex are fundamental to confirm several proposals related with: i) the overall protein folding, ii) the effect of the distal residues in the ligand selection and stabilization, iii) the planarity and the stereochemistry of the heme.

2. OBJECTIVES

Our main goals are to i) design and develop a pH function crystallographic structural analysis for Oxy complex of HbII-III, ii) obtain the HbIII structural models for the Oxy and Cyano complexes. The pH study will contribute to evaluate the oxygen release mechanism. The HbIII analysis will be used to gain a better insight about the function of the HbIII protein in the clam. To fulfil these goals, we will carry out the following objectives.

2.1. To isolate and purify HbIII from the HbII-III complex

Optimize the IEC methodology to obtain high quantities of pure HbIII from the HbII-III moiety. The purified fraction will be characterized by tandem MS/MS to validate the employed methodology.

2.2. To design a crystallization methodology to obtain crystals for the Oxy and Cyano complexes of HbIII

Design and develop HDVD and CCD screening experiments to obtain the crystallization conditions of the HbIII Oxy and Cyano complexes.

2.3. To develop a pH dependence crystallization experiment for the Oxy complex of HbII-III as a pH function of 4 to 9

Design and obtain the CCD crystallization condition for the Oxy complex from HbII-III as a pH function (García-Ruiz, 2003; Nieves-Marrero et al., 2010).

2.4. To develop an X-ray methodology to elucidate structural models of the Oxy and Cyano complexes of HbIII and the complex of Oxy-HbII-III as a pH function 4 to 8

X-ray data will be acquired using the synchrotron radiation to obtain highest resolution. Molecular replacement methodology will be employed using the phases from 2OLP and 3PT7 to

solve the structure for the Oxy and Cyano complexes for HbIII and for the Oxy complex of HbII-III.

2.5. To perform a comparative analysis between the crystallographic structures of the Oxy homodimer of HbII with the Oxy heterodimer of HbII-III complex within a pH range from 4 to 8

The comparison between the Oxy-HbII and the Oxy-HbII-III complex is essential to evaluate the protein folding effect in a homo and heterodimer structures. We will correlate HbIII properties from comparison of these structures. The solved structures during this study will be deposited into the RCSB Protein Data Bank.

3. METHODOLOGY

3.1. Extraction, isolation and purification of *Lucina pectinata* hemoglobins

Hemoglobins extraction of *Lucina pectinata* from the ctenidia (Figure 3.1) was performed according to previous methods (Kraus et al., 1990) with slight modifications (Pietri et al., 2005). 100 mL of extraction solution (10.0 mM HEPES, 5.0 mM EDTA and 1.0 mM DTT), per 25.0 g of ctenidia tissue was employed in a 4 °C ice-cold reservoir. The medium was adjusted to pH 7.5 with triethanolamine (TEA) buffer.

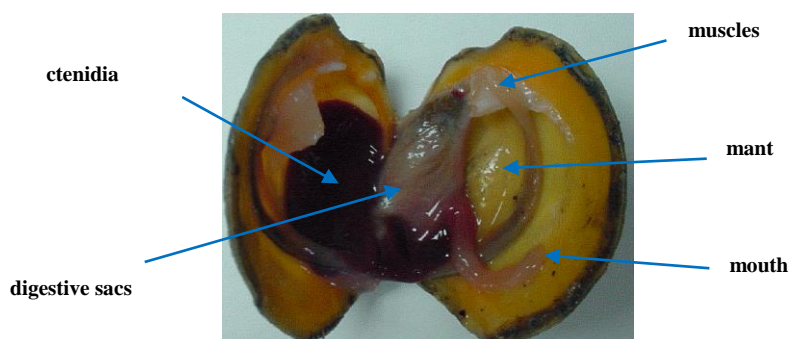


Figure 3.1. The *Lucina pectinata* clam.

The extract was homogenized, bubbled for 15 min with carbon monoxide (CO) and centrifuged at 19,000 rpm for 1.0 hour at 4.0 °C constant temperature. Supernatant was filtered using a 0.45 µm filter and stored at -80°C. This extract is our “raw material” or “crude extract”. Size exclusion chromatography (SEC) with a HiLoad 26/60 Superdex 200 prep grade column (ÄKTA FPLC, Amersham Bioscience) was used to isolate the different hemoglobins. The elution buffer (50.0 mM of sodium phosphate monobasic (NaH₂PO₄) with 0.5 mM of ethylenediaminetetraacetic acid (EDTA)), was adjusted to pH 7.5 (Ruiz-Martínez et al., 2009). The SEC column used a flow rate of 1.0 mL/min and a maximum pressure of 0.15 MPa. Figure 4.1 shows the elution profile obtained for the HbI/pCys, HbII-III complex and the yellow fractions.

Different fractions were duly separated by SEC, the HbII-III complex oxidation state and concentration were verified. The UV-Vis spectra showed the characteristic 414 nm Soret band and the 540 and 576 nm Q bands; all corresponding to the Oxy state. Sample concentration range was between 0.15 to 0.20 mM before separated by ion exchange chromatography (IEC). The HbII-III complex fraction was separated into HbII and HbIII using a new chromatographic procedure with IEC. This method was developed using a fast performance liquid Chromatography (FPLC) instrument with a XK 16/70 column (GE, healthcare life science), packed with a Q Sepharose High Performance (QHP, from GE healthcare life science), a strong anion exchanger, and a HiTrap QHP pre-column (GE, healthcare life science). Figure 3.2 shows the arrangement for the separation of Oxy-HbII-III complex.



Figure 3.2. XK 16/70 column with strong anion exchange Q Sepharose High Performance (QHP).

IEC column was equilibrated with the running Buffer A (10.0 mM of TEA/sodium acetate at pH 7.5) prior to run. The sample (10 mL with a concentration between 0.15 to 0.20

mM) was loaded using elution Buffer B (10 mM TEA/sodium acetate and 180 mM sodium chloride at pH 7.5). This new IEC methodology used the following chronology and parameters:

- a) 12.0 mL: 100% buffer A / 0% of buffer B at 2.0 mL/min (sample injection)
- b) 1.0 mL: 95% buffer A / 5% buffer B at 2.0 mL/min
- c) 2.0 mL: 95% to 60% buffer A / 5 to 40% buffer B at 2.5 mL/min
- d) 810.0 mL: 60% buffer A / 40% buffer B at 2.5 mL/min
- e) 300.0 mL: 60 % to 0% buffer A / 40 to 100% buffer B at 2.5 mL/min
- f) 225.0 mL: 0 to 100% buffer A / 100 to 0% buffer B at 2.5 mL/min

Figure 4.4 shows the chromatographic separation profile of HbII and HbIII complexes monitored with a UV-Vis detector. To confirm the integrity of the Oxy-HbIII complex, tandem MS/MS technique was used. The purified HbIII sample (100 µg/mL) were separated by one-dimensional electrophoresis. The band, with the characteristic molecular weight of our sample corresponding to the hemoglobin HbIII, were cut and subjected to protein-digestion (using trypsin and overnight incubation at 37 °C). Peptide were extracted with 0.1% of trifluoroacetic acid (60% ACN), dried and purified using zip-tip (C18 from Millipore Corp). The obtained peptide were resuspended in 0.1% formic acid in HPLC graded water (Pérez-Laspiur et al., 2007; Toro-Nieves et al., 2009; Rivera-Rivera et al., 2012). These peptide were fractionated on a microcapillary RP-C18 column followed by fragmentation with ESI-LC-MS/MS system (ProteomeX system with LTQ XL) in a nano-spray configuration. Mass Spectrometric analysis was searched using Mascot (Matrix Science, London UK; version 2.4.0). Mascot was searched with a fragment ion mass tolerance of 0.8 Da and a parent ion tolerance of 10.0 PPM. Mascot use the carbamidomethyl of cysteine as a fixed modification and S-carbamoylmethylcysteine cyclation on the n-terminus, oxidation of methionine and acetyl of the n-therminus as a variable modification.

To validate the peptide and protein identified by MS/MS were used Scaffold (version Scaffold 4.2.1, Proteome Software inc., Portland, OR). The peptide identification were accepted if they could be established at 80% or greater than this by the Peptide Prophet algorithm (Keller et al., 2002) with Scaffold delta-mass correction. To identify the protein in the MS/MS, this accepts the protein identification if they could be establish at greater than 90% probability and contained at least 2 identified peptides (Nesvizhskii et al., 2003). The proteins that have similar peptides and do not be distinguished based on MS/MS spectrometry analysis alone will be grouped to please the principle of parsimony.

The samples of HbII-III complex and HbIII complexes (Oxy and Cyano) were concentrated using a regenerated cellulose membrane YM-10 with an Amicom® ultrafiltration concentrator system for further utilization in crystallization experiment.

3.2. Preparation of crystallization samples of *Lucina pectinata* HbII-III and HbIII

Protein samples used for the crystallization experiment were in the Oxy form. The spectroscopic validation of all complexes was verified using an Agilent UV-Vis spectrophotometer. The characteristic bands for HbII-III complex were observed at 414 nm (Soret) and 540 nm and 576 nm (Q). Confirmation for HbIII showed bands at 414 nm (Soret) and 540 nm and 576 nm (Q). Concentration range for both complexes was established between 5 to 30 mg/mL. These concentration values were determined with the corresponding average absorptivity coefficients reported by Kraus and co-workers elsewhere (Kraus et al., 1990). Samples that do not have the corresponding spectroscopic markers for the oxygen ligands were further treated to bring them to an Oxy state. The stabilization of these samples was achieved by exposure to an argon atmosphere to achieve deoxygenation. Under anaerobic conditions, an excess of a freshly prepared sodium dithionite (5.0M, Merck) was added to obtain the ferrous

oxidation state. This produces deoxy-HbIII with Soret band at 431 nm (Kraus and Wittenberg, 1990). The excess of sodium dithionate was eliminated using a Centricon centrifugal filter (Amicon) with an YM-10 membrane. Preparation of the Oxy-HbII-III and Oxy-HbIII was accomplished by equilibrating the sample in a chamber with an oxygen saturated environment of 1.0 atm.

3.3. Preparation of Cyano-HbIII from *Lucina pectinata*

The protocol used to prepare the Cyano-HbIII samples has been reported previously (Kraus et al., 1990; Ruiz-Martinez et al., 2009). To generate the Cyano-complex, the ferric HbIII was obtained adding an excess of 10% of the total sample volume of potassium ferricyanide ($K_3Fe(CN)_6$) 10.0 mM (pH 5.0). Complex formation was completed by addition of 50 mM NaCl/20 mM NaCN prepared at pH 5.0. The HbIII-CN complex was confirmed spectrophotometrically using as reference the reported Soret (419 nm) and Q bands (538 nm). See Figure 4.6.

3.4. Crystallization screening techniques

Vapor Diffusion by Hanging Drop (HDVD) and Capillary Counterdiffusion (CCD) Crystallization methods were employed to initial the optimum crystallization conditions.

3.4.1. Vapor diffusion method-hanging drop technique

The HDVD crystallization technique is the most popular method used to obtain crystals of different biological macromolecules (McPherson, 1999). The Crystal Screen ITM (HR2-110) from Hampton Research Corp. is a sparse matrix, containing 50 crystallization conditions used and reported in the literature by Jancarik and co-workers (Jancarik et al., 1991). The evaluation of the crystallization condition for HbII-III complex and HbIII was performed using this vapor diffusion technique with the HR2-110 Crystal Screen ITM kit. The protein used in the experiment

was in distilled water at a concentration between 5 and 30 mg/mL. Previously, 50 wells on VDX plates were prepared using vacuum grease on top of each well. Each well was filled with 1.0 mL of the different HR2-110 Crystal Screen ITM reagents. The Oxy-HbII-III complex and Oxy and Cyano HbIII crystallization sample drops consist of 2.0 μ L of the reservoirs solution and 2.0 μ L of the protein solution. The drop was placed over siliconized coverslips. Each VDX well was covered with coverslips, exposing the protein solution in the drop to the solution inside the well. Figure 3.3 shows a schematic diagram of the HDVD experiment. The observations of the HDVD experiment were completed using an optical microscope.

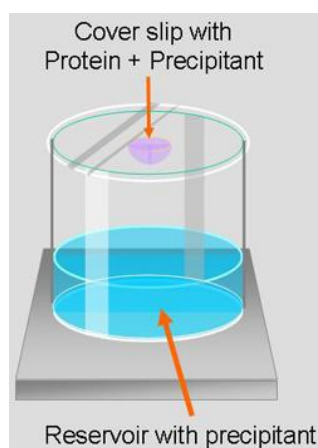


Figure 3.3: Vapor diffusion experiment using the hanging drop method.

3.4.2. Capillary counterdiffusion technique

The Capillary Counterdiffusion (CCD) technique is a non-equilibrium technique for macromolecular crystallization (García-Ruiz, 2003). This crystallization technique was carried out in two parts: i) an initial crystallization screening and ii) the final optimization phase. The CCD technique employs the second generation Granada Crystallization Box (GCB2TM) with a 24 optimal conditions for the proteins' crystallization (Kimber et al., 2003). This crystallization kit was developed by Triana Science and Technology Corporation at Granada, Spain. As Figure 3.4

shows, inside the GCB2TM all 24 domino-like boxes contained precipitant agent solutions at specific concentration covered with a layer of agarose gel to control the nucleation of the protein. The capillaries with inner diameter of 0.1 to 0.5 mm were filled with Oxy-HbIII, Cyano-HbIII and Oxy-HbII-III complex. The upper part of the capillary was sealed using plastiline. The capillary was introduced inside the domino-like box through the agarose layer to generate a plug between the capillary and the precipitant agent solution. Prior to the development of this screening step, an optimal concentration of the protein was required. In our study, the starting point of reference was the 30 mg/mL reported by Gavira and co-workers, Ruiz-Martinez and co-workers and, Nieves-Marrero and co-workers (Gavira et al., 2005; Ruiz-Martinez et al., 2009; Nieves-Marrero et al., 2010).

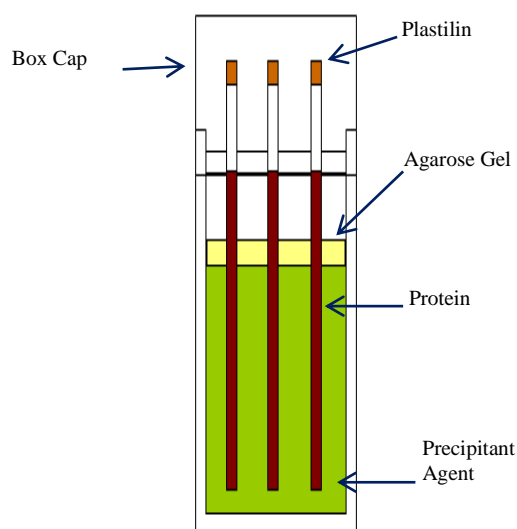


Figure 3.4: Schematic diagram for the Granada Crystallization Box (GCB2TM).

For the second part of the crystallization protocol, the same CCD technique was used to improve the quality and the size of the crystals. In this optimization stage, the GCB2TM consisted of six boxes with specific pH intervals from 4 to 9, with the same precipitant agent. The optimal protein concentration and the precipitant agent was used based on the results of the screening step.

3.5. Structure solution and refinement

3.5.1. X-ray diffraction and crystal mounting

The crystal used for data acquisition will be selected from the CCD optimization step. Crystals obtained from the HDVD technique was collected using a tiny loop with the aid of a microscope. The protein crystal was equilibrated in 50.0 μL of a cryo-protectant solution before exposure to the X-ray source. The cryo-protectant solution containing 15% (v/v) glycerol and the precipitating agent used to grow the crystals was briefly applied to prevent ice formation, crystal breaking, and freezing based on drastic temperature changes. Such changes may happen during the use of a liquid nitrogen jet stream at 100 K (Gavira et al., 2006; Garman and Schneider, 1997). It also prevents protein degradation based on possible radiation damage from the exposure to the high intensity synchrotron radiation during data acquisition.

The selected crystals grown by CCD were prepared by cutting the section of the capillary that contains the crystals. These crystals were extracted and equilibrated with the cryo-protectant solution as previously described. The removal of the crystal from the capillary was performed with extreme care to avoid crystal damage based on manipulation. Figure 3.5 summarizes the crystal manipulation.



Figure 3.5. Crystal collection and mounting.

- The crystal that grew inside the capillary was extracted and equilibrated with the cryo-protectant solution.
- Crystal of Oxy-HbIII grown at pH 4 in sodium formate as precipitant agent, mounted on a nylon loop and flash-cooled in a 100K liquid nitrogen stream.

3.5.2. X-ray data acquisition and structure refinement and resolution

Data acquisition and structure refinement and resolution for the Oxy-HbII-III complex, Oxy-HbIII and Cyano-HbIII complexes were performed following previously published procedure with slightly modifications (Gavira et al., 2005 and 2008). The X-rays source used was at the European Synchrotron Radiation Facility (ESRF). The beamlines used at the ESRF were the BM16 and BM14U. The wavelength and detector were 0.96 Å and a MAR CCD 165, respectively. At the BM14U beamline, the wavelength and detector used were 0.954 Å and a MAR CCD 225, respectively. The structure resolution of all Hb complexes was carried out using molecular replacement methods. Crystallography and NMR System (CNS) suite are commonly used to elucidate the structures of proteins. The structure refinement was accomplished using CNS, PHENIX and REFMAC5 from Collaborative Computational Project, number 4 (CCP4) Suite (Adams et al., 2010; Vagin et al., 2004 and Collaborative Computational Project, N° 4, 1994). The building of the structural model against the electron density maps was obtained with the computational program COOT (Emsley and Cowtan, 2004). Additional refinement was carried with REFMAC5, using TLS parameters (Vagin et al., 2004; Painter et al., 2006). The inclusion of TLS parameters in the refinement process improved the minimization of the R-factor and R-free factor for the crystallographic structure. The secondary structures were obtained using the STRIDE program (Frishman and Argos, 1995). A structural comparison among crystallographic structure were achieved by using root mean square (RMS) analyses on the superposition of the protein backbone main atoms and all side chain residues. Relative displacements were detected using the CCP4 program LSQKAB (Kabash, 1976). The structural information of the protein was supplemented by analyzing the protein-protein interface, using PISA program (Krissinel and Henrick, 2005) and LigPlot+ 1.4.5 version (Laskowisky and

Swindells, 2011). Information related to the accessible surface areas values, as well as the protein cavities were obtained, using NACCESS and CASTp program (Hubbard et al., 1993; Binkowski et al., 2003). The structural model and the corresponding rotamers were reviewed using MolProbity (Davis et al., 2007). After structural evaluation with the corresponding programs, the deposition of the final structures was made using PROCHECK (Lovell et al., 2003; Laswosky et al., 1993). All tridimensional (3D) structural representations and related information for the crystallographic models were obtained using PyMOL Molecular Graphic Systems 1.3, Schrödinger, LLC. Figure 3.6 summarizes graphically the complete procedure to obtain the protein crystallographic structure.

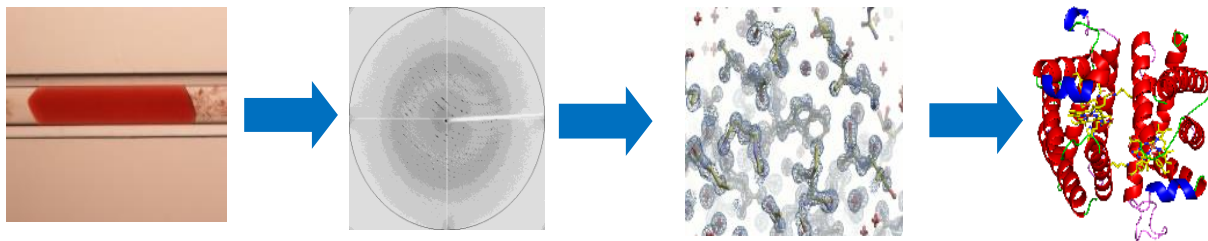


Figure 3.6. Schematic illustration for a protein crystallographic structure.

1. Crystal selection.
2. X-ray source, X-ray diffraction data and hkl 2000 (indexing, scaling and integration).
3. Molecular Replacement with CCP4-COOT and Structural Model Refinement (REFMAC).
4. Final Crystallographic Structural Model.

4. RESULTS AND DISCUSSION

4.1. Isolation and purification of hemoglobins from *L. pectinata*

Crystallographic studies require pure proteins because their crystallization need a high level of purity (McPerson, 2004). The first step in the process is the isolation of the protein from the raw material (crude extract) from the clam. There are multiple proteins in the crude extract. To separate them, the first chromatographic step is the Size Exclusion Chromatography (SEC). The proteins obtained from this separation are HbII-III complex, HbI/p-Cys and others (Kraus and Wittenberg, 1990). Figure 4.1 shows the chromatographic spectra obtained from the crude extract following with the UV-Vis spectrophotometry, detected segment $\lambda_{\max} = 238$ nm.

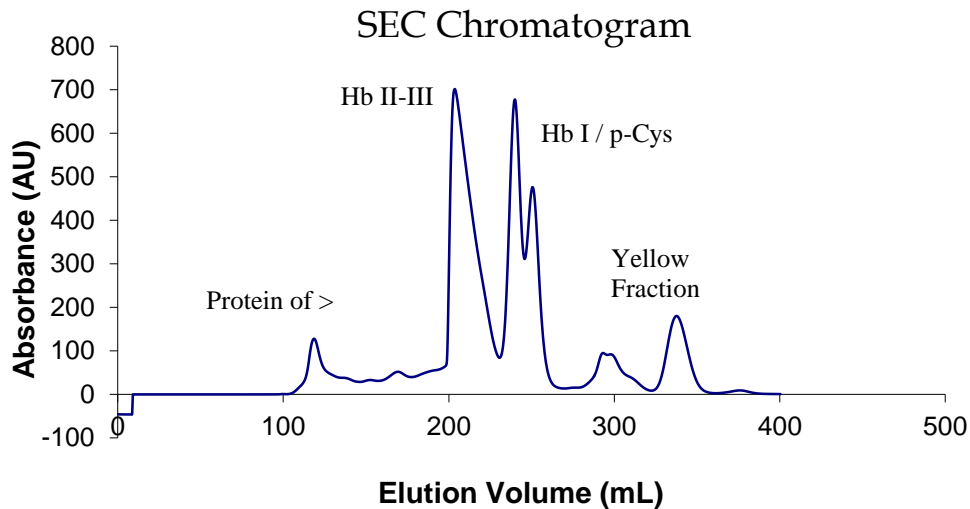


Figure 4.1. SEC chromatogram of the crude extract from the clam *L. pectinata*.

Chromatogram analysis shows five different components: one protein with a high molecular weight, an HbII-III complex (this complex has two components: the hemoglobins HbII and HbIII), the third one is a combination of HbI and the rich cysteine proteins (p-Cys) and the last two are unknown and not characterized yet, known as the yellow fractions. SEC is an effective way to separate the protein of interest, the complex HbII-III. The HbII-III fraction was

collected, switched to distilled water and concentrated for further purification. The HbII and HbIII were separated by IEC.

4.1.1. Purification of HbII and HbIII with ion exchange chromatography (IEC)

Ion Exchange Chromatography was carried out using a HiPrep 16/10 column, loaded with a strong anionic matrix, $-N^+(CH_3)_3$, with a 90 μm mean spherical particles. This column was coupled to a HiTrap QFF pre-column with the same matrix and size particle previously described. Figure 4.2 show an IEC chromatogram data of HbII-III using the HiPrep 16/10 column. HbII is the first major component identified in the figure and the second component is HbIII protein. The pH of the column and the buffers used to separate the HbII-III complex was 8.3, as described in the methodology. After separation, HbII and HbIII fractions were collected, buffer switched to distilled water, and concentrated. HbIII sample purity was analyzed with a second IEC chromatography step. An absorption signal at 55 min elution time showed a peak, indicating that HbIII was contaminated with HbII component (Figure 4.3.). Our data demonstrates that this procedure does not separate the fractions of HbII and HbIII from the HbII-III complex on a 100% basis.

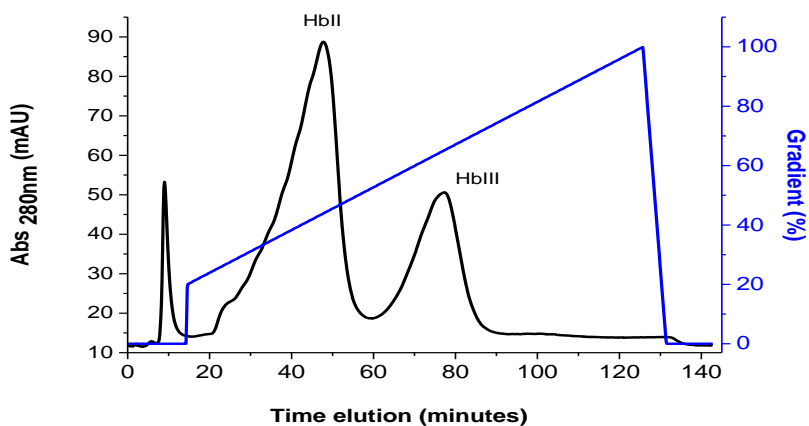


Figure 4.2. IEC for the HbII-III complex with HiPrep 16/10 QFF column.

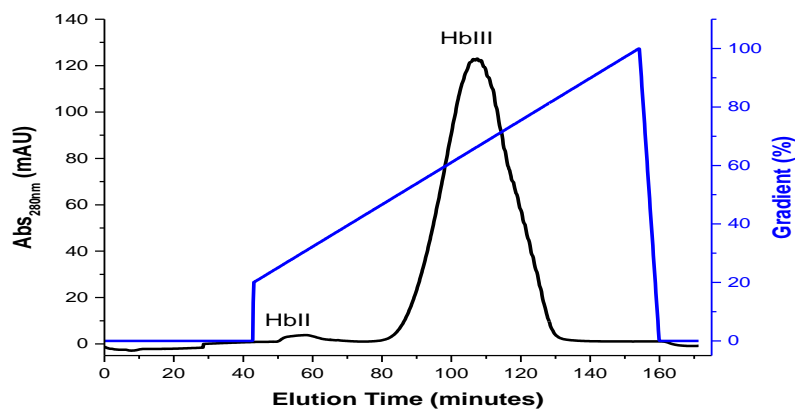


Figure 4.3. IEC for HbIII to confirm the purity of the protein.

The purification procedure was improved pursuing a total purification of the HbIII fraction. Our analysis of the previous data suggested carrying out an IEC with a new column that had the same anionic matrix, but a smaller mean bead size (34 μm). A new column XK 16/70 from GE healthcare life science was packed with Q Sepharose High Performance (QHP, GE healthcare life science) matrix. This new column was coupled to a pre-column (HiTrap QHP). The program used to separate the components from the complex was modified, as described in the methodology. The pH of the column and buffer was adjusted at 7.5. Chromatogram spectrum using the modified parameters is shown in Figure 4.4. The first peak represents the HbII component and the second represents HbIII component. A comparative analysis between chromatographic spectra as shown in Figure 4.2 and Figure 4.4 demonstrate: i) a better resolution, judged by the separation of the peaks, using the conditions described in the new procedure, ii) a better definition of the baseline was obtained as it approach to zero. HbIII purity analysis was further accomplished using a Tandem MS/MS technique. MS/MS data analysis shows the presence of Hemoglobin-3 (OS=Phacoides pectinatus; Table 4.1). The Tandem MS/MS analysis was performed in duplicate and it identified 31 and 32 unique peptides respectively, for HbIII in each test. HbIII was identified with high confidence and HbII unique

peptides were not found. Table 4.1 shows the proteins components obtained in the MS/MS analysis from HbIII.

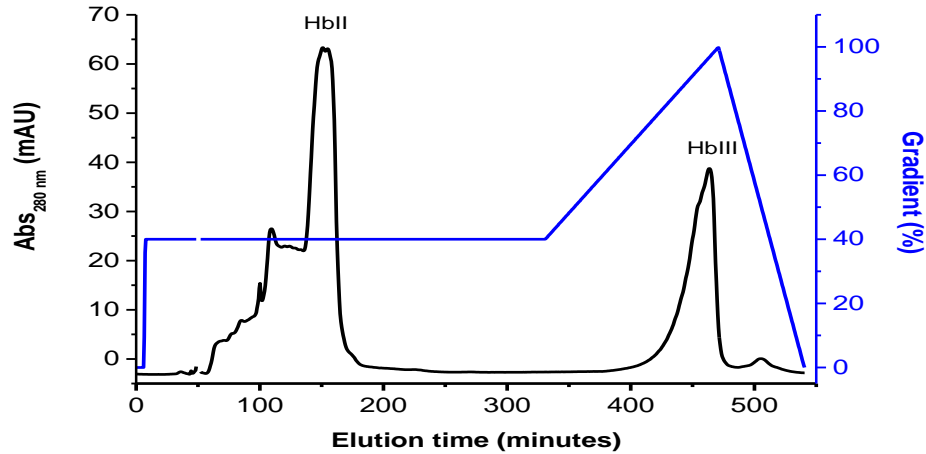


Figure 4.4. IEC for the HbII-III complex with QHP matrix with HK 16/70 column.

Table 4.1. Proteins identified by MS/MS.

Proteins	Accession number	Molecular Weight kDa	Number of peptide	
			Sample 1	Sample 2
Hemoglobin-3 OS = Phacoides pectinatus PE = 1 SV = 2	GLB3_PHAPT	18	31	32
Keratin, type I cytoskeletal 10 OS = Homo sapiens GN=KRT10 PE = 1 SV = 6	K1C10_HUMAN	59	0	3
Keratin, type I cytoskeletal 9 OS = Homo sapiens GN=KRT9 PE = 1 SV = 3	K1C9_HUMAN	62	2	1
Phosphate binding protein OS= Unknown prokaryotic organism PE =1 SV =1	PHBP_UNKP	39	3	2
Trypsin OS=Sus scrofa PE=1 SV=1	TRYP_PIG	24	6	4

The Hemoglobin-3 (OS=Phacoides pectinatus), sample 1 for HbIII presents 9 exclusive unique peptides, 17 exclusive unique spectra, 31 total spectra, 82/153 amino acids (54% coverage), and 100% protein identification. Sample 2 for HbIII presents 10 exclusive unique peptides, 18 exclusive unique spectra, 32 total spectra, 84/153 amino acids (55% coverage), and 100% protein identification. Figure 4.4.1 and Figure 4.4.2 shown the peptide identified with

MS/MS for sample 1 and 2 respectively (sequence in yellow). These results validated the new procedure as a tool to separate HbIII from HbII-III complex.

GLB3_PHAPT (100%), 17,560.6 Da
Hemoglobin-3 OS=Phacoides pectinatus PE=1 SV=2
9 exclusive unique peptides, 17 exclusive unique spectra, 31 total spectra, 82/153 amino acids (54% coverage)

```

M S S G L T G P Q K A A L K S S W S R F M D N A V T N G T N F Y M D L F K A Y P D T L T P F K S L F
E D V S F N Q M T D H P T M K A Q A L V F C D G M S S F V D N L D D H E V L V V L L Q K M A K L H F
N R G I R I K E L R D G Y G V L L R Y L E D H C H V E G S T K N A W E D F I A Y I C R V Q G D F M K
E R L

```

Figure 4.4.1. Peptide sequence identified with MS/MS spectrometry, sample 1.

GLB3_PHAPT (100%), 17,560.6 Da
Hemoglobin-3 OS=Phacoides pectinatus PE=1 SV=2
10 exclusive unique peptides, 18 exclusive unique spectra, 32 total spectra, 84/153 amino acids (55% coverage)

```

M S S G L T G P Q K A A L K S S W S R F M D N A V T N G T N F Y M D L F K A Y P D T L T P F K S L F
E D V S F N Q M T D H P T M K A Q A L V F C D G M S S F V D N L D D H E V L V V L L Q K M A K L H F
N R G I R I K E L R D G Y G V L L R Y L E D H C H V E G S T K N A W E D F I A Y I C R V Q G D F M K
E R L

```

Figure 4.4.2. Peptide sequence identified with MS/MS spectrometry, sample 2.

4.1.2. Spectroscopic confirmation of the Cyano and Oxy complex for HbIII

The determination of the oxidation state for the Oxy-HbIII is necessary to establish the crystallization conditions. Oxy state from HbIII sample was determined by UV-Vis spectrophotometry. The UV-Vis band reported by Kraus and Wittenberg for Oxy-HbIII was 414 nm Soret and two Q bands at 540 and 575 nm (Kraus and Wittenberg, 1990). The experimental spectrum of our sample shows a 414 nm for the Soret band and two Q bands at 541 and 576 nm (Figure 4.5). Oxy-HbIII concentration was determined using the molar extinction coefficient of the bands.

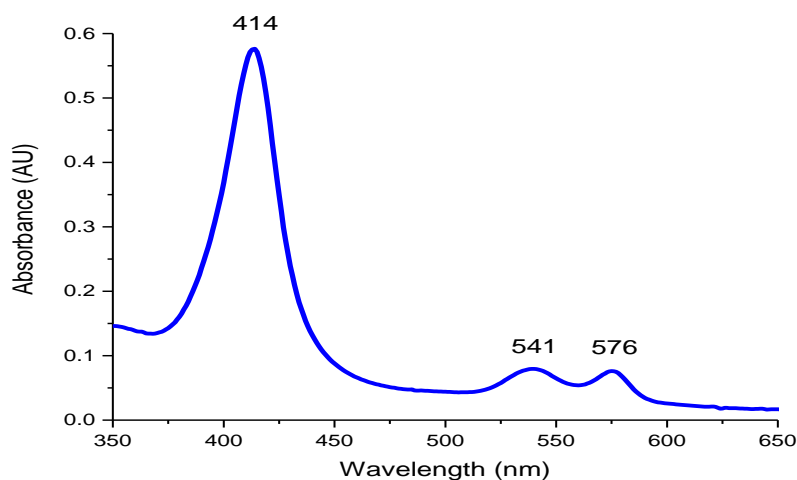


Figure 4.5. UV-Vis spectrum for Oxy-HbIII.

Electronic absorption bands reported by Kraus and Wittenberg for the Cyano complex of HbIII, were 419 nm for the Soret band and one Q band at 537 nm (Kraus and Wittenberg, 1990). The Cyano complex obtained with the procedure reported in the methodology (Figure 4.6) agrees with Kraus' report. The spectrum shows the Soret band at 419 nm and a Q band at 537 nm. Cyano-HbIII concentration was determined using the molar extinction coefficient of the bands. Both spectra shown in Figure 4.5 and 4.6 ratify the hemeprotein have the Oxy ligand and the Cyano ligand, respectively.

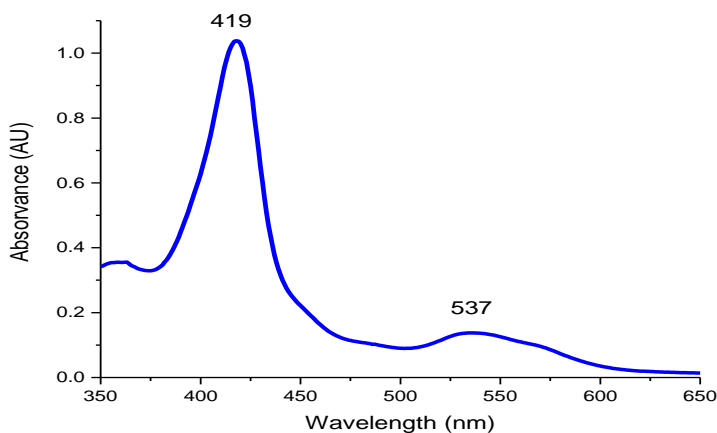


Figure 4.6. UV-Vis spectrum for Cyano-HbIII.

4.2. Crystallization of the hemoglobins from *L. pectinata*

The crystallization process of the hemoglobin from *L. pectinata* is based on the work described by Gavira and co-workers, Nieves-Marrero and co-workers, and Ruiz- Martínez and co-workers (Gavira et al., 2008; Nieves-Marrero et al., 2010; Ruiz-Martínez et al., 2009). The most relevant crystallization process used in this research is the CCD developed by Juan Manuel García-Ruiz (García-Ruiz, 2003). Crystallization conditions for Oxy-HbIII and Cyano-HbIII were obtained with the HDVD technique using the HR2-110 Crystal Screen from Hampton ResearchTM kit. A second approach to determine the crystallization condition for the Oxy and Cyano complex of HbIII was the 24 Precipitant for Screening by Capillary Counterdiffusion kit, (24-PRECIP-KIT) from Triana Science & Technology.

CCD technique using capillary counterdiffusion kits, (KIT-AS-49 (ammonium sulfate) and KIT-SF-49 (sodium formate)) from Triana Science & Technology was used to determine the crystallization condition for Oxy-HbII-III complex at different pH.

4.2.1. Crystallization conditions for Oxy-HbIII and Cyano-HbIII

Based on the results obtained by Nieves-Marrero and co-workers (Nieves Marrero et al., 2010) and Ruiz-Martínez and co-workers (Ruiz-Martínez et al., 2009), the procedure described in the methodology section was applied to obtain the crystals for HbIII (Oxy and Cyano). The first step to obtain crystallization condition for these proteins was to use the 24-PRECIP-KIT with a concentration of 30.0 mg/mL and the HR2-110 for HDVD with the same conditions. Only CCD technique with the 24-PRECIP-KIT presented one crystallization condition for Cyano-HbIII and none for Oxy-HbIII. The HDVD technique did not present crystallization conditions for both proteins. The crystallization condition found for Cyano-HbIII was condition #21, 6.0 M of sodium formate.

To improve the crystallization condition obtained by 24-PRECIP-KIT and to generate a good optical quality single crystal for both hemoglobins, we use the KIT-AS-49 and KIT-SF-49 with a pH range from 4 to 9 with the concentration of 30.0 mg/mL for each protein (Kemlin et al. 1991; Doyle et al., 1994; Gavira et al., 2006). Some Oxy-HbIII crystals were obtained with 2.8 M ammonium sulfate precipitant agent of pH 4. Cyano-HbIII crystals were obtained with 5.0 M sodium formate precipitant agent at different pH, 5 to 9. Figure 4.7 shows the prismatic ruby red crystal formed by Cyano-HbIII, whereas Oxy-HbIII has a ruby-red color without a regular prismatic shape. Table 4.2 summarizes the crystallization conditions for Oxy-HbIII and Cyano-HbIII.

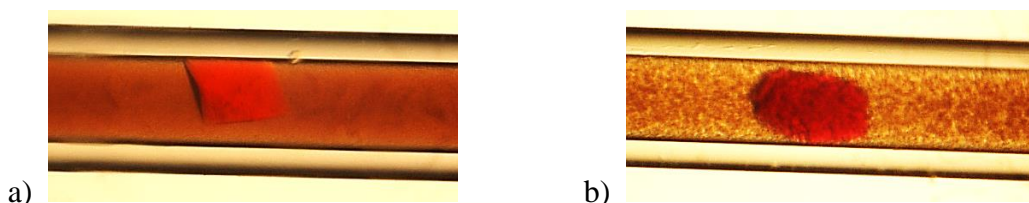


Figure 4.7. a) Crystal for Cyano-HbIII at pH 5 with precipitant agent of sodium formate and b) Oxy-HbIII at pH 4 with precipitant agent of ammonium sulfate.

Table 4.2. Crystallization conditions for Oxy-HbIII and Cyano-HbIII.

protein	ammonium sulfate	sodium formate
Oxy-HbIII	pH 4 - sodium acetate 0.1 M/ ammonium sulfate 2.8 M	N/A
Cyano-HbIII	N/A	pH5 sodium acetate 0.1 M/ sodium formate 5.0M
	N/A	pH6 Bis Tris-HCl 0.1 M/ sodium formate 5.0 M
	N/A	pH7 Tris-HCl 0.1 M/ sodium formate 5.0 M
	N/A	pH8 Tris-HCl 0.1 M/ sodium formate 5.0 M
	N/A	pH9 Tris-HCl 0.1 M/ sodium formate 5.0 M

The poor crystallization conditions for Oxy-HbIII and Cyano-HbIII suggest that HbIII is not stable without the HbII component. The fact that the HbIII protein changes color from red to brown after several days, may indicate that the protein has a tendency to autoxidation and change

from oxy state to aquo-met state. The UV-Vis spectrum for HbIII shows a Soret and Q bands of 408 nm, 541 nm and 576 nm, respectively, after few days, which indicate the mixture of Oxy and aquo-met state (data not shown).

4.2.2. Crystallization conditions for Oxy-HbII-III complex at different pH

The complex Oxy-HbII-III was obtained from the crude extract of *L. pectinata* with SEC chromatography described previously. Protein concentration conditions of 30.0 mg/mL was based on the work reported by Ruiz-Martínez and co-workers (Ruiz-Martínez et al., 2009). To confirm the Oxy state from HbII-III complex, they used a UV-Vis spectrophotometry. The UV-Vis band reported by Kraus and Wittenberg for Oxy-HbII-III complex was 414 nm Soret and two Q bands at 540 and 575 nm (Kraus and Wittenberg, 1990). Figure 4.8 shows the experimental spectrum for Oxy-HbII-III complex. The extinction coefficient of the three bands was used to calculate the concentration for crystallization procedure.

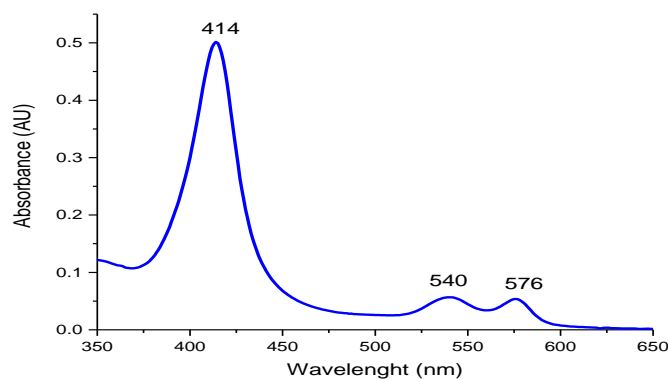


Figure 4.8. UV-Vis spectrum for the Oxy-HbII-III complex.

The CCD technique was used to grow crystals at different pH for the Oxy complex of HbII-III. The kits used for the crystallization procedure were KIT-AS-49 and KIT-SF-49 at pH 4 to 9. Both kits produced a good ruby red crystal at all pH. Figure 4.9 shows an example of some

crystal for Oxy-HbII-III complex at pH8 with sodium formate and ammonium sulfate. Table 4.3 summarizes the crystallization condition of Oxy-HbII-III complex.



Figure 4.9. Crystals for Oxy-HbII-III complex at pH 8 with different precipitant agents. a) sodium formate and b) ammonium sulfate.

Table 4.3. Crystallization conditions for Oxy-HbII-III complex.

pH	ammonium sulfate	sodium formate
4	sodium acetate 0.1 M/ ammonium sulfate 2.8 M	sodium acetate 0.1 M/ sodium formate 5.0 M
5	sodium acetate 0.1 M/ ammonium sulfate 2.8 M	sodium acetate 0.1 M/ sodium formate 5.0 M
6	Bis Tris-HCl 0.1 M / ammonium sulfate 2.8 M	Bis Tris-HCl 0.1 M/ sodium formate 5.0 M
7	Tris-HCl 0.1 M / ammonium sulfate 2.8 M	Tris-HCl 0.1 M/ sodium formate 5.0 M
8	Tris-HCl 0.1 M / ammonium sulfate 2.8 M	Tris-HCl 0.1 M/ sodium formate 5.0 M
9	Tris-HCl 0.1 M / ammonium sulfate 2.8 M	Tris-HCl 0.1 M/ sodium formate 5.0 M

The crystallization condition for these hemoglobins obtained by capillary counterdiffusion established a good technique to acquire crystal for macromolecules. There are more crystallization conditions for Oxy-HbII-III complex than Oxy-HbIII and Cyano-HbIII. These results imply that the stability of HbII-III complex is greater than the stability of HbIII, in addition to the affinity that may exist between the components of HbII and HbIII (Ruiz-Martínez, 2011). The size and shape of the crystals are different between Oxy-HbII-III complex and Oxy-HbIII. These differences indicate that HbIII prefers to form a complex with HbII rather than to stand alone. The number of crystallization hits obtained by HbIII vs HbII-III complex with oxygen ligand differ. Oxy-HbII-III complex had 12 hits while Oxy-HbIII had only one, using CCD technique (see Tables 4.2 and 4.3 for more details). Comparison of these data with

the one reported by Ruiz-Martínez (Ruiz-Martínez, 2011), in which Oxy-HbII-III complex had 12 crystallization hits with the HDVD technique using the HR2-101 Kit from Hampton Research and for Oxy-HbIII had zero hits. In addition, comparison of data reported by Ruiz-Martínez, 2011 using the CCD technique with the 24-PRECIP-KIT from Triana Science & Technology for Oxy-HbII-III complex and Oxy-HbIII, they report 16 crystallization hits for the Oxy-HbII-III complex and one hit for the Oxy-HbIII. This comparison supports our interpretation, indicating that HbIII protein prefers to form a complex with HbII rather than stand alone.

The crystal used for diffraction to obtain the crystallographic structure for Oxy-HbII-III complex at pH range from 4 to 8 are: precipitant agent; sodium formate, pH 4, 6 and 8 and precipitant agent: ammonium sulfate, pH 7. For Oxy-HbIII, the crystal growing in precipitant agent of ammonium sulfate at pH 4 and for Cyano-HbIII the crystal used from the precipitant agent of sodium formate at pH 5 to 8, were used for crystallographic experiment. The results obtained from the diffracted crystals grown in the precipitant agent described above, presented the best resolution. The different pH was the only variable affecting the crystal growth during the crystallization process.

The use of sodium formate and ammonium sulfate to grow crystals for the present work create an appropriate state of super-saturation for our proteins (McPherson, 2004). These organic salts modify the solubility of the media creating a salting in and salting out process and water molecules hydrate the salt ions and the water available to solubilize the protein was reduced (Nieves-Marrero, 2011). During the nucleation process, it is necessary to have intermolecular interactions between the proteins, allowing crystal formation, growth, and therefore good quality crystals arise (Nieves-Marrero, 2011).

The pH affects the crystallographic structure. For example, at pH 4 it is possible that the carbonyl group for some amino acids, like aspartic acid, was protonated; losing the negative charge to neutral charge (Nieves-Marrero, 2011). This variation possibly influences the interaction between the chains of the proteins and others, by altering the formation of the protein crystal because it could interfere with the formation of the electrostatic interactions (Nieves-Marrero, 2011). When these interactions decrease, they could interfere in the stability of the crystal contact (McPherson, 1995).

The crystals obtained at different pH for Oxy-HbII-III complex provided a good range of diffraction resolution between 1.86Å to 2.65Å. The crystal was grown in capillaries of 0.2 mm. The pH could optimize the size, the quality of the crystal and the resolution, maybe altering the habit or the unit cell (McPherson, 1995 and 1999). For our crystals from Oxy-HbII-III complex, the crystals maintained the same space group, but altered the unit cell parameters slightly.

The CCD crystallization technique employed in this work was performed to complete a pH screening for the protein of Oxy-HbII-III complex. This technique allows the process of nucleation and crystal growth simultaneously in the same capillary (Ng et al., 2003). The juxtaposition of the proteins with the precipitant agent allows a faster interaction between both components, resulting in a formation of an amorphous precipitate at the beginning of the capillary. Microcrystals formation occurs according to the nucleation process along the capillary (Otalora et al., 2009). Larger and good quality crystals were obtained as the precipitant solution goes through the capillary. Protein concentration decreased after the amorphous precipitate appeared, the precipitant agent continued the diffusion process, inducing a progressive supersaturation gradient which constantly allows the nucleation and the crystal formation (Nieves-Marrero, 2011). The process stopped when the protein was consumed and crystals with different

shape and size were obtained around the capillary (García-Ruiz, 2003). Figures 4.7 and 4.9 show protein crystals of Cyano-HbIII, Oxy-HbIII and Oxy-HbII-III complex, respectively with different precipitant agent.

4.3. Crystallographic results for the Oxy complex of HbII-III at pH 4 to 8

The acquisition of the crystallographic data was obtained using an X-ray synchrotron radiation. This X-ray data allows us to obtain the crystallographic structure with better resolution of Oxy and Cyano HbIII complexes and Oxy-HbII-III complex at different pH. The crystallographic structure models were solved with different programs designed for analyzing X-ray data sets. The crystallographic data obtained for the crystal for Oxy-HbIII and Cyano-HbIII complexes were poor. The resolution obtained for this crystal was about 8 Å which does not allow us to get a crystallographic structure for these hemoglobins (data not shown). The lack of a crystallographic structure may indicate that HbIII protein prefers to form a complex with HbII as a heterodimer instead of being alone as a homodimer.

X-ray diffraction data was obtained for Oxy-HbII-III complex at different pH (from 4 to 8). The statistics and refinements results for each crystal are summarized in Table 4.4. The crystals of Oxy-HbII-III complex at different pH from 4 to 8 show a $P4_22_12$ space group. All parameters were supported in the literature with the reported findings for HbII and HbII-III. (Gavira et al., 2008; Nieves-Marrero, 2011; Ruiz-Martínez, 2011). The structure of this work presents two monomers in the asymmetric unit for Oxy-HbII-III complex. The data collection for this hemoglobin at different pH was collected at the beam-line BM-16 and BM-14U of the European Synchrotron Radiation Facilities (ESRF). Table 4.4 shows the complete data collection for the hemoglobin Oxy-HbII-III complex. The resolution obtained for these crystals range from 1.85 to 2.65 Å. The unit cell edges have an average from $a = b = 74.46$ Å and $c =$

152.41 Å and the angle of the cell is 90° for all structures. These kinds of parameters are characteristic of tetragonal systems. Figure 4.10 shows diffraction frames for Oxy-HbII-III complex at pH 6 and 7. The data completeness for the structure is over 98.9% and for pH 4 is almost a 100% (99.9). Others results are included in Table 4.4.

Table 4.4. Summary of X-ray data collection, statistics and refinements results for Oxy-HbII-III complex crystals precipitated with sodium formate and ammonium sulfate at different pH values. Statistical values for the highest resolution shell for crystal growth are given in parentheses in the Resolution range row. Values in parenthesis belong to the highest resolution shell.

Data Collection	pH 4.0	pH 5.0*	pH 6.0	pH7.0	pH 8.0
Wavelength (Å)	0.907	0.886	0.954	0.954	0.9075
Temperature (K)	100	100	100	100	100
Distance (mm)	269.08	199.64	213.21	187.45	171.4
Oscillation angle (°)	0.50	0.50	0.50	0.50	0.50
Space group	P 4 ₂ 2 ₁ 2				
a = b, c (Å)	73.90, 151.87	74.07, 152.06	75.41, 153.29	74.91, 151.91	74.36, 152.27
α, β, γ (°)	90	90	90	90	90
Mol/Asym. Unit	2	2	2	2	2
Resolution range (Å)	19.90-2.65 (2.91-2.65)	19.94-2.15 (2.24-2.15)	53.32-2.24 (2.34-2.24)	43.45-1.86 (1.95-1.86)	19.91-1.85 (1.92-1.85)
Observed reflections	12909 (1263)	253,034	197,014	246,986	37,050 (3622)
Matthews coef. (Å ³ Da ⁻¹)	2.89	3.02	3.21	3.14	2.93
Data completeness (%)	99.9 (100)	99.4 (100)	98.9 (100)	99.1 (100)	99.2 (100)
Refinement					
Rfactor (%)	18.22 (21.64)	18.9 (21.4)	19.78 (28.38)	21.27 (27.75)	20.05 (27.27)
Rfree (%)	23.84 (30.37)	24.5 (27.4)	25.50 (35.36)	25.26 (35.75)	23.66 (31.50)
Reflection in working set	12244 (1188)	23,658 (2468)	21774	33862	35159 (2629)
Reflection in test set	2987 (148)	1214 (130)	1118	2000	1853 (139)
Water molecules	74	160	123	242	272
Average B factor (Å ²)	51.37	40.14	39.14	32.83	29.69
Ramachandran Plot					
Preferred Regions (%)	95.74	97.79	96.42	95.21	97.05
Allowed Regions (%)	3.61	2.21	3.26	4.15	2.3
Outliers (%)	0.66	0	0.33	0.64	0.66

†Rmerge = $\sum hkl \sum i |I_i(hkl) - \langle I(hkl) \rangle| / \sum hkl \sum i I_i(hkl)$, where $I_i(hkl)$ is the i^{th} measurement of reflection hkl , and $\langle I(hkl) \rangle$ is the weighted mean of all measurements. *Reported by Ruiz-Martínez, 2011.

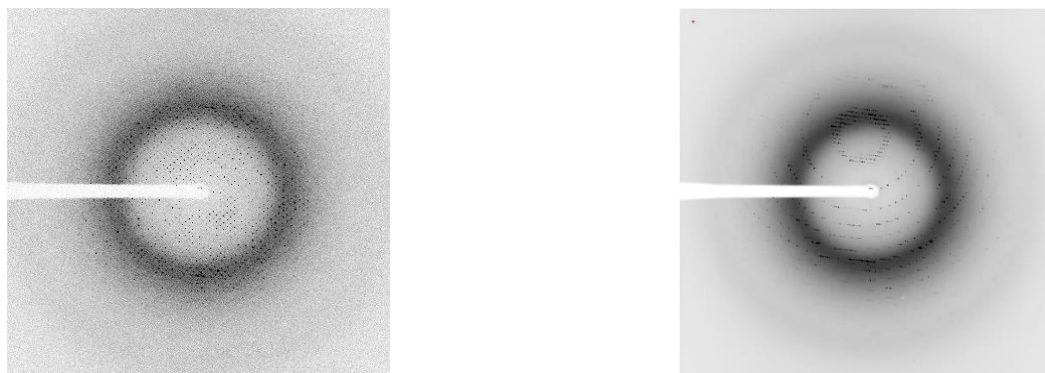


Figure 4.10. X-ray diffraction frames for the Oxy-HbII-III complex, (a) at pH 6 with a resolution of 2.24 Å obtained at 100 K; and (b) at pH 7 with a resolution of 1.86 Å obtained at 100 K.

4.3.1. *Structural model finding for primary structure for Oxy-HbII-III complex*

The structural composition for the hemoglobins at different pH confirm the composition of the heterodimer reported by Ruiz-Martínez (Ruiz-Martínez, 2011). The heterodimer is composed by two proteins component, HbII and HbIII. The sequence analysis for the component on chain A has 151 residues and for chain B it has 152 residues corresponding for HbII and HbIII, respectively. The amino acids sequence for HbII reported by Hockenhull-Jhonson and co-workers (Hockenhull-Jhonson et al., 1991) using Edman degradation, in comparison with the sequence reported by Torres-Mercado and co-workers (Torres-Mercado et al., 2003), using full-length cDNA, shows that Torres-Mercado differentiates in one amino acid at position 84, for an Asp vs Met. Gavira and co-workers report the amino acids sequence using a crystallographic structure and found the same sequence reported by Torres-Mercado and co-workers (Gavira et al., 2007).

Hockenhull-Johnson and co-workers (Hockenhull-Johnson et al., 1993) report the HbIII amino acids sequence using Edman degradation. The weight for HbIII from c-DNA is 18,068 Da (with the heme group) and the estimated molecular weight, without heme group after subtracting N-terminal methionine is 17,410 Da. This molecular weight concurs with the Edman degradation reported by Kraus and Wittenberg (Kraus and Wittenberg, 1990; Rivera et al., 2008). The HbIII molecular weight reported by Sanoguet, obtained through MALDI-MS, was 17,494.3 Da (Sanoguet, 1999). A comparison between them shows that the differences of molecular weight was attributed by the first two N-terminal serine residues, which are acetylated (Rivera et al, 2008). Rivera and co-workers reported the amino acids sequence derived from a full-length cDNA and deposited the amino acids sequence in the Gene Data Bank, ID: A7UAU9 (Rivera et al., 2008). Ruiz-Martínez reported the amino acids sequence derived from

crystallographic structure for Oxy-HbII-III complex at pH 5, PDB number: 3PT7. An HbIII amino acid sequence analysis (reported in NCBI protein data base, P41262.2 and ABS87592.1) demonstrates an amino acid differences summarized in the Table 4.5. The sequence comparison between P41242.2, ABS87592.1 and 3PT7 was acquired using the BLAST software (Morgulis, et al., 2008).

Table 4.5. Amino acid sequence of HbIII, according to Hockenull-Johnson (P41262.2), Rivera (ABS87592.1) and Ruiz-Martínez (3PT7).

Amino Acids						
						72
<i>Hockenull</i>						Asp
<i>Rivera</i>						Asn
	21	50	51	59	67	72
<i>Hockenull</i>	Asp	Glu	Asp	Asp	Ala	Asp
<i>Ruiz</i>	Asn	Gln	Asn	Asn	Ser	Asn
	21	50	51	59	67	
<i>Rivera</i>	Asp	Glu	Asp	Asp	Ala	
<i>Ruiz</i>	Asn	Gln	Asn	Asn	Ser	

The crystal structures analyzed in this work for Oxy-HbII-III complex at different pH, 4 to 8, confirm the composition reported by Ruiz-Martínez for HbIII. But the BLAST alignment analysis only evidence five differences in amino acids sequences between the Rivera and Ruiz-Martínez findings for HbIII. These five differences can be attribute technique profile and execution. Although, every technique has a limitations and possibilities of incorrect identifications could not be ruled out 100%. The amino acid sequence reported by Rivera and co-workers (Rivera et al., 2008) for the component HbIII using the full length mRNA coding for HbIII extracted from the clam ctenidia tissue is a standardized methodology with a low probability of false positives (Ruiz-Martínez, 2011). In the other hand, the amino acid sequence reported by Ruiz-Martínez is based on the contour map analysis can involve in the discrepancies is different in terms on the side chain compositions and their Van der Walls volumes (Ruiz-Martínez, 2011). The probability of incorrect identification using the solving, refinements, and validations strategies is possible, since it is dependent of the resolution of the technique when

data was obtained in the acquisition process. During the paramagnetic methodology like X-ray, it is necessary to have quantitative indicators to describe the internal consistency of data processing. Moreover, this shows systematic random errors in the data used for construction structural models (Evans et al., 2011).

4.3.2. *Secondary and tertiary structure for Oxy-HbII-III complex*

The heterodimeric HbII-III complex structures at pH 4, 6, 7 and 8 have been deposited in the RCSB Protein Data Bank. To confirm the quality models and structures for HbII-III complex, the following programs were used; SFCHECK, PROCHECK. PHENIX and Molprobit (Murshudov et al., 1997; Vaguine et al., 1998; Vagin et al., 2004; Adams et al., 2010). Ramachandran plots were used as a validation parameters for the amino acids conformers (Ramakishnan et al., 1965). These plots showed the favorable conformation based on the values calculated dihedral angle. The general conformation of a polypeptide depends on the arrangement of secondary structure motifs relative to each other. The angle for the bond between the nitrogen atom on the peptide and the alpha (α) carbon atom is Phi (Φ) and the angle of the bond between the α -carbon atom and the carbon for the carbonyl is Psi (Ψ). These measurements of Phi and Psi angles were made in degrees from 0° to 180° and from 0° to -180° , respectively. Ramachandran plots show the secondary conformation of the structure such as: alpha (α) helix, beta (β) strand or turns. The conformers adopted for the amino acids in the proteins were classified in three general regions: the right-handed α -helix, the β -strand and the left-handed alpha (α) helix.

Our Ramachandran plot presents an output results with no outliers for all pH structures and with all residues in preferred regions. These Ramachandran plots for the hemoglobins of Oxy-HbII-III complexes at pH 4, 6, 7, and 8 are shown in Figure 4.11. We used the MolProbit

4.0 web server program to obtain the Ramachandran plot (Lowell et al., 2003). At all pH, the majority of the residues are located inside the right-handed alpha helix region. At pH 4, 95.7 % of all residues were in favored regions, when the Phi (Φ) values are between -40 to -90 and the Psi (Ψ) values between 0 to -60. For pH 6, the behaviors are similar to pH 4, the 96.4 % of all residues are in favored regions and the Phi (Φ) values and the Psi (Ψ) are the same at pH 4. At pH 7, the 95.2 % of all residues were in favored regions, when the Phi (Φ) values are between -50 to -90 and the Psi (Ψ) values between -10 to -60. At pH 8, the 97.1 % of all residues were in favored regions and the Phi (Φ) values are between -50 to -90 and the Psi (Ψ) values between 0 to -60. Some residues were located in the strand region and few were located in the left-hand alpha helix. These crystallographic structures do not present β -strand for any structure of Oxy-HbII-III complexes at different pH. All of the Oxy-HbII-III complexes structures fold into a classical helical globin with two monomers per asymmetric unit (Gavira et al., 2008; Nieves-Marrero, 2011). The heterodimeric structures for these hemoglobins of Oxy-HbII-III complex apparently exhibit the highest stability among other possibilities, like tetramer assembly or others obtained with PISA web server (Krissinell et al., 2005).

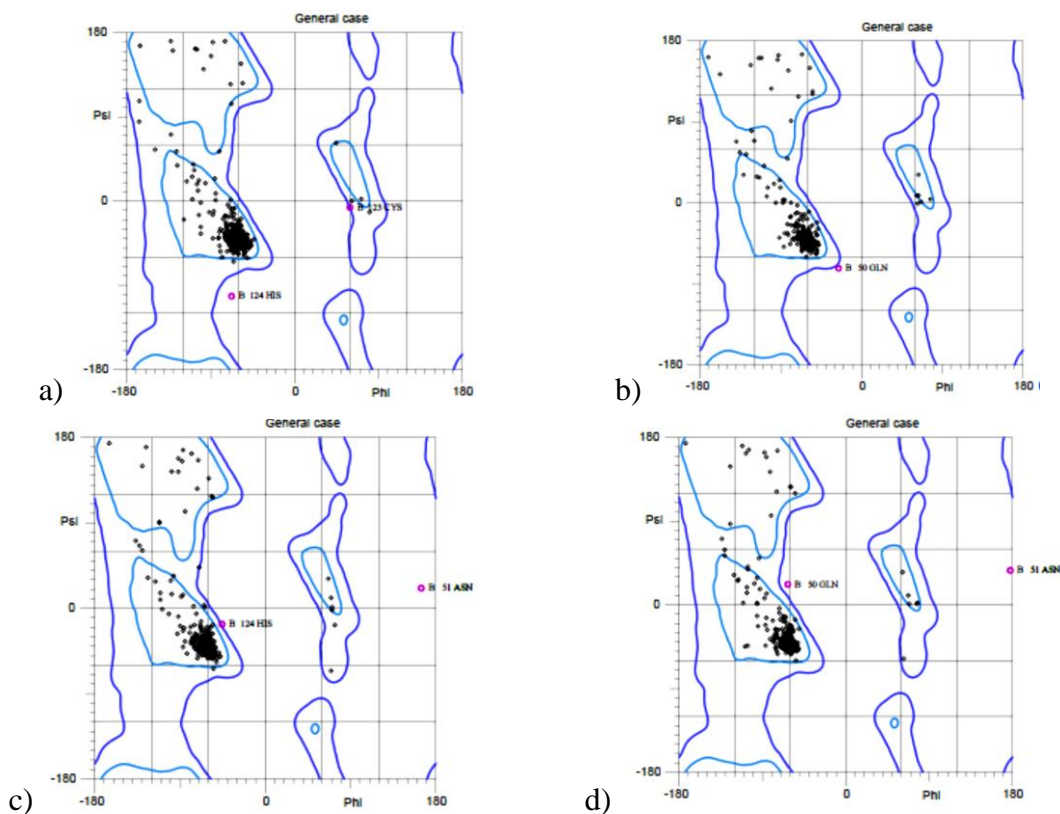


Figure 4.11. Ramachandran plots for the Oxy-HbII-III complex at pH a) 4, b) 6, c) 7 and d) 8. Each plot was produced by the MolProbity 4.0 web server program.

Ramachandran plots confirms the structure present in the heterodimer of Oxy-HbII-III complex with the torsion of the angle Ψ and Φ in the protein back bond (Figure 4.11). Analysis of the helix length and amino acids distribution shows variations (Table 4.6). These variations in the secondary structure, although small, can be a consequence of the effect of pH.

The hemoglobin Oxy-HbII-III complex was submitted to other secondary structure analysis to find out the effect of the pH in the overall structure regarding the distribution of its secondary structure. To determine this, the STRIDE web server was used (Heinig and Frishman 2004). The distribution for the secondary structure for each monomer by chain A (HbII) and chain B (HbIII) at pH 4, 5, 6, 7, and 8 are summarized in Table 4.6.

It was found that two types of secondary structures are present, an alpha helix and a 3_{10} helix, where the alpha helix is a secondary structure predominant. This kind of helix presents a classical three over three (“3-over-3”) helical assembling behaviors in all structures (Phillips, 1980; Rizzi et al., 1994). The composition of these helical assembling is shown in Table 4.6. The observed distribution remains identical for chain A at all pH except pH 4, but in chain B the variations in the distribution are at pH 6 to 8. The 3-over-3 assembling of alpha helix is different when chain A and chain B are compared at all pH (Nieves-Marrero, 2011).

Table 4.6 evidences the variations in the distribution of the helix when the pH increases. At pH 4, the total number of helix observed are 8 in chain A; but at pH 8, we observed 9. However, in chain B at pH 4 the number of helix observed are 8, but at pH 8, they decrease to 7. Analysis of the secondary structure at pH 5 and 6 shows that the number of helix remain in 9 for chain A, but change in chain B from 8 to 7. Overall, when pH increases, the number of helix increases in chain A, but in chain B it decreases. Table 4.7 summarizes these results.

Comparison of the 3_{10} helix between chain A and B reveals some variations. Chain A has two 3_{10} helices at all pH, but in chain B at pH 4 and 5 there are two, at pH 6 to 8, the number of 3_{10} helix decreases to one (Table 4.6).

Table 4.6. Secondary structure distribution for *Lucina pectinata* Oxy-HbII-III complex using the STRIDE web server (Heinig and Frishman, 2004).

	Chain A (HbII)				Chain B (HbIII)			
	Helix	Range	Type	N ^o of residues	Helix	Range	Type	N ^o of residues
pH4	A	5-36	alpha	32	A	6-21	alpha	16
	B	38-40	3 ₁₀	3	B	23-37	alpha	15
	C	44-49	alpha	6	C	39-45	3 ₁₀	7
	D	53-55	3 ₁₀	3	D	54-56	3 ₁₀	3
	E	60-78	alpha	19	E	61-80	alpha	20
	F	83-99	alpha	17	F	84-100	alpha	17
	G	104-121	alpha	18	G	105-122	alpha	18
	H	128-149	alpha	22	H	127-151	alpha	25
	I	N/A	N/A	N/A	I	N/A	N/A	N/A
# of helix		8	6*/2*			8	6*/2*	
pH5[□]	A	5-20	alpha	16	A	6-21	alpha	16
	B	22-36	alpha	15	B	23-37	alpha	15
	C	38-44	3 ₁₀	7	C	39-45	3 ₁₀	7
	D	45-49	alpha	5	D	54-56	3 ₁₀	3
	E	53-55	3 ₁₀	3	E	61-79	alpha	19
	F	60-78	alpha	19	F	84-100	alpha	17
	G	83-99	alpha	17	G	105-122	alpha	18
	H	104-121	alpha	18	H	127-151	alpha	25
	I	128-149	alpha	22	I	N/A	N/A	N/A
# of helix		9	7*/2*			8	6*/2*	
pH6	A	5-20	alpha	16	A	6-21	alpha	16
	B	22-36	alpha	15	B	23-37	alpha	15
	C	38-44	3 ₁₀	7	C	39-45	3 ₁₀	7
	D	45-49	alpha	5	D	61-79	alpha	19
	E	53-55	3 ₁₀	3	E	84-100	alpha	17
	F	60-78	alpha	19	F	105-122	alpha	18
	G	83-99	alpha	17	G	128-150	alpha	23
	H	104-121	alpha	18	H	N/A	N/A	N/A
	I	128-149	alpha	22	I	N/A	N/A	N/A
# of helix		9	7*/2*			7	6*/1*	
pH7	A	5-20	alpha	16	A	6-21	alpha	16
	B	22-36	alpha	15	B	23-37	alpha	15
	C	38-44	3 ₁₀	7	C	39-45	3 ₁₀	7
	D	45-49	alpha	5	D	61-79	alpha	19
	E	53-55	3 ₁₀	3	E	84-100	alpha	17
	F	60-78	alpha	19	F	105-122	alpha	18
	G	83-99	alpha	17	G	128-151	alpha	24
	H	104-121	alpha	18	H	N/A	N/A	N/A
	I	128-149	alpha	22	I	N/A	N/A	N/A
# of helix		9	7*/2*			7	6*/1*	
pH8	A	5-20	alpha	16	A	6-21	alpha	16
	B	22-36	alpha	15	B	23-37	alpha	15
	C	38-44	3 ₁₀	7	C	39-45	3 ₁₀	7
	D	45-49	alpha	5	D	61-79	alpha	19
	E	53-55	3 ₁₀	3	E	84-100	alpha	17
	F	60-78	alpha	19	F	105-122	alpha	18
	G	83-99	alpha	17	G	127-150	alpha	24
	H	104-121	alpha	18	H	N/A	N/A	N/A
	I	128-149	alpha	22	I	N/A	N/A	N/A
# of helix		9	7*/2*			7	6*/1*	

* = alpha helix, ♦ = 3₁₀ helix, □ = reported by Ruiz-Martínez 2011.

Table 4.7. Summary of total number of helices for the Oxy-HbII-III complex.

pH	HbII-III complex	
	Chain A	Chain B
4	8	8
5	9	8
6	9	7
7	9	7
8	9	7

Analysis of the turns and coils present in the secondary structures for Oxy-HbII-III complex at different pH reveals the presence of different types of turns. For all pH, type I, II and IV are present; but at pH 4 and 7 a gamma classic turn was found and at pH 7 a turn VIII was observed. All of these types of turns are summarized in Table 4.8.

Table 4.8. Different types of turns for the Oxy-HbII-III complex.

pH	HbII-III
4	I, II, IV, gamma classic
5	I, II, IV
6	I, II, IV
7	I, II, IV, VIII, gamma classic
8	I, II, IV

The number of residues for chain A change from 32 at pH 4 for the alpha helix A, to 16 for the other structures from pH 5 to 8. In chain B, the numbers of residues are the same at all pH. The distributions for the number of residues are presented in Table 4.6.

Table 4.9 summarizes the distribution of coils and turns for Oxy-HbII-III complex. In chain A, the coils and turns remain identical, 7 and 3, respectively. In contrast, chain B, there are some differences because the number of coils and turns decrease when the pH increases.

Figure 4.12 presents the globin-like crystallographic structures for each pH without the heme group. All sequences contain an acetyl group at each N-terminal. The incorporation of non-proteins molecules are present into the crystallographic structure like water molecules. The total water molecules are: 76, 160, 150, 248 and 295 for pH 4 to 8, respectively, and they increase when the pH increases.

Table 4.9. Summary of the different coils and turns for the Oxy-HbII-III complex.

pH	HbII-III			
	Chain A		Chain B	
	Coil	Turn	Coil	Turn
4	6	4	7	4
5	7	3	7	3
6	7	3	6	2
7	7	3	6	3
8	7	3	6	2

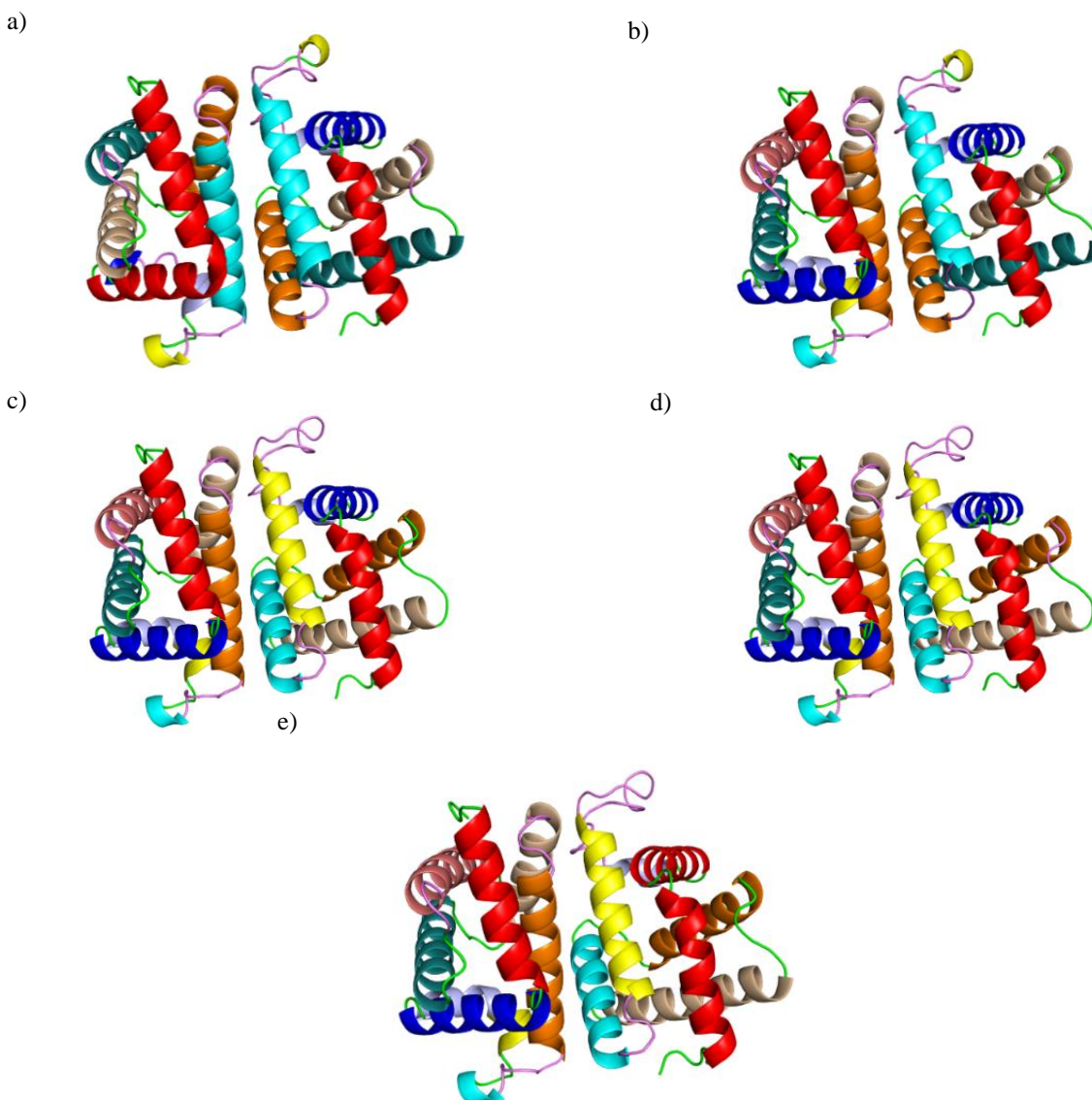


Figure 4.12. Crystallographic structure for Oxy-HbII-III complex without the heme group. Chain A (left) and chain B (right) at pH a) 4, b) 5, c) 6, d) 7 and e) 8. Each helix, A to H, are identified by colors: red, blue, light blue, yellow, cyan, orange, wheat, cyan-deep teal and deep salmon respectively. The coils are green and the turns are violet.

Using the Stride web server shown in Figure 4.13, a color code distribution of secondary structure for the Oxy complex of HbII-III at pH 4 to 8 is demonstrated. Data shows that all 3_{10} helix are among the first 38 residues for chain A and the first 39 residues for chain B. All chains A have two 3_{10} helix; and chain B has two 3_{10} helix at pH 4 and 5, but only one 3_{10} helix at pH 6 to 8. The predominant number of residues for the 3_{10} helix is 7 and 3, respectively; at pH 4 chain A has 3 residues in both 3_{10} helix. The first 3_{10} helix on chain A is found between residues 38 to 44 except at pH 4, which is located between residues 38 to 40. The second 3_{10} helix is between residues 53 to 55 at all pH. In chain B, the first 3_{10} helix is found between residues 39-45 and the second, at pH 4 and 5, is located between residues 54-56. The effect of pH can be observed more markedly in chain B; when the pH increases the number of 3_{10} helix decrease, from two to one.

Overall, the 3-over-3 globin fold for Oxy-HbII-III complex does not affect significantly when the pH changes. If we overlap the crystallographic structure of Oxy-HbII-III complex at all pH from 4 to 8, we will observe that the majority of the differences are in the segments of turns and coils at the structures (see Figure 4.14). The folding of the globin was maintained based on the electrostatic hydrogen bonding and all hydrophobic interactions into the protein (Kleywegt, 2000).

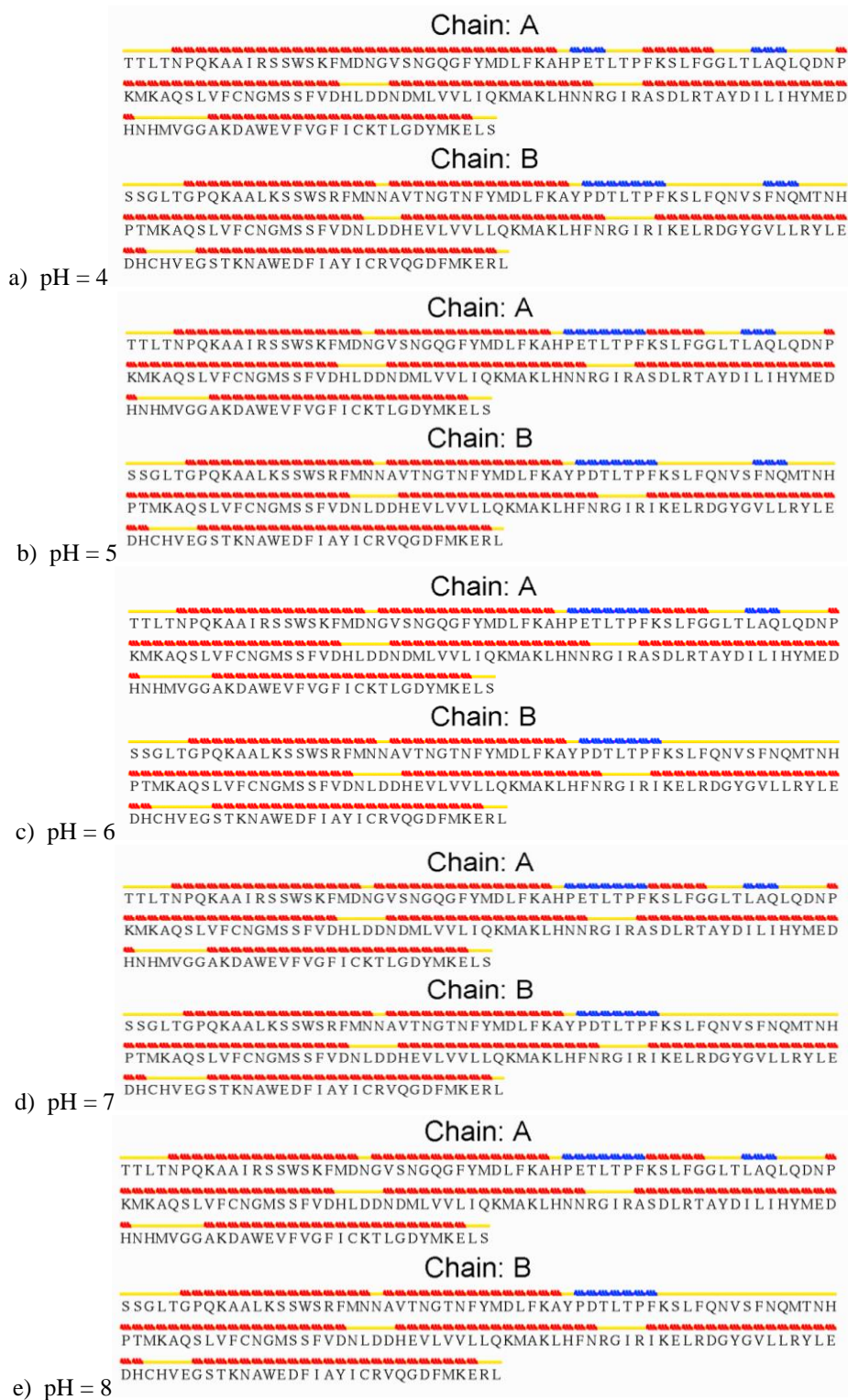


Figure 4.13. STRIDE web server output for secondary structure comparison of Oxy-HbII-III complex at pH 4 to 8. The red color indicate an alpha helix, blue, 3_{10} helix and yellow, turn or coil.



Figure 4.14. Crystallographic structures of the Oxy-HbII-III complexes overlapping using PyMOL at pH 4 (green), pH 5 (red), pH 6 (yellow), pH 7 (magenta) and pH8 (cyan).

To evaluate the pH effect in the protein folding of the Oxy complex of HbII-III, overlapping chains analysis was performed between the structures at different pH. We used the Root Mean Square Deviation (RMSD) to measure the similarity or the difference in structure of globular proteins conformations (Maiorov and Crippen, 1994). RMSD measures the average change in displacement of the selected atoms and provides insights into its structural conformation throughout simulations. The RMSD plot analysis shows the main peptide backbone C, N, O and C α (m-RMSD); an overlapping analysis of chain A and B for all structures at different pH, 4 to 8, was obtained based on the main chain back bond. An all-RMSD overlapping analysis was done for all the site chain residues. The m-RMSD and all-RMSD results are: 1.0501 Å and 1.2001 Å for pH4, 1.0087 Å and 1.2053 Å for pH 5, 0.9532 Å and 1.1577 Å for pH6, 1.0023 Å and 1.3166 Å for pH7 and 1.0478 Å and 1.2001 Å for pH 8, respectively for the heterodimer of Oxy-HbII-III complex. The overlapping of the main chain

back bond in the heterodimer for each chain (A/B) revealed a m-RMSD obtained for pH 4 vs 8 of 0.4610 Å and 0.4228 Å and for pH7 vs 8 of 0.2092 Å and 0.3754 Å. Statistical analysis demonstrates a 76.29% similarity between the Oxy complexes chains analyzed. Figure 4.15 shows the m-RMSD and all-RMSD plots for pH 4 vs pH8 with the same chain. The blue line corresponds to the HbII (chain A) at pH 4 vs pH 8 and the orange line corresponds to the HbIII (chain B) at pH 4 vs pH 8. These results were obtained with the NOC program.

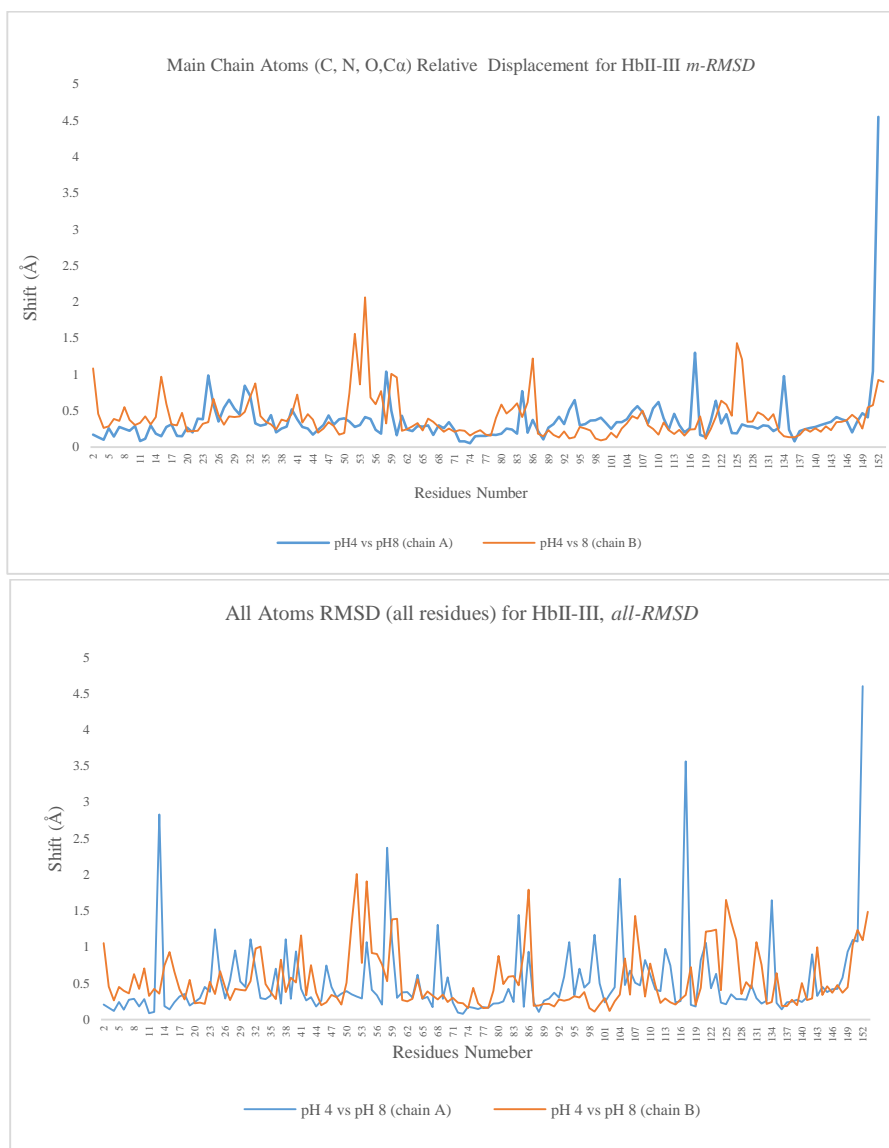


Figure 4.15. RMSD plot for the overlapping of chain A with chain B for the Oxy-HbII-III complex at pH 4 and 8.

4.3.3. Tertiary structure of Oxy-HbII-III complex at different pH

The protein-protein interactions are important to establish the residues present in the interface between chain A and B in Oxy-HbII-III complex and to determine how the pH affects this interaction. Protein-protein interaction for the heterodimer Oxy-HbII-III complex interface in each structure with pH variation was determined using the LigPlot+ program (Laskowski and Swindells, 2011). The number of residues involved in the protein-protein interaction between the dimer of HbII-III complex, the interface area, and the number of hydrogen bonds were determined (see Figure 4.15.1). Table 4.10 summarizes the number of residues present in the protein-protein interaction. The total interaction practically remains the same at pH 4 to 6, but decreases as pH increases.

Table 4.10. LigPlot+ interactions between chain A and B for the Oxy-HbII-III complex at pH 4 to 8 and Cyano-HbII-III complex at pH 5.

<i>pH</i>	<i>Water molecules</i>	<i>Hydrogen-bond interactions (H₂O-aa)</i>	<i>%</i>	<i>Hydrogen-bond Interactions (aa-aa)</i>	<i>%</i>	<i>Hydrophobic Interaction (aa-aa)</i>	<i>%</i>	<i>Total interactions</i>
4	2	4	14	2	7	22	79	28
5	2	4	14	3	10	22	76	29
6	1	2	7	4	14	23	79	29
7	2	4	17	3	12	17	71	24
8	2	4	17	3	12	19	73	26
5 (CN)	2	5	18	3	11	20	71	28

All interactions were obtained using LigPlot+ (version 1.4.5, Laskowski and Swindells, 2011).

The residues in the hydrogen bond interaction between the heterodimer are 2, 3, 4, 3 and 3 for pH 4, 5, 6, 7 and 8, respectively. At pH 6, the HbII-III complex has the most hydrogen bond interaction (four). The hydrogen bond interaction of Gln65(A)-Lys93(B) and Lys 92(A)-Gln66(B) are present at all pH (see Figure 4.15.2). Hydrogen bond interaction between Ser46(A)-Lys96(B) is lost at pH 7. Lys95(A)-Ser47(B) is present at pH 6 and 7. We suggest that the Gln and Lys residues, present at all pH having hydrogen bond and non-bonded contact residues, are the responsible for the stabilization between chains of the heterodimer in Oxy-HbII-III complex (Kraus and Wittenberg, 1990; Gavira et al., 2008). Data shown in Table 4.10

evidences that the lowest total interaction with 24 is at pH 7, and it is also the lowest percentage of hydrophobic interactions between chains. This suggests that the stability of the heterodimer at pH 7 is lower than the others; therefore, we allowing the oxygen release from the heme pocket.

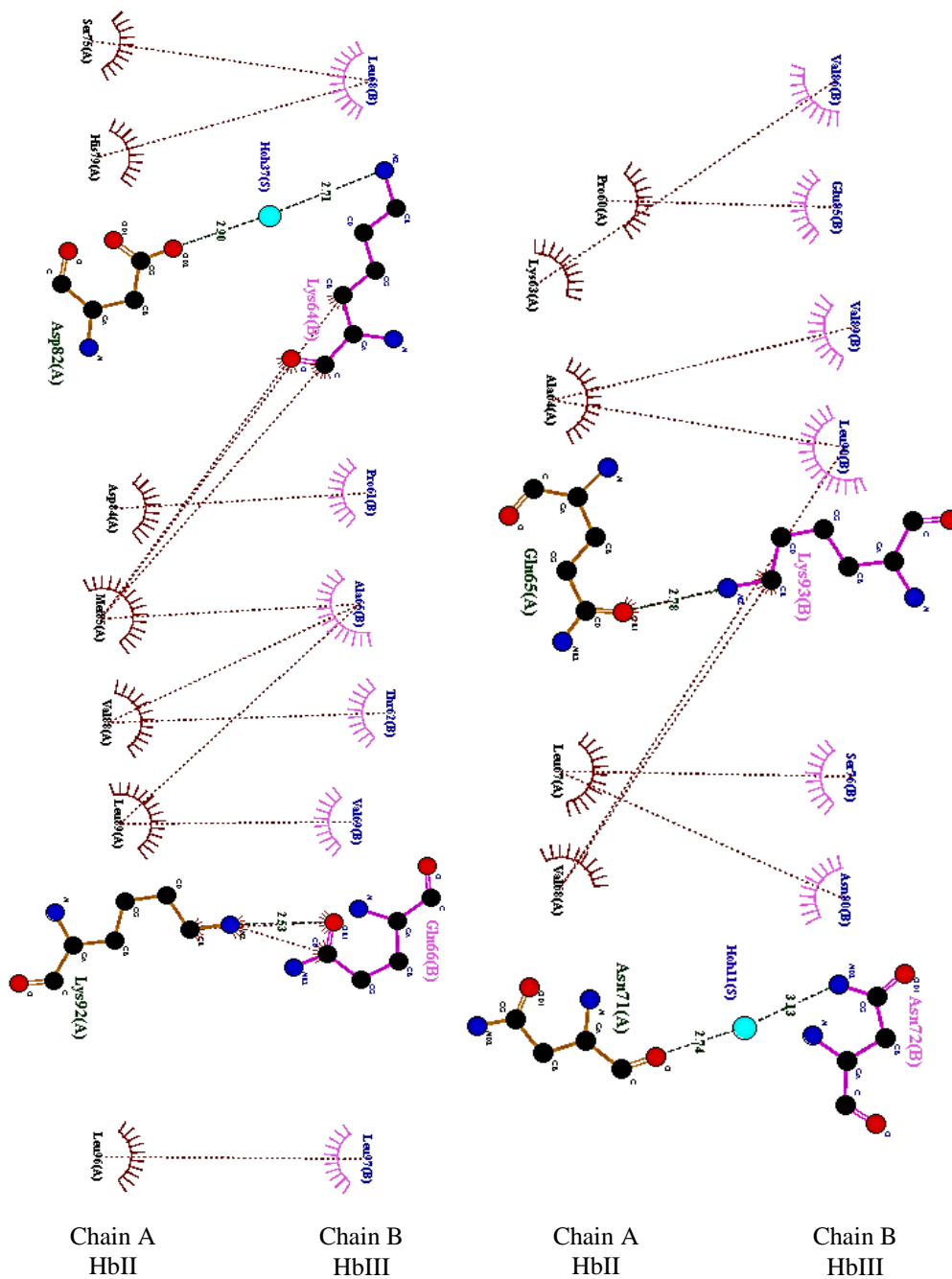


Figure 4.15.1. Residues found in the protein-protein interaction between dimers of the Oxy-HbII-III complex at pH 4 using LigPlot+ program.

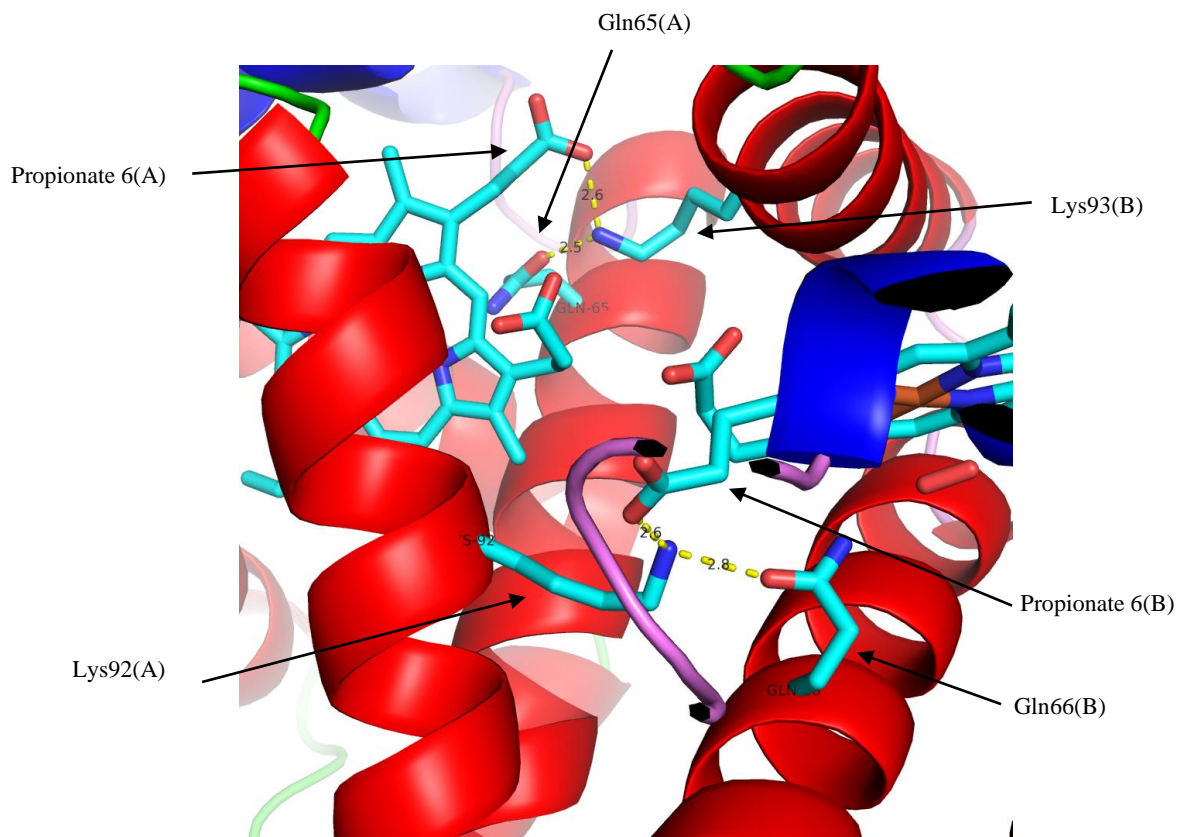


Fig 4.15.2. Gln and Lys residues interaction between chains A (HbII, left) and chain B (HbIII, right) at pH 7.

Comparison of the Oxy-HbII-III complex at all pH with the Cyano-HbII-III complex at pH 5, when the oxidation state is different, do not show significant differences in the total amino acids interactions (Table 4.10). These show more hydrogen bond interaction between amino acids and water molecules. The different oxidation state does not change the protein-protein interaction.

Table 4.11 summarizes the protein-protein interaction residues present for Oxy-HbII-III complex at all pH (4 to 8). Data show i) a 10 amino acids interaction at all pH; ii) one amino acids interaction at pH 7 to pH 8; and iii) five amino acids interaction at pH 4 to 6. The total residues involved in the protein-protein interactions analysis at different pH show: i) 32 residues (16 for both chain A and B) interact at pH 4; ii) 30 residues (15 for both chain A and B) at pH 5

and 6; iii) 25 residues (12 for chain A and 13 for chain B) at pH 7 and iv) 28 residues (14 for both chain A and B) at pH8 (data not shown). At pH 7, the interactions between chains were lower indicating that, at this pH, the stability of the heterodimer decreases, allowing the release of the oxygen ligand.

Table 4.11. Residues found in the protein-protein interaction between dimers of the Oxy-HbII-III complex. All interactions were obtained using LigPlot+ program version 1.4.5 (Laskowski and Swindells, 2011).

aa interaction in all pH (Chain A-Chain B)	aa interaction into pH7 to pH8 (Chain A-Chain B)	aa interaction into pH4 to pH6 (Chain A-Chain B)
Pro60 - Glu85	Ala64 - Leu90	Lys63 - Val86
Ala64 - Val89		Leu67 - Ser76
Gln65 - Lys93		Val68 - Leu90
Leu67 - Asn80		Leu89 - Ala65
His79 - Leu68		Leu89 - Val69
Asp84 - Pro61		
Met85 - Lys64		
Met85 - Ala65		
Val88 - Ala65		
Lys92 - Gln66		

The Cyano complex data of HbII-III at pH 5 show: 32 amino acids into the protein-protein interaction (16 amino acids for both chains), nine of those interactions are the same at all pH when compared to Oxy-HbII-III complex at all pH. The amino acids in the interactions are: Pro60(A)-Glu85(B), Ala64(A)-Val89(B), Gln65(A)-Lys93(B), Leu67(A)-Asn80(B), His79(A)-Leu68(B), Asp84(A)-Pro61(B), Met85(A)-Lys64(B), Met85(A)-Ala65(B), Lys92(A)-Gln66(B). Cyano-HbII-III complex pH behavior shows, at acidic pH, four residues interaction and at basic pH three residues interactions (data not shown). Only Tyr146(A) is not involved in the interactions when compared with the Cyano and Oxy HbII-III complexes.

Area and volume analysis for Oxy-HbII-III complex at all pH were done using the CASTp (Computer Atlas of Surface Topography of proteins) web server program with a probe radius of 1.4 Å (Dundas et al., 2006; Liang et al., 1998). The area and the volume increased between pH 5 to 6 and decreased from pH 6 to 8. The results for the calculation of area and

volume are summarized in Table 4.12. Overall, when the pH increases, the area and the volume decrease. This behavior is in agreement with the idea that the protein loses its oxygen ligand.

Table 4.12. Area and volume of the protein-protein interaction for the Oxy-HbII-III complex.

pH	Area	Volume
4	1019.7	1302.9
5	775.5	946.7
6	1161.4	1460.1
7	1070.4	1377.1
8	901.8	1115.1

4.3.4. Heme pocket analysis for Oxy-HbII-III complex at different pH

The heme group (heme pocket) is associated to the functionality of the hemoglobin and the chemistry around the porphyrin ring (Weber and Vinogradof, 2001; Kakar et al., 2010). Residues at the distal and proximal site play an important role on the interaction with the ligand. One of the interactions observed in the Oxy heterodimer complex of HbII-III is the hydrogen bond network between the proximal amino acids, TyrB10 and GlnE7 residues, with the oxygen ligand and the non-bonding network with PheE11. HbISi (hemoglobin I *Scapharca inaequalvis*) from *Scapharca inaequalvis* (Chiancone et al., 1981), *Ascaris suum* (HbAs) (Yang et al., 1995) are examples of hemoglobins with the same non-bonding network and a similar heme system.

To understand the configuration of the heme ring, it is important to know the numbering of the peripheral residues, and the stereochemistry of the vinyl and propionate group. Figure 4.16 shows the heme pocket for chain A at pH 4. The vinyl groups stereochemistry was determined using the methyl group, 1-methyl for 2-vinyl and 3-methyl for the 4-vinyl as a reference (Desbois et al., 1984; Yamamoto et al., 1989; Silfa et al., 1998). When the vinyl group

is oriented into the methyl, it has a *cis* conformation, but when it is in the opposite direction regarding the methyl group, it is in a *trans* conformation.

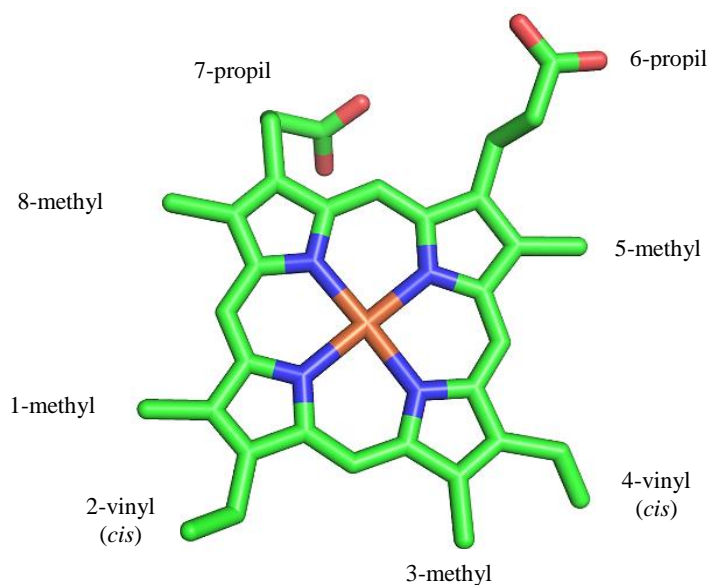


Figure 4.16. Heme A of the HbII-III complex at pH4.

The 2-vinyl group has a different stereochemistry (*cis*, *trans*) between chain A and B in the Oxy-HbII-III complex (table 4.14). Chain A shows a *trans* stereochemistry for the 2-vinyl group at pH 7, while the others pH are *cis*. In chain B, the stereochemistry is *trans* at all pH. Otherwise, the stereochemistry of the 4-vinyl group remains *trans* for both chains. We establish that the pH has an effect on the 2-vinyl group by crystallographic data analysis as shown in Table 4.13 and Figure 4.17. We propose that the conformational change of 2-vinyl group in heme A at pH 7 allows a decrease in the electron density at the heme group, increasing the Fe-O bond and allowing the oxygen ligand to be released when the pH increases. This explains the absence of oxygen at pH 8 in both heme pockets. When the first oxygen was released from the heme A, the release of the oxygen from the heme pocket in chain B is provoked.

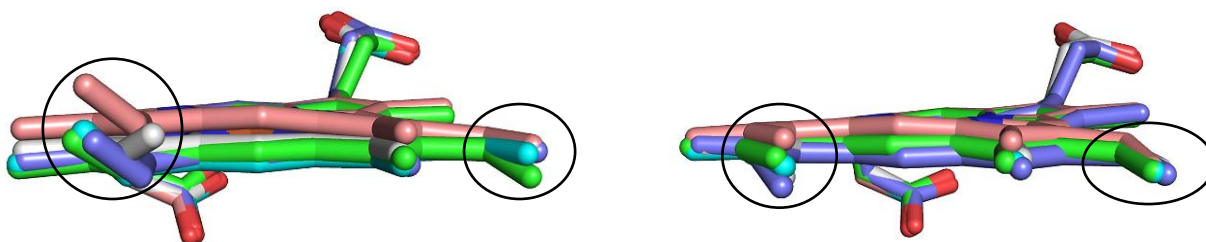


Figure 4.17. Heme A (left) and heme B (right) of the Oxy-HbII-III complex at pH 4 (green), pH 5 (cyan), pH 6 (violet), pH 7 (grey-white) and pH 8 (dark salmon) which show the stereochemistry for the 2- and 4 vinyl groups.

Table 4.13. Summary of the stereochemistry of the 2- and 4-vinyl groups for the Oxy-HbII-III complex at a pH range of 4 to 8.

pH	2-vinyl		4-vinyl	
	Chain A	Chain B	Chain A	Chain B
4	<i>cis</i> twisted out	<i>trans</i> in plane	<i>cis</i> twisted out	<i>cis</i> twisted out
5	<i>cis</i> twisted out	<i>trans</i> twisted out	<i>cis</i> in plane	<i>cis</i> twisted out
6	<i>cis</i> twisted out	<i>trans</i> twisted out	<i>cis</i> in plane	<i>cis</i> twisted out
7	<i>trans</i> twisted out	<i>trans</i> twisted out	<i>cis</i> in plane	<i>cis</i> twisted out
8	<i>cis</i> twisted out	<i>trans</i> in plane	<i>cis</i> in plane	<i>cis</i> twisted out

In the NMR study realized by Silfa and co-workers, they observed the 2-vinyl group in the heme plane for the HbI from the *L. pectinata* (Silfa et al., 1998). This study located the 2-vinyl group slightly out of plane (twisted out) with a *trans* stereochemistry; while the 4-vinyl group present a *cis* stereochemistry with an in-plane orientation. The electron withdrawing effect and the orientation of the vinyl group could affect the heme group (Silfa et al., 1998; Cao et al., 2003).

In Oxy-HbII-III complex, at pH 6, the orientation of the oxygen ligand in heme pocket for chain A and B is different when compared with pH 7. At pH 7, the oxygen ligand is parallel to the iron and the bond strength between iron and oxygen ligand decrease, allowing the oxygen ligand to be released when the pH increases. That is why the oxygen ligand is not present in the crystal structure of the heme A and B at pH8. Figure 4.18 indicates the crystallographic structure of heme A and B at pH 6, 7 and 8 (no oxygen) which shows the behavior of the ligand.



Figure 4.18. Crystallographic structure of the heme A (left) with oxygen ligand and heme B (right) for the HbII-III complex at pH 6 (magenta), 7 (yellow) and 8 (orange).

Figure 4.19 illustrates the crystallographic structure for the heme A and B for Oxy-HbII-III complex at pH 5, 6 and 7. The orientation of the oxygen ligand changes as the pH changes. The oxygen ligand at pH 7 is perpendicular to heme plane. In chain A at pH 5, the bond angle for the oxygen ligand between O₁-O₂-Fe on heme A is 119.0°, at pH 6 is 104.2° and at pH 7 is 89.5°. This data shows the movement of the oxygen ligand when the pH changes. In heme B the behavior is the same at heme A. The bond angle changes when the pH increases. Table 4.14 shows the bond angle for the oxygen ligand in both chains. We propose that an increase in pH will create a repulsive environment in the heme pocket, inducing a change in oxygen stability and allowing the oxygen release.



Figure 4.19. Heme A (left) and B (right) with the oxygen ligand at pH 5 (cyan), 6 (magenta) and 7 (yellow).

Table 4.14. Bond angles between O₁-O₂-Fe in the heme pocket of the Oxy-HbII-III complex.

pH4 (°)		pH5 (°)		pH6 (°)		pH7 (°)		pH8 (°)	
Chain A	Chain B								
113.7	111.8	119.0	128.2	104.2	144.5	89.5	76.8	N/A*	N/A*

The distance between the heme iron and the oxygen ligand are different since the distance in heme B is shorter than the distance in chain A. At pH 5, 6 and 7, an increase is observed in

both heme group and the bond strength decreases, facilitating the oxygen release. Table 4.15 summarizes this data.

The pH has an effect in the planarity of the heme group ring. At pH 5 to 7, chain A did not show differences in the planarity, but at pH 8, we observed a twist in the planarity. A comparison between the heme at pH 4 and pH 8 showed a distortion in the heme group in chain A, but in chain B it remains the same. Figure 4.20 shows the heme crystallographic structure demonstrating the twist in planarity observed for chains A and B at pH 4 and 8. We propose that the change in the planarity affects the electron density in the heme ring, causing the weakening of the bond strength between the ligand and the iron in the heme pocket.

Table 4.15. Heme contacts in the Oxy-HbII-III complex at different pH values.

Distal Site Interactions	pH4		pH5		pH6		pH7		pH8	
	Chain A (Å)	Chain B (Å)								
Fe – O2	2.2	2.1	2.1	1.8	2.5	2.0	2.2	2.3	N/A	N/A
Fe – O1	3.0	2.8	2.9	2.7	3.1	3.1	2.5	2.3	N/A	N/A
O1 – O2	1.2	1.2	1.2	1.2	1.2	1.2	1.2	1.2	N/A	N/A
Fe – OH-(TyrB10)	5.0	4.6	4.9	4.4	5.1	4.8	4.5	4.0	3.6	3.6
O1 – OH-(TyrB10)	2.5	2.7	2.6	2.5	2.0	1.8	2.4	2.2	N/A	N/A
O2 – OH-(TyrB10)	2.8	2.5	2.8	2.6	3.1	3.0	2.4	1.9	N/A	N/A
O1 – NE2-(GlnE7)	3.6	4.0	3.9	4.0	3.7	3.4	3.9	3.7	N/A	N/A
O2 – NE2-(GlnE7)	2.8	3.1	3.1	3.3	2.8	2.9	2.9	2.6	N/A	N/A
Fe – NE2-(GlnE7)	4.3	4.4	4.5	4.4	4.4	4.4	4.5	4.3	4.2	4.0
(TyrB10)-OH – NE2-(Gln E7)	3.1	2.6	2.9	3.0	3.0	3.0	3.0	2.9	3.1	3.1
(LysF3)-NZ – OE1-(Gln E7)*	2.8	2.5	2.6	2.6	2.5	2.6	2.5	2.8	2.8	2.8
(LysF3)-NZ – Propionate O1D*	2.4	2.5	2.6	2.7	2.8	2.8	2.6	2.6	2.6	2.7
(MetE15)-SD – 2-Vinyl CA ^x	5.5	5.6	5.4	5.0	5.5	5.3	5.1	5.3	5.6	5.1
(MetE15)-SD – 2-Vinyl CB ^x	4.5	6.5	7.0	6.0	7.0	7.0	6.5	6.8		
			6.0	8.2	6.0		7.0	7.6		
Proximal Site Interaction										
(MetF4)-SD – 2-Vinyl CA [♦]	5.4	5.1	5.1	5.1	5.4	5.2	5.5	5.1	5.7	5.5
(MetF4)-SD – 2-Vinyl CB [♦]	6.2	6.0	5.8	6.0	6.3	5.8	6.6	5.8	6.4	6.4
			6.7							
Fe – NE2-(HisF8)	2.4	2.3	2.2	2.2	2.4	2.4	2.3	2.4	2.4	2.4
(HisF8)-NE2 – OH-(TyrB10)	7.2	6.8	7.0	6.5	7.4	7.1	6.7	6.4	5.8	5.9
(HisF8)-NE1 – H ₂ O (W)	3.8	3.4	3.4	3.3	3.5	3.5	3.5	3.2	3.3	3.3
Propionate O2A – H ₂ O (W)	3.3	2.8	2.9	2.7	2.7	2.7	2.8	2.7	2.6	2.7
Propionate O2A – (ArgF11)-N1	3.3	2.9	3.0	2.9	3.2	3.0	3.1	2.9	3.1	2.9
Propionate O1A – (ArgF11)-N2	3.0	2.9	2.7	2.4	2.9	2.8	2.7	2.5	2.7	2.7

(*) Inter-chain contact

(†) This measurement was with a water molecule acting as a ligand at the sixth coordination site

(N/A) Does not apply

(x) Two orientation was observed of MetE15 at pH 5, 6 and 7

(♦) Two orientations of MetF4 are observed at pH 5

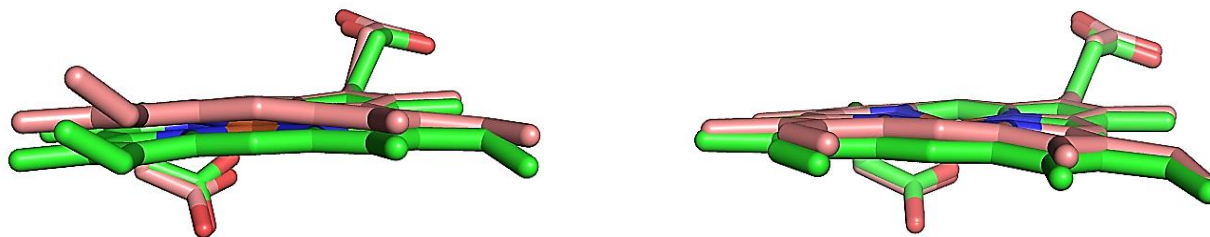


Figure 4.20. Overlapping Heme A (left) and heme B (right) of the Oxy-HbII-III complex at pH 4 (green) and pH8 (dark salmon).

The distal amino acids in chains A and B show differences among them. TyrB10, GlnE7 and PheE11 are the residues in the heme pocket in chains A and B affected when the pH changes. Phenylalanine (Phe) is a hydrophobic unreactive residue in proteins but it contributes to the stabilization of the ligand (Navarro et al., 1996; Pietri et al., 2006). Glutamine (Glu) and tyrosine (Tyr) play a major contribution in the stabilization by establishing hydrogen bonds with the oxygen ligand (Huang et al., 1996; Peterson et al., 1997; Kuwada et al., 2010; Nieves-Marrero, 2011). The hydroxyl on the TyrB10 establishes a hydrogen bond with the oxygen ligand, and the polar residue of GlnE7 could make a hydrogen bond at the $-NH_2$ with the oxygen ligand. The average distance of 2.4 Å for chain A and 2.3 Å for chain B between $-OH$ from the TyrB10 and the oxygen ligand support the idea of the formation of hydrogen bond stabilizing the oxygen ligand and controlling the heme reactivity in the heterodimer of Oxy-HbII-III complex (Pietri et al., 2005). One example of these distal residues interactions in the heme pocket comes in *Ascaris suum*, where these residues interact with the oxygen ligand to stabilizing the oxygen (Yang et al., 1995; Bolognesi et al., 1997; Peterson et al., 1997).

The TyrB10 at pH 5 is closer to the iron and the oxygen ligand, while at pH 6 it moves away from the iron in both chains. The interaction between GlnE7 and the oxygen ligand is maintained with an average distance of 3.2 Å for chain A and 3.0 Å for chain B. These differences in distance between GlnE7 and the oxygen ligand in heme A and heme B can

indicate that the ligand in heme A is less stabilized, whereas in heme B it is more stable, therefore indicating that the heme A is more reactive than the heme B.

In chain A, the PheE11 moves away at pH 5 when compared with pH 6, but in chain B the PheE11 remains in the same position. Figure 4.21 shows this behavior at pH 5 and 6 for the heme group in chains A and B. In distal position, TyrB10 and GlnE7 could establish a shared interaction with the oxygen ligand across the hydrogen bond network between the residues. This shared stabilization between both amino acids could be responsible for the slow oxygen dissociation rate (Kraus and Wittenberg, 1990; Pietri et al., 2005).

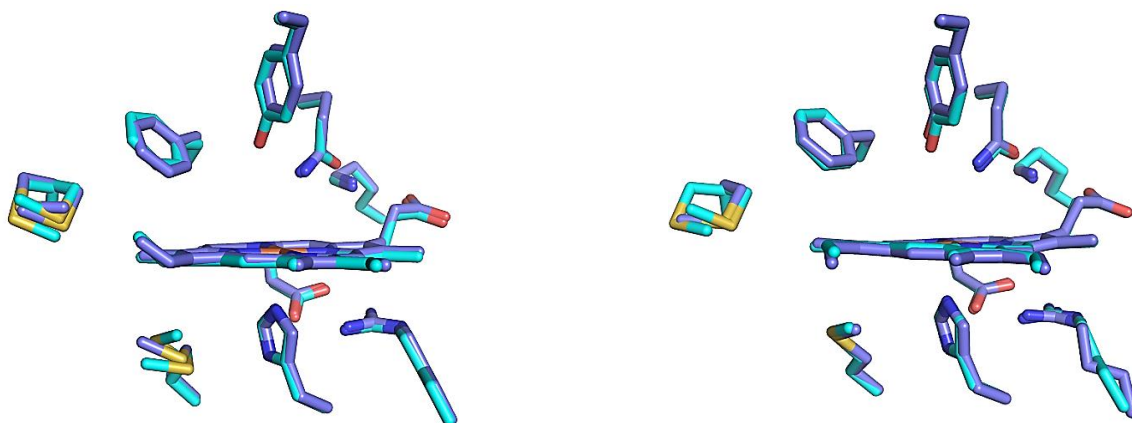


Figure 4.21. Heme groups and the residues for chain A (left) and B (right) at pH 5 (cyan) and 6 (purple) for the complex of HbII-III.

The orientation of the GlnE7 is important, because these residues play an important role in the stabilization of the Oxy-HbII-III complex at all pH. GlnE7 in chain A was involved in the inter-chain salt bridge with the nitrogen from the Lys93 (chain B) and the nitrogen from Lys92 (chain A) with the GlnE7 in chain B (Nieves-Marrero, 2011).

Figure 4.22 shows the major differences between the residues in the distal site for the heme pocket in chains A and B. When the pH increases, the distal amino acids go away and other amino acids approach the iron. These behaviors are observed in the crystallographic structure at pH 6 to 8. The TyrB10 and GlnE7 approaches the iron, but the PheE11 moves away

from the heme pocket in chains A and B. We suggest that movement of the PheE11 facilitates the oxygen release from the heme pocket when pH increases.

The distance between –OH from the TyrB10 and the iron in the heme pocket for both heme groups at pH 6 to 8 decrease when the pH increases from 5.1 Å to 3.6 Å in chain A and from 4.8 Å to 3.6 Å in chain B. The shorter distance between TyrB10 and the iron at the heme pocket at pH8 indicate that the residue of TyrB10 participates in the stabilization of the iron in both heme pockets (see Table 4.16). Distance between the GlnE7 and the iron in the heme pocket remains the same at pH 4 to 7 in heme B. GlnE7 moves closer to the iron in the heme pocket A, at pH 7 to 8, from 4.5 Å to 4.2 Å, and the GlnE7 also moves closer to the iron in heme pocket B from 4.4, (pH 6) to 4.0 Å (pH 8). We suggest that GlnE7 does not participate in the stabilization of the iron at pH 8 when the oxygen ligand was absent.



Figure 4.22. Heme A (left) and heme B (right) for the HbII-III complex at pH 6 (magenta), pH 7 (yellow) and pH 8 (orange). The heme A and B at pH 8 show the absence of an oxygen ligand. The Tyr(B10) shows different distances as a function of pH, being closer to Fe at pH 8.

The bond distance between iron and oxygen ligand increases at pH 5 and 6 in heme A, from 2.1 Å to 2.5 Å, respectively. In chain B, the same behavior at pH 5 and 6 was observed for the bond distance, changing from 1.8 Å to 2.0 Å, respectively. The distance at pH 6 and 7, in chain A is the same (2.5 Å), but the distance in chain B increases from 2.0 Å to 2.3 Å. These

results demonstrate a relationship between the pH and the bond distance, which will cause a decrease in bond strength and the oxygen ligand will be easily released.

The crystallographic structure in chain A for HisF8 shows a slightly movement to the left site (rocking) when compared to all pH, a remarkable difference was seen at pH 4 and pH 8 (Figure 4.23). Chain A at pH 4 and pH 8 show a larger separation for the HisF8 than the one observed in chain B. Data reflects the presence of a water molecule on the proximal site. This water molecule forms a hydrogen bond with the 7-propionate in the heme pocket. The distance of the water molecule in heme A is 3.3 Å at pH 4 changes to 2.6 Å at pH 8. These results indicate an inverse relationship between the specific pH mentioned above and the bond distance in heme A. The distance in heme B is the same at all pH. The water molecule has an interaction with the HisF8 through a weak hydrogen bond with an average distance of 3.5 Å in heme A and 3.4 Å in heme B. This suggests that the interaction at the proximal site may play a significant role in the regulation of the ligand affinity (Gavira et al., 2008; Nieves-Marrero, 2011). This data suggests that the heme A is more reactive than heme B in the of Oxy-HbII-III complex.



Figure 4.23. Crystallographic structures of heme A (left) and heme B (right) with a water molecule (proximal site) and the residues for HbII-III complex at pH 4 (green) and pH 8 (orange).

The volume and the area analysis for the heme group of Oxy-HbII-III complex at different pH was performed using the CASTp web site without the heme group. At pH 5, the area and the volume is less when compared with the pH 6 for both chains. At pH 4, 5 and 7, the area and the volume is less in chain B than in chain A. At pH 6 and 8, the area and volume increase in chain B and decrease in chain A. A comparison of pH 4 with pH 8 reveals that the area and the volume decrease when the pH increases. At pH 8, the area and volume in both chains are less than the other pH because the oxygen was not present in the heme group. Table 4.16 summarizes the area and the volume for the Oxy-HbII-III complex and the number of residues. Analysis of the number of residues at pH 5 and 6 demonstrate an increment in the number of residues when the pH increases in both chains, but at pH 8 the numbers of residues decrease in both chains.

Table 4.16. Area and volume of the heme pockets A and B for the Oxy-HbII-III complex*.

pH	Area		Volume		N° of residues	
	A	B	A	B	A	B
4	588.3	540.5	919.2	866.6	27	23
5	582.7	551.4	875.3	849.7	25	24
6	610.9	615.6	935.4	994.5	27	27
7	613.8	551.6	934.6	877.3	27	24
8	534.6	592.1	808.3	854.8	23	25

*The volume and areas calculation for the heme pocket was realized without the heme group, the ligand. This function was selected in the CASTp program. CASTp probe radius is 1.4 Å.

4.4. Crystallographic structure comparison between the Oxy heterodimer of HbII-III complex with the Oxy homodimer of HbII at different pH from 4 to 8

4.4.1. Secondary structure distribution between the homodimer of Oxy-HbII and the heterodimer of Oxy-HbII-III complex at pH 4 to 8

The secondary structure distributions in globular proteins are predominantly helicoidally (Perutz, 1963; Philips, 1980). The helicoidal distribution reported in Table 4.6, indicated the type of helix present for Oxy-HbII-III complex, and the number of residues as a pH function.

The secondary structure at pH 8 for the heterodimer HbII-III complex shows some discrepancies such as: i) the total number of helix (9 for chain A and 7 for chain B); and ii) the distribution of the alpha helix and 3_{10} helix (seven alpha helix and, two 3_{10} helix for chain A) and (six alpha helix and, one 3_{10} helix for chain B). These variations are present in all of the heterodimers at different pH.

Proteins are dynamic and exhibit conformational changes to maintain the stability of the three-dimensional structure. This stability is preserved even after the protein crystal is formed. The models of the HbII-III protein complex at different pH (4 to 8) show the formation of an antiparallel heterodimer similar to the homodimer of the Oxy-HbII. When these proteins are exposed to drastic changes in pH, the tertiary structure is conserved due to a conformational change mechanism that sustains the tertiary structure. Evidence of these changes in the secondary structure for the Oxy heterodimer HbII-III complex at different pH (4-8) are presented in Table 4.6. We compare the structures of the Oxy heterodimer of HbII-III complex with the Oxy homodimer of HbII. We found structural differences at pH 4 to 8.

To determine the secondary structure present in Oxy-HbII-III complex and in Oxy-HbII at different pH, we use the STRIDE web server (Hening and Frishman, 2004). The Oxy homodimer HbII structure at pH6 has been deposited at the RCSB Protein Data Bank. The programs used to verify the quality model structure for Oxy HbII at pH 6 are described in section 4.3.2. Table 4.17 and 4.18 show the distribution of the secondary structure for the Oxy homodimer of HbII and the Oxy heterodimer of HbII-III complex. We found two types of secondary structures present, an alpha helix and a 3_{10} helix in both dimers, being the alpha helix the predominant secondary structure. Both dimers present a classical three over three assembling behaviors in all structures (Phillips, 1980; Rizzi et al., 1994).

Table 4.17. Secondary structure distribution for chain A of the Oxy dimers of HbII and HbII-III complex in *Lucina pectinata*, using STRIDE web server (Heinig and Frishman, 2004).

pH4	Chain A HbII-II				Chain A HbII-III			
	Helix	Range	Type	N ^o of residues	Helix	Range	Type	N ^o of residues
	A	5-18	alpha	14	A	5-36	alpha	32
	B	19-21	3 ₁₀	3	B	38-40	3 ₁₀	3
	C	22-36	alpha	15	C	44-49	alpha	6
	D	38-44	3 ₁₀	7	D	53-55	3 ₁₀	3
	E	53-56	alpha	4	E	60-78	alpha	19
	F	60-78	alpha	19	F	83-99	alpha	17
	G	83-100	alpha	18	G	104-121	alpha	18
	H	104-121	alpha	17	H	128-149	alpha	22
	I	128-148	alpha	21	I	N/A	N/A	N/A
# of helix		9	7*/2♦			8	6*/2♦	
pH5	A	5-36	alpha	32	A	5-20	alpha	16
	B	38-44	3 ₁₀	7	B	22-36	alpha	15
	C	45-49	alpha	5	C	38-44	3 ₁₀	7
	D	53-55	3 ₁₀	3	D	45-49	alpha	5
	E	60-78	alpha	19	E	53-55	3 ₁₀	3
	F	83-100	alpha	18	F	60-78	alpha	19
	G	104-121	alpha	18	G	83-99	alpha	17
	H	128-149	alpha	22	H	104-121	alpha	18
	I	N/A	N/A	N/A	I	128-149	alpha	22
# of helix		8	6*/2♦			9	7*/2♦	
pH6	A	5-20	alpha	16	A	5-20	alpha	16
	B	22-36	alpha	15	B	22-36	alpha	15
	C	38-44	3 ₁₀	7	C	38-44	3 ₁₀	7
	D	45-49	alpha	5	D	45-49	alpha	5
	E	53-55	3 ₁₀	3	E	53-55	3 ₁₀	3
	F	60-78	alpha	19	F	60-78	alpha	19
	G	83-99	alpha	7	G	83-99	alpha	17
	H	104-121	alpha	18	H	104-121	alpha	18
	I	128-149	alpha	22	I	128-149	alpha	22
# of helix		9	7*/2♦			9	7*/2♦	
pH7	A	5-20	alpha	16	A	5-20	alpha	16
	B	22-36	alpha	15	B	22-36	alpha	15
	C	38-44	3 ₁₀	7	C	38-44	3 ₁₀	7
	D	45-49	alpha	5	D	45-49	alpha	5
	E	53-55	3 ₁₀	3	E	53-55	3 ₁₀	3
	F	60-78	alpha	19	F	60-78	alpha	19
	G	83-99	alpha	17	G	83-99	alpha	17
	H	104-121	alpha	18	H	104-121	alpha	18
	I	128-149	alpha	22	I	128-149	alpha	22
# of helix		9	7*/2♦			9	7*/2♦	
pH8	A	5-36	alpha	32	A	5-20	alpha	16
	B	38-44	3 ₁₀	7	B	22-36	alpha	15
	C	45-49	alpha	5	C	38-44	3 ₁₀	7
	D	53-55	3 ₁₀	3	D	45-49	alpha	5
	E	60-78	alpha	19	E	53-55	3 ₁₀	3
	F	83-99	alpha	17	F	60-78	alpha	19
	G	104-121	alpha	18	G	83-99	alpha	17
	H	128-149	alpha	22	H	104-121	alpha	18
	I	N/A	N/A	N/A	I	128-149	alpha	22
# of helix		8	6*/2♦			9	7*/2♦	

* = alpha helix, ♦ = 3₁₀ helix

Table 4.18. Secondary structure distribution for chain B of the Oxy dimers of HbII and the HbII-III complex *Lucina pectinata*, using STRIDE web server (Heinig and Frishman, 2004).

pH4	Chain B HbII-II				Chain B HbII-III			
	Helix	Range	Type	N ^o of residues	Helix	Range	Type	N ^o of residues
	A	5-36	alpha	32	A	6-21	alpha	16
	B	38-41	3 ₁₀	4	B	23-37	alpha	15
	C	42-45	alpha	4	C	39-45	3 ₁₀	7
	D	53-55	3 ₁₀	3	D	54-56	3 ₁₀	3
	E	60-78	alpha	19	E	61-80	alpha	20
	F	83-100	alpha	18	F	84-100	alpha	17
	G	104-121	alpha	18	G	105-122	alpha	18
	H	128-147	alpha	20	H	127-151	alpha	25
	I				I	N/A	N/A	N/A
# of helix		8	6*/2♦			8	6*/2♦	
pH5	A	5-20	alpha	16	A	6-21	alpha	16
	B	22-36	alpha	15	B	23-37	alpha	15
	C	38-44	3 ₁₀	7	C	39-45	3 ₁₀	7
	D	60-78	alpha	19	D	54-56	3 ₁₀	3
	E	83-100	alpha	18	E	61-79	alpha	19
	F	104-121	alpha	18	F	84-100	alpha	17
	G	128-149	alpha	22	G	105-122	alpha	18
	H	N/A	N/A	N/A	H	127-151	alpha	25
	I	N/A	N/A	N/A	I	N/A	N/A	N/A
# of helix		7	6*/1♦			8	6*/2♦	
pH6	A	5-20	alpha	16	A	6-21	alpha	16
	B	22-36	alpha	15	B	23-37	alpha	15
	C	38-44	3 ₁₀	7	C	39-45	3 ₁₀	7
	D	60-78	alpha	19	D	61-79	alpha	19
	E	83-99	alpha	17	E	84-100	alpha	17
	F	104-121	alpha	18	F	105-122	alpha	18
	G	128-150	alpha	23	G	128-150	alpha	23
	H	N/A	N/A	N/A	H	N/A	N/A	N/A
	I	N/A	N/A	N/A	I	N/A	N/A	N/A
# of helix		7	6*/1♦			7	6*/1♦	
pH7	A	5-20	alpha	19	A	6-21	alpha	16
	B	22-36	alpha	15	B	23-37	alpha	15
	C	38-44	3 ₁₀	7	C	39-45	3 ₁₀	7
	D	45-48	alpha	4	D	61-79	alpha	19
	E	53-55	3 ₁₀	3	E	84-100	alpha	17
	F	60-78	alpha	19	F	105-122	alpha	18
	G	83-100	alpha	18	G	128-151	alpha	24
	H	104-121	alpha	18	H	N/A	N/A	N/A
	I	128-150	alpha	23	I	N/A	N/A	N/A
# of helix		9	7*/2♦			7	6*/1♦	
pH8	A	5-20	alpha	16	A	6-21	alpha	16
	B	21-36	alpha	15	B	23-37	alpha	15
	C	38-44	3 ₁₀	7	C	39-45	3 ₁₀	7
	D	53-55	3 ₁₀	3	D	61-79	alpha	19
	E	60-78	alpha	19	E	84-100	alpha	17
	F	83-99	alpha	17	F	105-122	alpha	18
	G	104-121	alpha	18	G	127-150	alpha	24
	H	128-149	alpha	22	H	N/A	N/A	N/A
	I	N/A	N/A	N/A	I	N/A	N/A	N/A
# of helix		8	6*/2♦			7	6*/1♦	

* = alpha helix, ♦ = 3₁₀ helix

The comparison of the secondary structure distribution for Oxy HbII and Oxy HbII-III complex have a close approximation to the number of helix in chain A. Chain A analysis is as follows: at pH 6 and 7 both dimers have the same number of alpha helix. At pH 5 and 8, Oxy-HbII has one more alpha helix than HbII-III complex and at pH 4, HbII has one more helix than Oxy-HbII-III complex. The 3_{10} helix remains the same at all pH for both dimers. Table 4.19 summarizes the total number of helix for both Oxy dimers of HbII and HbII-III complex.

Table 4.19. Summary of the helices for Oxy-HbII and the Oxy-HbII-III complex.

pH	Chain A		Chain B	
	HbII	HbII-III	HbII	HbII-III
4	9	8	8	8
5	8	9	7	8
6	9	9	7	7
7	9	9	9	7
8	8	9	8	7

Turn type data analysis is as follows: i) all HbII and HbII-III complex show turn type I, II and IV at all pH; ii) at pH 7 HbII has an additional turn type II'; iii) at pH 4 and 7 HbII-III complex has a gamma classic turn; and iv) at pH 7 HbII-III complex shows an VIII turn type. Turns types data is summarized in Table 4.20.

Table 4.20. Summary of the different types of turns for the Oxy dimers of HbII and the HbII-III complex.

pH	HbII	HbII-III
4	I, II, IV	I, II, IV, gamma classic
5	I, II, IV	I, II, IV
6	I, II, IV	I, II, IV
7	I, II, IV, II'	I, II, IV, VIII, gamma classic
8	I, II, IV	I, II, IV

Table 4.21 summarizes the coil and turn number for the dimer HbII-III complex and HbII. Chain A comparison for both hemoglobins reveals no changes in the number of turn but there are variations in the number of coils. At pH 4 and 6, they have the same number of coil but at pH 5, 7 and 8 HbII-III complex have more coils than HbII. HbII chain B analysis at pH 6 to 8

have more turns than HbII-III complex and at pH 4 and 5 the number of turns remain the same. The number of coils in HbII chain B presented a different behavior too. At pH 4 and 5, HbII has less coils than HbII-III complex, but at pH 7 and 8, HbII have more coils than HbII-III complex. At pH 6, the number of coils are the same for both dimers.

Table 4.21. Summary of the different coils and turns for Oxy-HbII and the Oxy-HbII-III complex.

pH	Chain A				Chain B			
	HbII		HbII-III		HbII		HbII-III	
	Coil	Turn	Coil	Turn	Coil	Turn	Coil	Turn
4	6	4	6	4	6	4	7	4
5	5	3	7	3	6	3	7	3
6	7	3	7	3	6	3	6	2
7	6	3	7	3	7	4	6	3
8	6	3	7	3	7	4	6	2

4.4.2. Tertiary structure comparison between the homodimer of Oxy-HbII and the heterodimer of Oxy-HbII-III complex at pH 4 to 8; protein-protein interaction

The protein-protein interaction between the dimer of HbII shows: i) a 10 amino acids interactions at all pH, ii) at pH 7 to pH 8, a five amino acids interactions, and iii) at pH 4 to 6 it has a one amino acid interaction. A comparison of the interactions between HbII and HbII-III complex at all pH found: i) six conserve amino acids interactions in both dimers: (Gln65(A)-Lys92/93(B), His79(A)-Leu67/68(B), Asp84(A)-Pro60/61(B), Met85(A)-Lys63/64(B), and Lys92(A)-Gln65/66(B)); and ii) the rest of the interactions were different for both dimers complexes. Table 4.11 and 4.22 summarize the protein-protein interaction for both Oxy dimer, HbII-III complex and HbII, respectively. At pH 7 to 8, HbII presents five interactions, while HbII-III complex has only one. At pH 4 to 6, HbII presents only one interaction while HbII-III complex has five. Figure 4.23.1 shown the residues found in the protein-protein interactions between HbII-II with HbII-III at pH 8.

The total residues analysis for protein-protein interaction for the homodimer HbII and the heterodimer HbII-III complex shows that HbII has a larger number of residues involved in the interaction over HbII-III complex. This data is summarized in Table 4.23. The program LigPlot+ was used to identify the protein-protein interaction for both proteins at pH 4 to 8 (Laskowski and Swindells, 2011).

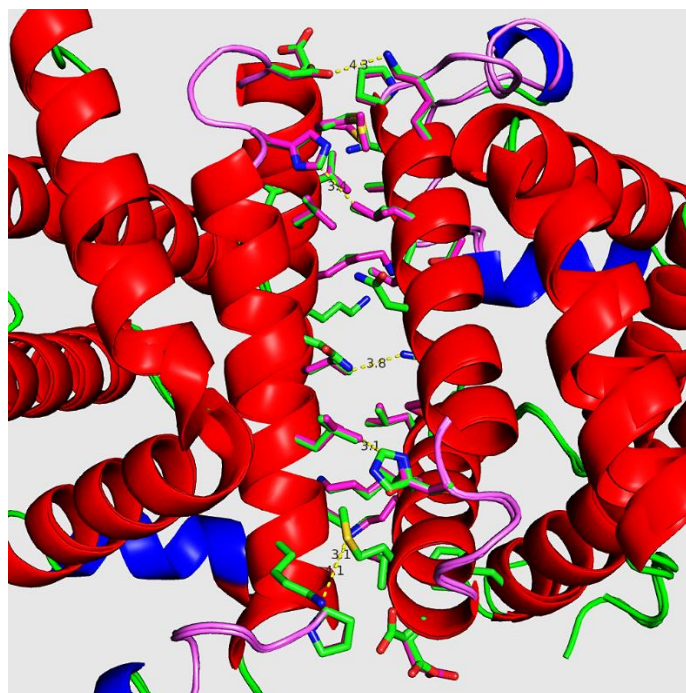


Figure 4.23.1. Residues found in the protein-protein interaction of HbII-II (green) and HbII-III (magenta) at pH 8.

Table 4.22. Residues found in the protein-protein interaction between the homodimer of Oxy-HbII. All interactions were obtained using LigPlot+ version 1.4.5 (Laskowski and Swindells, 2011).

aa interaction in all pH (Chain A-Chain B)	aa interaction into pH7 to pH8 (Chain A-Chain B)	aa interaction into pH4 to pH6 (Chain A-Chain B)
Lys63 – Met 85	Val68 – Leu89	Pro60 – Asp84
Ala64 – Leu89	Pro60 - Asp84	
Gln65 – Lys92	Lys95 – Ser46	
Leu67 – His79	Leu89 – Val68	
His79 – Leu67	Ala64 – Val88	
Asp84 – Pro60		
Met85 – Lys63		
Val88 – Ala64		
Lys92 – Gln65		
Ser46 – Lys95		

Table 4.23. Total amount of residues participating in protein-protein interactions for Oxy-HbII and the Oxy-HbII-III complex at pH 4 to 8.

pH	Chain A (HbII)	Chain A (HbII-III)	Chain B (HbII)	Chain B (HbII-III)
4	18	16	16	16
5	19	15	19	15
6	16	15	17	15
7	17	12	18	13
8	18	14	19	14

Table 4.24 summarizes the hydrogen bond interactions and hydrophobic interactions for the homodimer Oxy-HbII and the heterodimer of Oxy-HbII-III complex at pH 4 to 8. HbII has more interactions than HbII-III complex. The HbII contains more water molecule, more hydrogen-bond interactions, and more hydrophobic interaction than HbII-III complex. Only at pH 6, the behavior is different when HbII-III complex has more interaction than HbII. The hydrogen bond interactions between residues present at pH 4 are the same in both proteins, but at pH 5 to 8, the interaction are different. At pH 5 and 7, HbII has two extra interactions when compared with HbII-III complex. At pH 6, HbII-III complex has one extra interaction than HbII. At pH 8, HbII has only one extra interaction when compared with HbII-III complex.

Table 4.24. Interactions between chain A and B for Oxy-HbII and Oxy-HbII-III complex.

pH	proteins	Water molecules	Hydrogen-bond interactions (H ₂ O-aa)	% aa	Hydrogen-bond Interactions (aa-aa)	% aa	Hydrophobic Interaction (aa-aa)	% aa	Total interactions
4	HbII	0	0	0	2	6	29	94	31
	HbII-III	2	4	14	2	7	22	79	28
5	HbII	5	12	26	5	11	29	63	46
	HbII-III	2	4	14	3	10	22	76	29
6	HbII	0	0	0	3	12	23	88	26
	HbII-III	1	2	7	4	14	23	79	29
7	HbII	4	9	21	5	12	28	64	41
	HbII-III	2	4	17	3	12	17	71	24
8	HbII	7	16	38	4	10	22	52	42
	HbII-III	2	4	17	3	12	19	73	23

All interactions were obtained using LigPlot+ (version 1.4.5, Laskowski and Swindells, 2011).

The area and volume are different when the dimer of Oxy-HbII and Oxy-HbII-III complex are compared. At pH 5 and 8, the area and volume is larger in the homodimer HbII

than the heterodimer HbII-III complex, but at pH 4, 6 and 7 the behavior is opposite, HbII is smaller than HbII-III complex. We did not find a tendency within this parameter when the pH changes. The data is shown in Table 4.25.

Table 4.25. Area and volume from protein-protein interaction for Oxy-HbII and the Oxy-HbII-III complex.

pH	Area		Volume	
	HbII	HbII-III	HbII	HbII-III
4	826.3	1019.7	924.1	1302.9
5	964.7	775.5	1186.6	946.7
6	1071.4	1161.4	1351.8	1460.1
7	941.3	1070.4	1175.4	1377.1
8	964.9	901.8	1141.5	1115.1

Water molecules analysis for each structure at different pH presents differences. At pH 4, HbII data presents a low water molecules number due to the poor resolution (3.65 Å). But at pH 5, the number of water molecules increases in HbII in comparison with HbII-III complex. At pH 6 and 8, the behavior is the opposite of pH 5. At pH 7, the number of water molecules remains the same for both dimers. Table 4.26 summarizes the total number of water molecules in the crystallographic structure for both dimers.

Table 4.26. Total amount of water molecules found in the crystallographic structure of Oxy-HbII and Oxy-HbII-III complex at pH 4 to 8.

pH	HbII-II	HbII-III
4	4	76
5	239	160
6	75	150
7	248	248
8	268	295

4.4.3. Heme pocket analysis between the Oxy proteins HbII-III complex and HbII

The 2-vinyl stereochemistry for Oxy-HbII-III complex heterodimer and for Oxy-HbII homodimer from chain A and B are important to establish the differences or similarities between both heme groups in each hemoglobins. The 2-vinyl group presents several difference and similarities. In chain A at pH 5 and 6 the stereochemistry in HbII-III complex is *cis* but for HbII,

it is *trans*. At pH 7 in HbII-III complex, the 2-vinyl is *trans* but in HbII it is *cis*. Chain B has *trans* stereochemistry for HbII-III complex at all pH, while in HbII the stereochemistry is *cis* except at pH 5. Table 4.27 summarizes the stereochemistry of the vinyl groups in both oxy dimers. The 4-vinyl group stereochemistry remains *cis* at all pH in both chains except at pH 6 in which the HbII, is *trans*.

Table 4.27. Comparison between 2- and 4-vinyl group conformations in the dimers of Oxy-HbII and the Oxy-HbII-III complex at pH range of 4-8.

pH	2- vinyl				4-vinyl			
	HbII	HbII-III	HbII	HbII-III	HbII	HbII-III	HbII	HbII-III
	Chain A	Chain A	Chain B	Chain B	Chain A	Chain A	Chain B	Chain B
4	<i>trans</i> twisted out	<i>cis</i> twisted out	<i>cis</i> twisted out	<i>trans</i> in plane	<i>cis</i> twisted out	<i>cis</i> twisted out	<i>cis</i> twisted out	<i>cis</i> twisted out
5	<i>trans</i> twisted out	<i>cis</i> twisted out	<i>trans</i> twisted out	<i>trans</i> twisted out	<i>cis</i> twisted out	<i>cis</i> in plane	<i>cis</i> in plane	<i>cis</i> twisted out
6	<i>trans</i> twisted out	<i>cis</i> twisted out	<i>cis</i> twisted out	<i>trans</i> twisted out	<i>trans</i> twisted out	<i>cis</i> in plane	<i>cis</i> twisted out	<i>cis</i> twisted out
7	<i>cis</i> twisted out	<i>trans</i> twisted out	<i>cis</i> twisted out	<i>trans</i> twisted out	<i>cis</i> twisted out	<i>cis</i> in plane	<i>cis</i> twisted out	<i>cis</i> twisted out
8	<i>cis</i> twisted out	<i>cis</i> twisted out	<i>cis</i> in plane	<i>trans</i> in plane	<i>cis</i> in plane	<i>cis</i> in plane	<i>cis</i> twisted out	<i>cis</i> twisted out

The overlapping crystallographic structures for both heme in chain A and B at pH 5 and 6 shows the same planarity for the heme group. However, at pH 4, both heme groups have a different planarity according to their crystallographic structures. Figure 4.24 and 4.25 demonstrate the distortion of the heme ring for HbII at pH 4 when compared with Oxy-HbII-III complex.

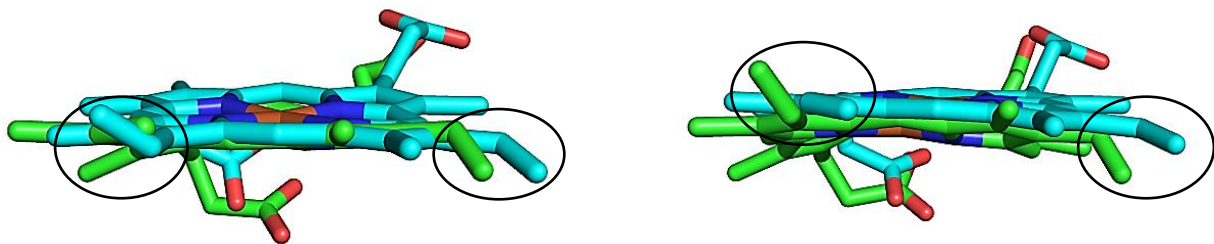


Figure 4.24. Heme A (left) of the HbII (green) overlapping with heme A of the Oxy-HbII-III complex (cyan) at pH 4. Heme B (right) of the HbII (green) overlapping with heme B of the Oxy-HbII-III complex (cyan) at pH 4.

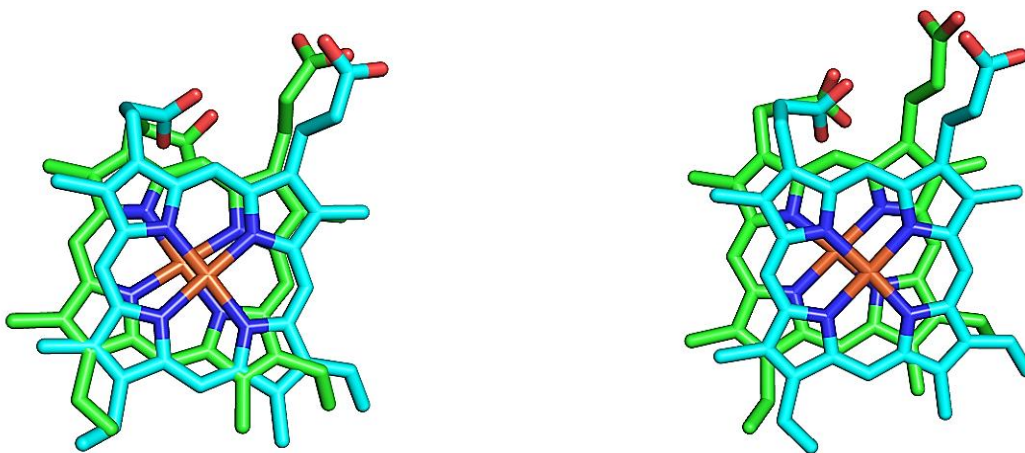


Figure 4.25. Heme A (left) of the HbII (green) overlapping with heme A of the Oxy-HbII-III complex (cyan) at pH 4. Heme B (right) of the HbII (green) overlapping with heme B of the Oxy-HbII-III complex (cyan) at pH 4, top view.

Figure 4.26 shows the crystallographic structure for the overlapping heme A and B at pH 8 for Oxy-HbII-III complex and Oxy-HbII. This figure shows the torsion in both heme A and B group for Oxy-HbII-III complex.

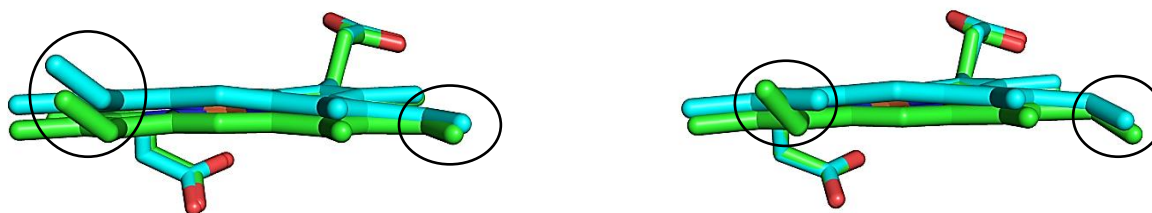


Figure 4.26. Heme A (left) of the HbII (green) overlapping with heme A of the Oxy-HbII-III complex (cyan) at pH 8. Heme B (right) of the HbII (green) overlapping with heme B of the Oxy-HbII-III complex (cyan) at pH 8.

The bond distance between oxygen ligand and the iron in the heme group for Oxy-HbII-III complex and Oxy-HbII at pH 4 to 8 reveals differences. The bond distance in the heterodimer Oxy-HbII-III complex is greater than the homodimer Oxy-HbII for both chains. In chain B, at pH 5 to 7, the bond distance increases when an increase in the pH of HbII-III complex occurs. Contrary to the behavior observed in HbII, in which the bond distance decreases. The bond distance for oxygen ligand and iron atom in the heme group are summarized in Table 4.28.

Table 4.28. Distance for Fe and oxygen ligand in HbII and the HbII-III complex.

Distal Site Interactions	pH4		pH5		pH6		pH7		pH8	
	Chain A (Å)	Chain B (Å)	Chain A (Å)	Chain B (Å)	Chain A (Å)	Chain B (Å)	Chain A (Å)	Chain B (Å)	Chain A (Å)	Chain B (Å)
HbII-III										
Fe – O1	2.2	2.1	2.1	1.8	2.5	2.0	2.2	2.3	N/A	N/A
Fe – O2	3.0	2.8	2.9	2.7	3.1	3.1	2.5	2.3	N/A	N/A
HbII										
Fe – O1	2.2 [†]	2.0 [†]	2.0	2.0	2.1	1.9	2.1	1.7	1.8	1.9
Fe – O2	n/a	n/a	2.9	2.8	3.0	2.9	2.9	2.8	2.6	2.6

([†]) This measurement was with a water molecule acting as a ligand at the sixth coordination site

The bond angle between O1–O2–Fe in HbII-III complex decreases at pH 6 and 7 in chain A when the pH increases in comparison to HbII. In Chain B at pH 5 and 6, the bond angle between O1–O2–Fe in HbII-III complex increases when the pH increases. The bond angle between O1–O2–Fe at pH 7 for chains A and B in HbII-III complex decrease when compared with HbII. Table 4.29 summarizes the bond angle for both dimers of HbII-III complex and HbII.

Table 4.29. Bond angle between O1–O2–Fe in the heme pocket for HbII and the HbII-III complex.

Protein	pH4 (°)		pH5 (°)		pH6 (°)		pH7 (°)		pH8 (°)	
	Chain A	Chain B								
HbII	N/A*	N/A*	120.1	120.8	123.1	104.2	123.2	162.7	115.0	114.8
HbII-III	113.7	111.8	119.0	128.2	104.2	144.5	89.5	76.8	N/A*	N/A*

N/A* = does not apply because no oxygen is present in pH 8 for Oxy-HbII-III complex.

N/A* = does not apply because water is present in pH 4 for Oxy-HbII.

The distal analysis for the TyrB10 with iron in heme A for Oxy-HbII-III complex and Oxy-HbII shows differences. At pH 5 to 8, the distance for the TyrB10 to the iron in heme A is shorter in Oxy-HbII-III complex than Oxy-HbII. The same behavior is observed in heme B. At pH 8 for Oxy-HbII-III complex, the distance is shorter than Oxy-HbII because the oxygen ligand is not present. We suggest that when the oxygen leaves from the heme pocket the TyrB10, it stabilizes the iron in the Oxy-HbII-III complex.

The distance between GlnE7 with the oxygen ligand (O1-NE2) in chain A at pH 5 to 7 for the heterodimer of Oxy-HbII-III complex and the homodimer Oxy-HbII are similar, which was expected since this residue plays a role in the hydrogen bond network that stabilizes the

ligand (Huang et al., 1996; Peterson et al., 1997; Pietri et al., 2005; Kuwada et al., 2010; Nieves-Marrero, 2011). The distance between GlnE7 and the oxygen ligand (O1-NE2) in chain B of Oxy-HbII-III complex at pH 5 and 6 is greater than the one found in Oxy-HbII. At pH 7, the behavior is the opposite. The distance between GlnE7 and the oxygen ligand (O1-NE2) in chain B of Oxy-HbII-III complex is lower than the one found in Oxy-HbII, which indicates that the stability of the oxygen ligand decreases, facilitating the ligand released in Oxy-HbII. Table 4.30 summarizes the distance for the distal site for both dimers. Figures 4.27 and 4.28 show the crystallographic structure for heme A and B at pH 5 and 6 for the Oxy dimers of HbII-III complex and HbII, respectively.

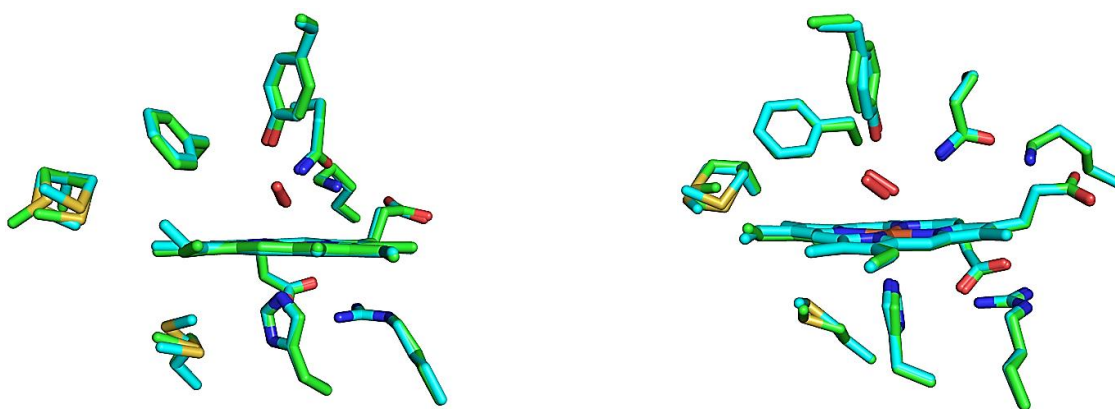


Figure 4.27. Heme A (left) of the HbII (green) overlapping with residues of the heme A of the Oxy-HbII-III complex (cyan) at pH 5. Heme B (right) of the HbII (green) overlapping with residues of the heme B of the Oxy-HbII-III complex (cyan) at pH 5.

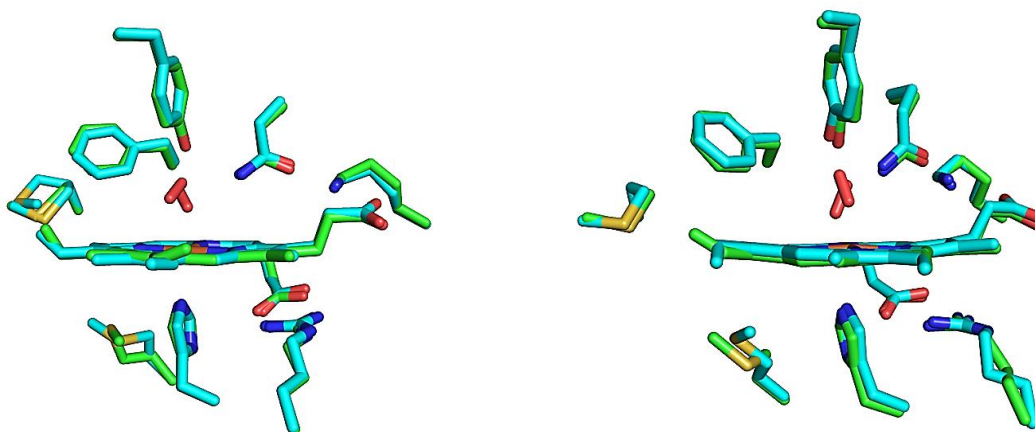


Figure 4.28. Heme A (left) of the HbII (green) overlapping with residues of the heme A of the Oxy-HbII-III complex (cyan) at pH 6. Heme B (right) of the HbII (green) overlapping with residues of the heme B of the Oxy-HbII-III complex (cyan) at pH 6.

Table 4.30. Distance for the distal site of the Oxy dimers of HbII and the HbII-III complex.

Distal Site Interactions	pH4		pH5		pH6		pH7		pH8	
	Chain A (Å)	Chain B (Å)								
HbII-III										
Fe – OH-(TyrB10)	5.0	4.6	4.9	4.4	5.1	4.8	4.5	4.0	3.6	3.6
O2 – OH-(TyrB10)	2.5	2.7	2.6	2.5	2.0	1.8	2.4	2.2	N/A	N/A
O1 – OH-(TyrB10)	2.8	2.5	2.8	2.6	3.1	3.0	2.4	1.9	N/A	N/A
O2 – NE2-(GlnE7)	3.6	4.0	3.9	4.0	3.7	3.4	3.9	3.7	N/A	N/A
O1 – NE2-(GlnE7)	2.8	3.1	3.1	3.3	2.8	2.9	2.9	2.6	N/A	N/A
Fe – NE2-(GlnE7)	4.3	4.4	4.5	4.4	4.4	4.4	4.5	4.3	4.2	4.0
(TyrB10)-OH – NE2-(Gln E7)	3.1	2.6	2.9	3.0	3.0	3.0	3.0	2.9	3.1	3.1
(MetE15)-SD – 2-Vinyl CA ^x	5.5	5.6	5.4	5.0	5.5	5.3	5.1	5.3	5.6	5.1
(MetE15)-SD – 2-Vinyl CB ^x	4.5	6.5	4.4	7.2	4.7	6.2	5.9	6.2	4.8	6.1
			6.0	8.2	6.0		7.0	7.6		
HbII										
Fe – OH-(TyrB10)	4.7	4.3	4.8	4.8	4.9	4.8	4.8	4.5	4.5	4.2
O2 – OH-(TyrB10)	2.7 †	2.4 †	2.4	2.1	2.0	1.9	1.9	1.8	2.4	2.2
O1 – OH-(TyrB10)	N/A	N/A	2.8	2.8	2.9	3.0	3.0	3.0	2.7	2.5
Fe – NE2-(GlnE7)	4.2	4.1	4.4	4.5	4.5	4.3	4.4	4.4	4.4	4.3
O2 – NE2-(GlnE7)	3.1 †	2.7 †	3.8	3.5	3.2	3.5	3.4	3.5	3.9	3.8
O1 – NE2-(GlnE7)	n/a	n/a	3.0	2.9	3.0	2.6	3.0	3.0	3.2	3.0
(TyrB10)-OH – NE2-(Gln E7)	2.6	2.7	2.9	3.2	2.8	2.6	3.0	3.1	3.0	2.7

(*) Inter-chain contact

(†) This measurement was with a water molecule acting as a ligand at the sixth coordination site (cut) The ArgF11 residue was partially cut during the structure refinement

(N/A) Does not apply

(x) Two orientations of MetE15 are observed at pH 5.

When the oxygen ligand at pH 6 (Figure 4.28) and pH 7 are analyzed (Figure 4.29), they have different orientation. At pH 7, the oxygen is parallel with the heme group in Oxy-HbII-III complex for both heme groups, but in Oxy-HbII the oxygen ligand is twisted.

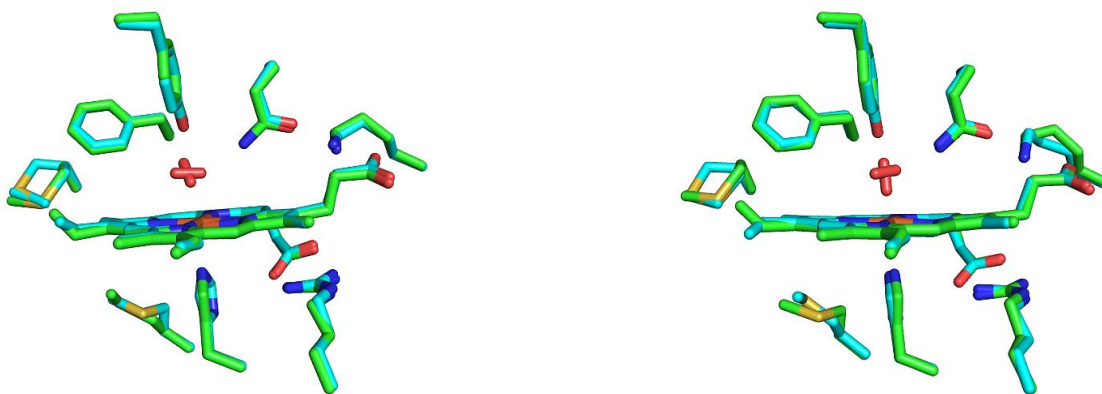


Figure 4.29. Heme A (left) of the HbII (green) overlapping with residues of the heme A of the Oxy-HbII-III complex (cyan) at pH 7. Heme B (right) of the HbII (green) overlapping with residues of the heme B of the Oxy-HbII-III complex (cyan) at pH 7.

Figure 4.30 shows the overlapping crystallographic structure for the heme A and B for both dimers, HbII-III complex and Oxy-HbII at pH 8. The TyrB10 and the GlnE7 are closer to iron in the heme pocket in HbII-III complex (cyan) than Oxy-HbII (green). The PheE11 residue, when compared with Oxy-HbII, moves away in HbII-III complex for both heme groups.

Figure 4.30 shows the heme groups for HbII-III complex (cyan) and Oxy-HbII (green) at pH 8. The comparison between the heme groups in HbII-III complex with the Oxy-HbII for both chains evidences that they are twisted. The TyrB10 is closer in HbII-III complex for both heme groups and the PheE11 moves away in HbII-III complex when compared with the heme group in Oxy-HbII, using the iron as a reference.

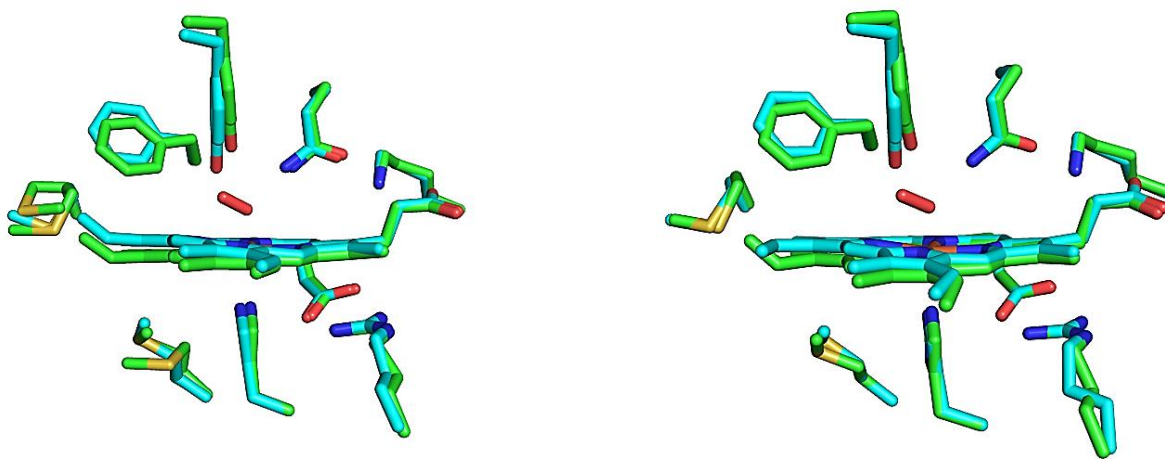


Figure 4.30. Heme A (left) of the HbII (green) overlapping with residues of the heme A of the Oxy-HbII-III complex (cyan) at pH 8. Heme B (right) of the HbII (green) overlapping with residues of the heme B of the Oxy-HbII-III complex (cyan) at pH 8.

HbII and HbII-III complex behave differently at pH 4. The TyrB10, the GlnE7 and the PheE11 are closer to the ligand in HbII than HbII-III complex for both heme groups. Figure 4.31 illustrates the overlapping crystallographic structure for both dimers. The heme for HbII and the heme of HbII-III complex are twisted. The propionates in HbII are twisted in both heme group when compared with the HbII-III complex.

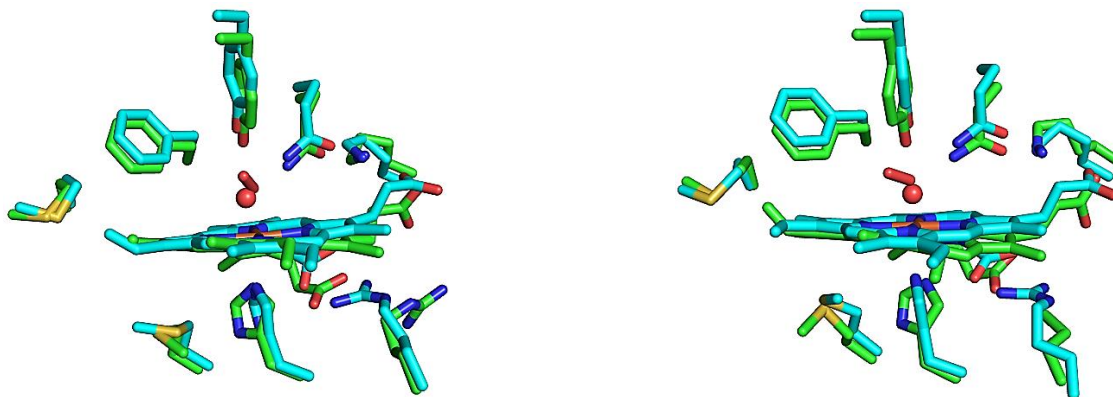


Figure 4.31. Heme A (left) of the HbII (green) overlapping with residues of the heme A of the Oxy-HbII-III complex (cyan) at pH 4. Heme B (right) of the HbII (green) overlapping with residues of the heme B of the Oxy-HbII-III complex (cyan) at pH 4.

The distance between HisF8 and the iron atom on the heme group at pH 5 and 6 in chains A and B are similar for both dimers. At pH 7 and 8, the HisF8 is closer in Oxy-HbII in both chains when compared with the dimer of Oxy-HbII-III complex. The water molecule is located at a proximal site (similar distance), in both dimers for chain A and B. At pH4 in HbII the HisF8 is twisted in both chains, when compared with HisF8 in Oxy-HbII-III complex. Table 4.31 summarizes the distance for the proximal site of the dimers for HbII-III complex and HbII.

Table 4.31. Distance for the proximal site of the Oxy dimers of HbII and the HbII-III complex.

Proximal Site Interactions	pH4		pH5		pH6		pH7		pH8	
	Chain	Chain								
	A (Å)	B (Å)	A (Å)	B (Å)						
HbII-III										
Fe – NE2-(HisF8)	2.4	2.3	2.2	2.2	2.4	2.4	2.3	2.4	2.4	2.4
(HisF8)-NE2 – OH-(TyrB10)	7.2	6.8	7.0	6.5	7.4	7.1	6.7	6.4	5.8	5.9
(HisF8)-NE1 – H ₂ O (W)	3.8	3.4	3.4	3.3	3.5	3.5	3.5	3.2	3.3	3.3
Propionate O2A – H ₂ O (W)	3.3	2.8	2.9	2.7	2.7	2.7	2.8	2.7	2.6	2.7
Propionate O2A – (ArgF11)-N1	3.3	2.9	3.0	2.9	3.2	3.0	3.1	2.9	3.1	2.9
Propionate O1A – (ArgF11)-N2	3.0	2.9	2.7	2.4	2.9	2.8	2.7	2.5	2.7	2.7
HbII										
(MetF4)-SD – 2-Vynyl CA*	4.9	4.8	5.4	5.2	4.8	5.7	5.3	5.5	5.2 5.8	5.4
(MetF4)-SD – 2-Vynyl CB*	5.7	5.9	6.3	6.3	6.1	6.5	6.4	6.5	5.8 6.8	6.2
Fe – NE2-(HisF8)	2.0	2.2	2.2	2.1	2.4	2.4	2.1	2.0	2.2	2.1
(HisF8)-NE2 – OH-(TyrB10)	6.6	6.4	6.9	6.9	7.2	7.0	6.9	6.5	6.6	6.3
(HisF8)-NE1 – H ₂ O (W)	N/A	N/A	3.3	3.3	3.5	3.3	3.5	3.4	3.3	3.3
Propionate O2A – H ₂ O (W)	N/A	N/A	2.8	2.7	2.4	2.9	2.6	2.6	2.7	2.6
Propionate O2A – (ArgF11)-N1	4.5	cut	2.9	2.9	3.0	2.9	3.0	2.9	3.0	2.9
Propionate O1A – (ArgF11)-N2	4.8	cut	2.7	2.5	2.3	2.4	2.7	2.5	2.6	2.6

(N/A) does not apply

(x) Two orientations of MetE15 are observed at pH 5.

(♦) Two orientations of MetF4 are observed at pH 8.

When we analyzed the area between these two dimers using the CASTp website program, we saw that the area in chain A of Oxy-HbII-III complex is larger at pH 4 to 6 than the area observed in Oxy-HbII. At pH 7, no visible differences are shown for both complexes; but at pH 8, the area of HbII-III complex decreases when compared with HbII. The chain B area behaves similarly to the one observed in chain A, with the exceptions at pH 4 and pH 8 in which the behavior is the opposite.

The volume for HbII-III complex in chain A is larger than HbII at pH 4, 6 and 7, but smaller at pH 5 than HbII. At pH 8, the volumes are the same. Otherwise, when the area for chain B at pH 5 to 7 is compared, it is larger in HbII-III complex than HbII. However, at pH 4 and 8, the area for HbII-III complex is smaller than HbII.

Volume in chain B, of HbII-III complex at pH 4 to 7 is larger than volume of HbII, but at pH 8, the volume for HbII-III complex is smaller than HbII. This behavior at pH 8 in HbII-III complex is due to the absence of the ligand in chain B. One would expect a lesser area and volume in HbII-III complex due to the absence of the oxygen ligand. Table 4.32 summarizes the area and the volume for both Oxy dimer, HbII-III complex and HbII.

Table 4.32. Area and volume of the heme pocket A and B* for Oxy-HbII and the Oxy-HbII-III complex.

pH	Area chain A		Area Chain B		Volume chain A		Volume chain B	
	<i>HbII</i>	<i>HbII-III</i>	<i>HbII</i>	<i>HbII-III</i>	<i>HbII</i>	<i>HbII-III</i>	<i>HbII</i>	<i>HbII-III</i>
4	578.6	588.3	575.9	540.5	852.1	919.2	847.5	866.6
5	579.8	582.7	523.9	551.4	881.4	875.3	842.8	849.7
6	534.5	610.9	605.0	615.6	862.4	935.4	956.1	994.5
7	612.1	613.8	537.6	551.6	912.6	934.6	831.9	877.3
8	542.7	534.6	621.4	592.1	807.6	808.3	879.7	854.8

*The volume and areas calculation for the heme pocket was realized without the heme group, the ligand. This function was selected in the CASTp program. CASTp probe radius is 1.4 Å.

The HbII homodimer and the HbII-III complex heterodimer comparisons were analyzed using the secondary structure distribution, tertiary structure and heme pocket environment as parameters. Several differences in all parameters previously discussed were found, as well as

similarities in both chains for both dimers. The differences found were related to the total number of helix, the protein-protein interactions, and the number of residues involved in the interactions, among others. The classic 3-over-3 globin fold structure remains unaffected in both dimers. These differences suggest that both hemoglobins work at different physiological conditions, (HbII at pH 4 and HbII-III complex at pH 8 without oxygen ligand present for both dimers) inside the clam. Figure 4.32 to 4.36 represent the overlapping globin crystallographic structure for each pH 4 to 8 of Oxy-HbII-III complex and Oxy-HbII.



Figure 4.32. Structure overlapping of Oxy-HbII (red) and the Oxy-HbII-III complex (cyan) at pH 4; chain A on the left side and chain B on the right side.

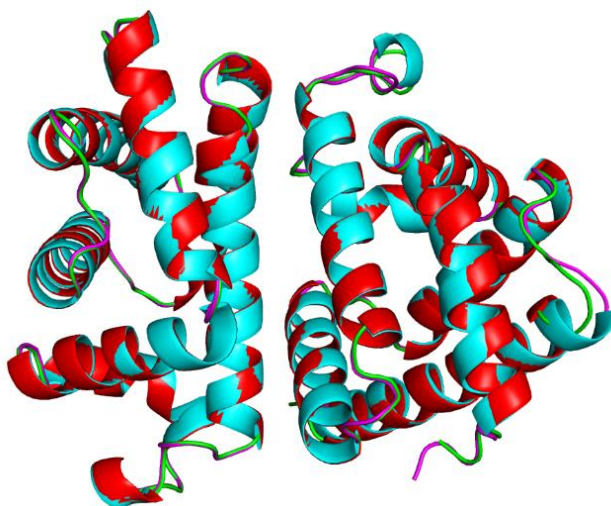


Figure 4.33. Structure overlapping of Oxy-HbII (red) and the Oxy-HbII-III complex (cyan) at pH 5; chain A on the left side and chain B on the right side.

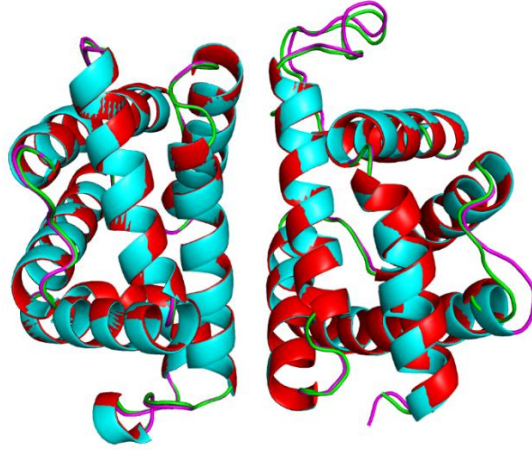


Figure 4.34. Structure overlapping of Oxy-HbII (red) and the Oxy-HbII-III complex (cyan) at pH 6; chain A on the left side and chain B on the right side.

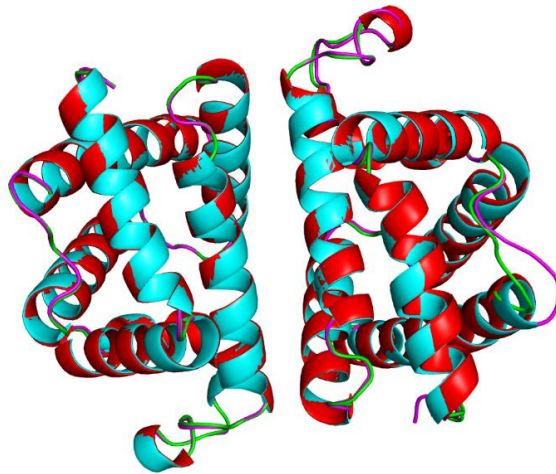


Figure 4.35 Structure overlapping of Oxy-HbII (red) and the Oxy-HbII-III complex (cyan) at pH 7; chain A on the left side and chain B on the right side.

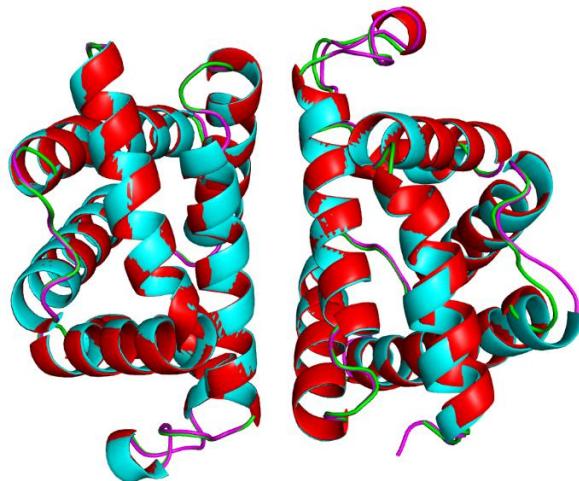


Figure 4.36. Structure overlapping of Oxy-HbII (red) and the Oxy-HbII-III complex (cyan) at pH 8; chain A on the left side and chain B on the right side.

5. CONCLUSIONS AND FUTURE WORK

5.1 Conclusions

Our research findings led us to contribute to the structure–function relationship of the invertebrate hemoglobins. The *Lucina pectinata* HbII-III complex was used as oxygen reactive protein model to obtain a better insight of the ligand discrimination and dissociation unknown mechanism.

As a part of our contribution, a new ion exchange chromatography purification protocol was developed, which allow us to isolated HbIII 100% pure from the HbII-III complex. The MS/MS spectrometry validated both, the protein purity and the efficiency of the isolation methodology. This developed protocol is applicable for similar proteins contained the heme group. Crystallization conditions for Oxy and Cyano complexes of HbIII were obtained using capillary counterdiffusion, but the X-ray diffraction data do not was obtained. The absence of the X-ray data support our hypothesis that the HbIII alone is a very unstable hemoglobin and needs the HbII component to form the stable HbII-III complex as a functional unit.

Crystallization conditions of the HbII-III complex at pH 4, 6, 7 and 8 were obtained using the capillary counterdiffusion technique. Using these crystals, five new crystallographic structures were solved. The structures of pH 4 and 6 are representatives of heme oxygen ligand, but the structures at pH 7 and 8 do not evidence the heme oxygen ligand. The absence of the oxygen ligand in the crystallographic structure of the HbII-III complex at pH 7 and 8 could be attributed to the photodissociation of the ligand provoked by X-ray radiation in the process of crystallographic data collection. The pH analysis confirms the structural variation in Oxy-HbII-III complex. These findings suggest that the pH is a driving force in the ligand release

mechanism for this invertebrate hemoglobin complex. Also, a new structure for the Oxy homodimer of HbII-II at pH 6 was solved.

The crystallographic structures of the Oxy heterodimer of HbII-III complex evidence the effect of the pH in the: i) distribution in the secondary structures; ii) the stereochemistry of the 2-vinyl group in heme pocket A; iii) peripheral change of the 2-vinyl group at the heme ring electron density; iv) distance and angle of the oxygen ligand; and v) distal and proximal residues.

The comparison between the homodimer of Oxy-HbII-II with the heterodimer of Oxy-HbII-III complex as pH function evidence several differences. The crystallographic structure of HbII-II at pH 4 do not shows the oxygen ligand, leading from Oxy to metaquo derivative HbII-II (Nieves-Marrero, 2011). However, the HbII-III complex showed an oxygen bond absence at pH 7 and 8. This finding suggests that the homodimer HbII-II and the heterodimer of HbII-III complex works in different biological conditions as reflect by the Oxy-HbII-II structural changes as pH function. The data also suggest that the functional part of the oxygen transport in *Lucina pectinata* can be attributed to the heterodimer of HbII-III and the homodimer of HbII-II, but not to the homodimer of HbIII-III.

5.2. Future Works.

Future works should address the crystallization and crystallographic analysis of HbIII, including enhancing the crystal quality for HbIII. Such research would lead to the design of a crystallographic study and solve a new crystallographic structure. This new investigation would require to development of an appropriate methodology for the data collection and processing, refinement and validation to determine the structure of HbIII. Having both crystallization and crystallographic results, we suggest that a complete pH study of HbIII is conducted in order to enhance the knowledge of the mechanism for the oxygen release in non-vertebrate hemoglobins.

6. REFERENCES

- Adams, P. D.; Afonine, P. V.; Bunkoczi, G.; Chen, V. B.; Davis, I. W.; Echols, N.; Headd, J. J.; Hung, L.-W.; Kapral, G. J.; Grosse-Kunstleve, R. W.; McCoy, A. J.; Moriarty, N. W.; Oeffner, R.; Read, R. J.; Richardson, D. C.; Richardson, J. S.; Terwilliger, T. C.; Zwart, P. H. PHENIX: a comprehensive Python-based system for macromolecular structure solution. *Acta Crystallogr., Sect. D: Biol. Crystallogr.* **2010**, 66 (2): 213-221.
- Antommattei-Pérez, F. M.; Rosado-Ruiz, T.; Cadilla, C. L.; López-Garriga, J. The cDNA-Derived Amino Acid Sequence of Hemoglobin I from *Lucina pectinata*. *J. Protein Chem.* **1999**, 18 (8): 831-836.
- Bellamy, H. D.; Snell, E. H.; Lovelace, J.; Pokross, M.; Borgstahl, G. E. O. The high-mosaicity illusion: revealing the true physical characteristics of macromolecular crystals. *Acta Crystallogr., Sect. D: Biol. Crystallogr.* **2000**, 56 (8): 986-995.
- Bolognesi, M.; Bordo, D.; Rizzi, M.; Tarricone, C.; Ascenzi, P. Nonvertebrate hemoglobins: Structural bases for reactivity. *Prog. Biophys. Mol. Biol.* **1997**, 68 (1): 29-68.
- Bolognesi, M.; Rosano, C.; Losso, R.; Borassi, A.; Rizzi, M.; Wittenberg, J. B.; Boffi, A.; Ascenzi, P. Cyanide binding to *Lucina pectinata* hemoglobin I and to sperm whale myoglobin: an x-ray crystallographic study. *Biophys. J.* **1999**, 77 (2): 1093-1099.
- Bonaventura, C.; Henkens, R.; De Jesús-Bonilla, W.; López-Garriga, J.; Jia, Y.; Alayash, A. I.; Siburt, C. J.; Crumbliss, A. L. Extreme differences between hemoglobins I and II of the clam *Lucina pectinata* in their reactions with nitrite. *Biochim. Biophys. Acta.* **2010**, 1804 (10): 1988-1995.
- Bustamante, J. P.; Abbruzzetti, S.; Marcelli, A.; Gauto, D.; Boechi, L.; Bonamore, A.; Boffi, A.; Bruno, S.; Feis, A.; Foggi, P.; Estrin, D. A. and Viappiani, C. Ligand Uptake Modulation by Internal Water Molecules and Hydrophobic Cavities in Hemoglobins. *J. Phys.Chem. B* **2014**, 118 (15), 1234–1254.
- Cao, C.; Zhang, Q.; Wang, Z.-Q.; Wang, Y.-F.; Wang, Y.-H.; Wu, H.; Huang, Z.-X. ¹H NMR studies of the effect of mutation at Valine45 on heme microenvironment of cytochrome b5. *Biochimie* **2003**, 85 (10): 1007-1016.
- Carugo, O.; Bordo, D. How many water molecules can be detected by protein crystallography? *Acta Crystallogr., Sect. D: Biol. Crystallogr.* **1999**, 55 (2): 479-483.
- Casale, E.; Lionetti, C.; Coda, A.; Merli, A.; Ascenzi, P.; Wittenberg, J. B.; Bolognesi, M.; Crystallization and preliminary data for the ferric form of *Lucina pectinata* hemoglobin I. *J. Mol. Biol.* **1991**, 222 (3): 447-449.

- Cerda, J.; Echevaria, Y.; Morales E.; López-Garriga J. Resonance Raman studies of the heme-ligand active site of hemoglobin I from *Lucina pectinata*. *Biospectroscopy*. **1999**, 4, 311–326.
- Collaborative Computational Project, N. The CCP4 suite: programs for protein crystallography. *Acta Crystallogr., Sect. D: Biol. Crystallogr.* **1994**, 50 (Pt 5): 760-763.
- Chiancone, E.; Vecchini, P.; Verzili, D.; Ascoli, F.; Antonini, E. Dimeric and tetrameric hemoglobins from the mollusc *Scapharca inaequivalvis*. Structural and functional properties. *J. Mol. Biol.* **1981**, 152, 577–592.
- Childress, J. J.; Girguis, P. R. The metabolic demands of endosymbiotic chemoautotrophic metabolism on host physiological capacities, *J Exp Biol.* **2011**, 214, 312-325
- Davis, I. W.; Leaver-Fay, A.; Chen, V. B.; Block, J. N.; Kapral, G. J.; Wang, X.; Murray, L. W.; Arendall, W. B. 3rd; Snoeyink, J.; Richardson, J. S.; Richardson, D. C. MolProbity: all-atom contacts and structure validation for proteins and nucleic acids. *Nucleic Acids Res.* **2007**, 35 (Web Server issue): W375-383.
- De Baere, I.; Perutz, M. F.; Kiger, L.; Marden, M. C.; Poyart, C. Formation of two hydrogen bonds from the globin to the heme-linked oxygen molecule in *Ascaris* hemoglobin. *Proc. Natl. Acad. Sci. USA* **1994**, 91 (4): 1594-1597.
- De Jesús-Bonilla, W.; Cruz, A.; Lewis, A.; Cerda, J.; Bacelo, D. E.; Cadilla, C. L.; López-Garriga, J. Hydrogen-bonding conformations of tyrosine B10 tailor the heme protein reactivity of ferryl species. *J. Biol. Inorg. Chem.* **2006**, 11: 334-342.
- Desbois, A.; Mazza, G.; Stetzkowski, F.; Lutz, M. Resonance raman spectroscopy of protoheme-protein interactions in oxygen-carrying hemoproteins and in peroxidases. *Biochim. Biophys. Acta, Protein Struct. Mol. Enzymol.* **1984**, 785 (3): 161-176.
- Doyle, M. A.; Vitali, J.; Wittenberg, J. B.; Vinogradov, S. N.; Walz, D. A.; Edwards, B. F.; Martin, P. D. Crystallization of hemoglobins II and III of the symbiont-harboring clam *Lucina pectinata*. *Acta Crystallogr., Sect. D: Biol. Crystallogr.* **1994**, 50 (Pt 5): 757-759.
- Drenth, J. Principles of Protein X-ray Crystallography. 3rd Ed., New York, 2007, Springer.
- Dundas, J.; Ouyang, Z.; Tseng, J.; Binkowski, A.; Turpaz, Y.; Liang, J. CASTp: computed atlas of surface topography of proteins with structural and topographical mapping of functionally annotated residues. *Nucleic Acid Research.* **2006**, 34:W116-W118.
- Edsall, J. T.; McKenzie, H. A. Water and Proteins. II. The location and dynamics of water in proteins systems and its relation to their stability and properties. *Adv. Biophys.* **1983**, 16: 53-183.
- Evans, G.; Axford, D.; Owen, R. L. The design of macromolecular crystallography diffraction experiments. *Acta Crystallogr. Sect. D: Biol. Crystallogr.* 2011, 67 (4), 261-270.

- Evans, P.; McCoy, A. An introduction to molecular replacement. *Acta Crystallogr., Sect. D: Biol. Crystallogr.* **2008**, 64 (1): 1-10.
- Feis, A.; Lapini, A.; Catacchio, B.; Brogioni, S.; Foggi, P.; Chiancone, E.; Boffi, A.; Smulevich, G. Unusually Strong H-Bonding to the Heme Ligand and Fast Geminate Recombination Dynamics of the Carbon Monoxide Complex of *Bacillus subtilis* Truncated Hemoglobin. *Biochemistry.* **2007**, 47 (3), 902–910.
- García-Ruiz, J. M. Counterdiffusion methods for macromolecular crystallization. *Methods Enzymol.* **2003**, 368: 130-154.
- Garman, E. ‘Cool’ crystals: macromolecular cryocrystallography and radiation damage. *Curr. Opin. Struct. Biol.* **2003**, 13 (5): 545-551.
- Garman, E. F.; Schneider, T. R. Macromolecular Crystallography. *J. Appl. Cryst.* **1997**, 30: 211-237.
- Gavira, J. A.; De Jesús-Bonilla, W.; Camara-Artigas, A.; López-Garriga, J.; García-Ruiz, J. M. Capillary crystallization and molecular-replacement solution of haemoglobin II from the clam *Lucina pectinata*. *Acta Crystallogr. Sect. F: Struct. Biol. Cryst. Commun.* **2006**, 62: 196–199.
- Gavira, J. A.; Camara-Artigas, A.; De Jesús-Bonilla, W.; López-Garriga, J.; Lewis, A.; Pietri, R.; Yeh, S. R.; Cadilla, C. L.; García-Ruiz, J. M. Structure and ligand selection of hemoglobin II from *Lucina pectinata*. *J. Biol. Chem.* **2008**, 283 (14): 9414-9423.
- Gersonde, K.; Sick, H.; Wollmer, A.; Buse, G. Heterotropic Allostereism of Monomeric Haemoglobins of *Chironomus thummi thummi*. *Eur. J. Biochem.* **1972**, 25, 181-189.
- Gibson, Q. H.; Wittenberg, J. B.; Wittenberg, B. A.; Bogusz, D.; Appleby, C. A. The kinetics of ligand binding to plant hemoglobins. Structural implications. *J. Biol. Chem.* **1989**, 264 (1): 100-107.
- Heinig, M.; Frishman, D. STRIDE: a web server for secondary structure assignment from known atomic coordinates of proteins. *Nucleic Acids Res.* **2004**, 32 (Web Server issue): W500-502.
- Helbing, J.; Bonacina, L.; Pietri, R.; Bredenbeck, J.; Hamm, P.; van Mourik, F.; Chaussard, F.; Gonzalez-Gonzalez, A.; Chergui, M.; Ramos-Alvarez, C.; Ruiz, C.; López-Garriga, J. Time-Resolved Visible and Infrared Study of the Cyano Complexes of Myoglobin and of Hemoglobin I from *Lucina pectinata*. *Biophys. J.* **2004**, 87, 1881-1891.
- Hockenhull-Johnson, J. D.; Stern, M. S.; Martin, P.; Dass, C.; Desiderio, D. M.; Wittenberg, J. B.; Vinogradov, S. N.; Walz, D. A. The Amino Acid Sequence of Hemoglobin II from the Symbiont-Harboring Clam *Lucina pectinata*. *J. Protein Chem.* **1991**, 10 (6): 609-622.

Hockenhull-Johnson, J. D.; Stern, M. S.; Wittenberg, J. B.; Vinogradov, S. N.; Kapp, O. H.; Walz, D. A. The Amino Acid Sequence of Hemoglobin III from the Symbiont-Harboring Clam *Lucina pectinata*. *J. Protein Chem.* **1993**, 12 (3): 261-277.

Hodge, K.; Ten Have, S.; Hutton, L.; Lamond, A. I. Cleaning up the masses: Exclusion list to reduce contamination with HPLC-MS/MS. *J. Proteomics.* **2013**, 88, 92-103.

Huang, S.; Huang, J.; Kloek, A. P.; Goldberg, D. E.; Friedman, J. M. Hydrogen bonding of tyrosine B10 to heme-bound oxygen in *Ascaris* hemoglobin. Direct evidence from UV resonance Raman spectroscopy. *J. Biol. Chem.* **1996**, 271 (2): 958-962.

Kakar, S.; Hoffman, F. G.; Storz, J. F.; Fabian, M.; Hargrove, M. S. Structure and reactivity of hexacoordinate hemoglobins. *Biophys. Chem.* **2010**, 152 (1-3): 1-14.

Kantardjieff, K. A.; Rupp, B. Matthews coefficient probabilities: Improved estimates for unit cell contents of proteins, DNA, and protein-nucleic acid complex crystals. *Protein Sci.* **2003**, 9: 1865-1871.

Keller, A.; Nesvizhskii, Al.; Aeresold, R. Empirical Statistical model to estimate the accuracy of peptide identifications by MS/MS and database search. *Anal. Chem.* **2002**, 74 (20), 5383-5392.

Keller, A.; Purvine, S.; Nesvizhskii, Al.; Stolyar, S.; Goodlett, D. R.; Kolker, E. Experimental Protein Mixture for Validating Tandem Mass Spectral Analysis. *OMICS.* **2002**, 6, 2.

Keller, B. O.; Sui, J. S.; Young, A. B.; Whittall, R. M. Interferences and contaminants encountered in modern mass spectrometry. *Anal. Chim. Acta.* **2008**, 627, 71-81.

Kemling, N.; Kraus, D. W.; Hockenhull-Johnson, J. D.; Wittenberg, J. B.; Vinogradov, S. N.; Walz, D. A.; Edwards, B. F.; Martin, P. Crystallization of a complex of hemoglobin components II and III of the symbiont-harboring clam *Lucina pectinata*. *J. Mol. Biol.* **1991**, 222 (3): 463-464.

Kimber, M. S.; Vallee, F.; Houston, S.; Necakov, A.; Skarina, T.; Evdokimova, E.; Beasley, S.; Christendat, D.; Savchenko, A.; Arrowsmith, C. H.; Vedadi, M.; Gerstein, M.; Edwards, A. M.. Data mining crystallization databases: knowledge-based approaches to optimize protein crystal screens. *Proteins* **2003**, 51 (4): 562-568.

Kleywegt, G. J. Validation of protein crystal structures. *Acta Crystallogr., Sect. D: Biol. Crystallogr.* **2000**, 56 (Pt 3): 249-265.

Kraus, D. W.; Wittenberg, J. B. Hemoglobins of the *Lucina pectinata*/bacteria symbiosis. I. Molecular properties, kinetics and equilibria of reactions with ligands. *J. Biol. Chem.* **1990**, 265 (27): 16043-16053.

Krissinel, E., Henrick, K., Berthold, M. R., Glen, R., Diederichs, K., Kohlbacher, O. and Fischer, I. Detection of Protein Assemblies in Crystals. *Computational Life Sciences*, Springer Berlin / Heidelberg. **2005**, 3695: 163-174.

Kuwada, T.; Hasegawa, T.; Takagi, T.; Sato, I.; Shishikura, F. pH-dependent structural changes in haemoglobin component V from the midge larva *Prosilocerus akamusi* (Orthoclaadiinae, Diptera)." *Acta crystallographica* **2010**, 66 (3): 258-267.

Lapini, A.; Di Donato, M.; Patrizi, B.; Marcelli, A.; Lima, M.; Righini, R.; Foggi, P.; Sciamanna, N.; Boffi, A. Carbon Monoxide Recombination Dynamics in Truncated Hemoglobins Studied with Visible-Pump MidIR-Probe Spectroscopy. *J. Phys. Chem. B.* **2012**, 116 (30), 8753–8761.

Laurent, M. C.; Gros, O.; Brulport, J. P.; Gaill, F.; Bris, N. L. Sunken wood habitat for thiotrophic symbiosis in mangrove swamps. *Mar Environ Res.* **2009**, 67, 83-88.

Laskowski, R. A. PDBsum new things." *Nucleic Acids Res.* **2009**, 37 (suppl 1): D355-D359.

Laskowski, R. A.; Chistyakov, V. V.; Thornton, J. M. PDBsum more: new summaries and analyses of the known 3D structures of proteins and nucleic acids." *Nucleic Acids Res.* **2005**, 33 (suppl 1): D266-D268.

Laskowisky, R. A.; Swindells, M. B. LigPlot+: Multiple Ligand-Protein Interaction Diagrams for Drug Discovery. *J Chem Inf Model.* **2011**, 51(10), 2778-86.

Lee, K.-B.; Jun, E., La Mar, G. N., Rezzano, I. N., Pandey, R. K., Smith, K. M., Walker, F. A., and Buttlare, D. H. Influence of heme vinyl- and carboxylate-protein contacts on structure and redox properties of bovine cytochrome b5. *J. Am. Chem. Soc.* **1991**, 113, 3576-3583.

Liang, J.; Edelsbrunner, H.; Woodward, C. Anatomy of protein pockets and cavities: measurement of binding site geometry and implications for ligand design. *Protein Sci.* **1998**, 7 (9): 1884-1897.

Lowell, S. C.; Davis, I. W.; Arendall-III, W. B.; Bakker. P. I. W.; Word, J. M.; Prisant, M. G.; Richardson, J. S.; Richardson, D. C. Structure validation by C α geometry: Φ , Ψ and C β deviation. *Proteins.* **2003**, 50, 437-450.

Lui, H.; Sadygov, R. G.; Yates, III, J. R. A model for random sampling and estimation of Relative Protein Abundance in Shotgun Proteomics. *Anal. Chem.* **2004**, 76, 4193-4201.

Maierov, V. N.; Crippen, G. M. Significance of Root-Mean-Square Deviation in Comparing Three-dimensional Structures of Globular Proteins. *J. Mol. Biol.* **1994**, 235, 625-634.

Matthews, B. W. Solvent content of protein crystals. *J. Mol. Biol.* **1968**, 33 (2): 491-497.
McPherson, A. Increasing the size of microcrystals by fine sampling of pH limits. *J. Appl. Crystallogr.* **1995**, 28 (3): 362-365.

McPherson, A. Crystallization of Biological Macromolecules. 1st Ed., New York, 1999, Cold Spring Harbor Laboratory Press.

McPherson, A. Introduction to protein crystallization. *Methods* **2004**, 34 (3): 254-265.

Moreno, A.; Rondón, D.; García-Ruiz, J. M. Growth of shaped single crystals of proteins. *J. Cryst. Growth* **1996**, 166 (1-4): 919-924.

Morgulis, A.; Coulouris, G.; Raytselis, Y.; Madden T. L.; Agarwala, R.; Schäffer, A. A. Database indexin for publication MegaBLAST searches. *Bioinformatics* **2008**, 24, 1757-1764.

Murshudov, G. N.; Vagin, A. A.; Dodson, E. J. Refinement of macromolecular structures by the maximum-likelihood method. *Acta Crystallogr., Sect. D: Biol. Crystallogr.* **1997**, 53 (Pt 3): 240-255.

Navarro, A. M.; Maldonado, M.; González-Lagoa, J.; López-Mejía, R.; López-Garriga, J.; Colón, J. L. Control of carbon monoxide binding states and dynamics in hemoglobin I of *Lucina pectinata* by nearby aromatic residues. *Lnor. Chim. Acta.* (1996)243: 161-166.

Nesvizhskii, Al.; Keller, A.; Kolker, E.; Aebersold, R. A statistical for identifying proteins by tandem mass spectrometry. *Anal. Chem.* **2003**, 75 (17), 4646-4658.

Ng, J. D.; Gavira, J. A.; García-Ruiz, J. M. Protein crystallization by capillary counterdiffusion for applied crystallographic structure determination. *J. Struct. Biol.* **2003**, 142: 218-231.

Nieves-Marrero, C. A.; Ruiz-Martínez, C. R.; Estremera-Andújar, R. A.; González-Ramírez, L. A.; López-Garriga, J.; Gavira, J. A. Two-step counterdiffusion protocol for the crystallization of haemoglobin II from *Lucina pectinata* in the pH range 4-9. *Acta Crystallogr., Sect. F: Struct. Biol. Cryst. Commun.* **2010**, 66: 264-268.

Nieves-Marrero, C. A. Crystallographic Structures of Hemoglobin II (HbII) from *Lucina pectinata* in the 4-9 pH Range. Ph.D. Thesis, University of Puerto Rico at Mayagüez, Mayagüez, P.R., May 2011.

Otalora, F.; Gavira, J. A.; Ng, J. D.; García-Ruiz, J. M. Counterdiffusion methods applied to protein crystallization. *Prog. Biophys. Mol. Biol.* **2009**, 101 (1-3): 26-37.

Otwinowski, Z.; Minor, W. Processing of X-ray diffraction data collected in oscillation mode. *Methods Enzymol.* **1997**, 276: 307-326.

Ouellet, H.; Ouellet, Y.; Richard, C.; Labarre, M.; Wittenberg, B.; Wittenberg, J.; Guertin, M. Truncated Hemoglobin HbN Protects Mycobacterium Bovis From Nitric Oxide. *Proc. Nat. Acad. Sci.* **2002**, 99, 9, 5902-5907.

Ouellet, H.; Juszczak, L.; Dantsker, D.; Samuni, U.; Ouellet, Y.H.; Savard, P.-Y.; Wittenberg, J.B.; Wittenberg, B.A.; Friedman, J.M.; Guertin, M. Reactions of mycobacterium tuberculosis truncated hemoglobin O with ligands reveal a novel ligand-inclusive hydrogen bond network, *Biochemistry*. **2003**, 42, 5764–5774.

Painter, J.; Merritt, E. A. TLSMD web server for the generation of multi-group TLS models." *J. Appl. Crystallogr.* **2006**, 39 (1): 109-111.

Pardanani, A.; Gambacurta, A.; Ascoli, F.; Royer Jr, W. E. Mutational destabilization of the critical interface water cluster in *Scapharca* dimeric hemoglobin: structural basis for altered allosteric activity. *J. Mol. Biol.* **1998**, 284 (3): 729-739.

Patrizi, B., Lapini, A., Di Donato, M., Marcelli, A., Lima, M., Righini, R., Foggi, P., Baiocco, P., Bonamore, A.; Boffi, A. Role of Local Structure and Dynamics of Small Ligand Migration in Proteins: A Study of a Mutated Truncated Hemoprotein from *Thermobifida fusca* by Time Resolved MIR Spectroscopy. *J. Phys. Chem. B* **2014**, 118, 9209–9217.

Pérez-Laspiur, J; Anderson, E. R.; Ciborowski, P.; Wojna, V.; Rozek, W.; Duan, F.; Mayo, R.; Rodríguez, E.; Plaud-Valentin, M.; Rodríguez-Orengo, J.; Gendelman, H. E.; Meléndes, L. M. CSF proteomic fingerprint for HIV-associated cognitive impairment. *J. Neuroimmunol.* **2007**, 192, 157-170.

Perutz, M. F. X-ray analysis of hemoglobin. *Science New York, N.Y* **1963**, 140: 863-869.

Peterson, E. S.; Huang, S.; Wang, J.; Miller, L. M.; Vidugiris, G.; Kloek, A. P.; Goldberg, D. E.; Chance, M. R.; Wittenberg, J. B.; Friedman, J. M. A comparison of functional and structural consequences of the tyrosine B10 and glutamine E7 motifs in two invertebrate hemoglobins (*Ascaris suum* and *Lucina pectinata*). *Biochemistry* **1997**, 36 (42): 13110-13121.

Phillips, S. E. Structure and refinement of oxymyoglobin at 1.6 Å resolution. *J. Mol. Biol.* **1980**, 142 (4): 531-554.

Pietri, R.; Granell, L.; Cruz, A.; De Jesús, W.; Lewis, A.; Leon, R.; Cadilla, C. L.; López-Garriga, J. L. Tyrosine B10 and heme-ligand interactions of *Lucina pectinata* hemoglobin II: control of heme reactivity. *Biochim. Biophys. Acta* (**2005**). 1747 (2): 195-203.

Pietri, R.; León, R. G.; Kiger, L.; Marden, M. C.; Granell, L. B.; Cadilla, C. L.; López-Garriga, J. Hemoglobin I from *Lucina pectinata*: A model for distal heme-ligand control. *Biochim. Biophys. Acta* **2006**, 1764: 758-765.

Pietri, R.; Nieves-Marrero, C.; Estremera-Andújar, R.; Ruiz-Martínez, C.; Gavira, J. A.; García-Ruiz, J. M.; López-Garriga, J. H₂S and pH effect on O₂ dissociation in the Hemoglobin II from *Lucina pectinata*. 2014, (**Submitted Biochemistry**).

Rabenstein, B.; Knapp, E. W. Calculated pH-dependent population and protonation of carbon-monoxo-myoglobin conformers. *Biophys. J.* **2001**, 80 (3): 1141-1150.

Ramakishnan, C.; Ramachandran, G. N. Stereochemical Criteria for Polypeptide and Protein Chain Conformations II. Allowed Conformations for a Pair of Peptide Units. *Biophys. J.* **1965**, 5: 909-933.

Ramos-Santana, B. J.; López-Garriga, J. Tyrosine B10 triggers a heme propionate hydrogen bonding network loop with glutamine E7 moiety. *Biochem. Biophys. Res. Commun.* **2012**, 424, 771-776.

Ravelli, R. B.; Garman, E. F. Radiation damage in macromolecular cryocrystallography. *Curr. Opin. Struct. Biol.* **2006**, 16 (5): 624-629.

Read, K. R. H. The characterization of the Hemoglobins of the Bivalve Mollusc *Phacoides Pectinata*. *Comp. Biochem. Physiol.* **1965**: 15, 137-158.

Reid, L. S.; Lim, A. G.; Mauk, A.G. Role of heme vinyl groups in cytochrome b5 electron transfer, *J. Am. Chem. Soc.* **1986**, 108, 8197-8201.

Rhodes, G. Crystallography made crystal clear: A guide for users of macromolecular models. 3rd Ed., USA (2006) Academic Press.

Rivera, L., López-Garriga, J.; Cadilla, C. L. Characterization of the full length mRNA coding for; *Lucina pectinata* HbIII revealed an alternative polyadenylation site. *Gene* **2008**, 410 (1): 122-128.

Rivera-Rivera, J.; Perez-Laspiur, J.; Colon, K. Inhibition of interferon response by cystain B: implication in HIV replication of macrophage reservoirs. *J. Neurovirol.* **2012**, 18 20-29.

Rizzi, M.; Wittenberg, J. B.; Coda, A.; Fasano, M.; Ascenzi, P.; Bolognesi, M. Structure of the sulfide-reactive hemoglobin from the clam *Lucina pectinata*. Crystallographic analysis at 1.5 Å resolution. *J. Mol. Biol.* **1994**, 244 (1): 86-99.

Rizzi, M.; Wittenberg, J. B.; Coda, A.; Ascenzi, P.; Bolognesi, M. Structural bases for sulfide recognition in *Lucina pectinata* hemoglobin I. *J. Mol. Biol.* **1996**, 258 (1): 1-5.

Ronda, L.; Bettati, S.; Henry, E. R.; Kashav, T.; Sanders, J. M.; Royer, W. E.; Mozzarelli, A. Tertiary and Quaternary Allostery in Tetrameric Hemoglobin from *Scapharca inaequalvis*. *Biochemistry* **2013**, 52, 2108-2117.

Rossmann, M. G. The molecular replacement method. *Acta Crystallogr., Sect. A: Found. Crystallogr.* **1990**, 46 (Pt 2): 73-82.

Royer, W.; Pardanani, A.; Gibson, Q.; Peterson, E.; Friedman, J. Ordered water molecules as key allosteric mediators in a cooperative dimeric hemoglobin. *Proc. Natl. Acad. Sci. USA* **1996**, 93 (25): 14526-14531.

Royer, W. E.; Jr.; Knapp, J. E.; Strand, K.; Heaslet, H. A. Cooperative hemoglobins: conserved fold, diverse quaternary assemblies and allosteric mechanisms. *Trends Biochem. Sci.* **2001**, *26*, 297-304.

Royer, W. E. Jr.; Zhu, H.; Gorr, T. A.; Flores, J. F.; Knapp, J. E. Allosteric hemoglobin assembly: diversity and similarity. *J. Biol. Chem.* **2005**, *280*, 27477-27480.

Ruiz-Martínez, C. R.; Nieves-Marrero, C. A.; Estremera-Andújar, R. A.; Gavira, J. A.; González-Ramírez, L. A.; López-Garriga, J.; García-Ruiz, J. M. Crystallization and diffraction patterns of the oxy and cyano forms of the *Lucina pectinata* haemoglobins complex. *Acta Crystallogr., Sect. F: Struct. Biol. Cryst. Commun.* **2009**, *65*: 25-28.

Ruiz-Martínez, C. R. New Crystallographic Structures of Oxy-HbII-III and CN-HbII-III from *Lucina pectinata*. Ph.D. Thesis, University of Puerto Rico at Mayagüez, Mayagüez, P.R., May 2011.

Samuni, U.; Dantsker, D.; Ray, A.; Wittenberg, J.B.; Wittenberg, B.A.; Dewilde, S.; Moens, L.; Ouellet, Y., Guertin, M.; Friedman, J.M. Kinetic modulation in carbonmonoxy derivatives of truncated hemoglobins, *J. Biol. Chem.* **2003**, *278* 27241– 27250.

Sanoguet Carrero, Z. Isolation and purification of *Lucina pectinata* Hemoglobins using preparative isoelectric focusing. MS. Thesis, University of Puerto Rico at Mayagüez, Mayagüez, P.R., May 1999.

Saroff, H. A. pH effects on the binding of oxygen to non-vertebrate monomeric hemoglobins. A linked function model. *J. Theor. Biol.* **2004**, *229* (1): 113-118.

Schneider, S.; Marles-Wright, J.; Sharp, K.H.; Paoli, M. Diversity and conservation of interactions for binding heme, *Nat. Prod. Rep.* **2007**, *24*, 621–630.

Silfa, E.; Almeida, M.; Cerda, J.; Wu, S.; López-Garriga, J. Orientation of the heme vinyl groups in the hydrogen sulfide-binding hemoglobin I from *Lucina pectinata*. *Biospectroscopy.* **1998**, *4*, (5): 311-326.

Sliz, P., Harrison, S. C.; Rosenbaum, G. How does radiation damage in protein crystals depend on X-ray dose? *Structure.* **2003**, *11* (1): 13-19.

Smit, J. D. G.; Sick, H.; Peterhenhs, A.; Gersonde, K. Acid Bohr effect of a monomeric haemoglobin from *Dicrocoelium dendriticum*, Mechanism of the allosteric conformation transition. *Eur. J. Biochem.* **1986**, *155*, 231-237.

Springer, B. A.; Sligar, S. G. Mechanism of Ligand Recognition in Myoglobin. *Chem. Rev.* (1994). *94*: 699-714.

Torres-Mercado, E.; Renta, J. Y.; Rodríguez, Y.; López-Garriga, J.; Cadilla, C. L. The cDNA-Derived Amino Acid Sequence of Hemoglobin II from *Lucina pectinata*. *J. Protein Chem.* **2003**, 22 (7/8): 683-690.

Toro-Nieves, D. M.; Rodríguez, Y.; Plaud, M.; Duan, F.; Pérez-Larpiur, J.; Wojna, V.; Meléndez, L. M. Proteomic analyses of monocyte-derived macrophages infected with human immunodeficiency virus type 1 primary isolates from Hispanic women with and without cognitive impairment. *J. Neurovirol.* **2009**, 15, 36-50.

Trent III, J. T.; Hvitved, A. N.; Hargrove, S. M. A Model of Ligand Binding to Hexacoordinate Hemoglobins. *Biochemistry.* **2001**, 40, 6155-6163.

Tronrud, D. E. Introduction to macromolecular refinement. *Acta Crystallogr., Sect. D: Biol. Crystallogr.* **2004**, 60: 2156-2168.

Vagin, A.; Teplyakov, A. MOLREP: an Automated Program for Molecular Replacement. *J. Appl. Cryst.* **1997**, 30 (6): 4.

Vagin, A. A.; Steiner, R. A.; Lebedev, A. A.; Potterton, L.; McNicholas, S.; Long, F.; Murshudov, G. N. REFMAC5 dictionary: organization of prior chemical knowledge and guidelines for its use. *Acta Crystallogr., Sect. D: Biol. Crystallogr.* **2004**, 60 (Pt 12 Pt 1): 2184-2195.

Vaguine, A. A.; Richellea, J.; Wodak, S. J. SFCHECK: a unified set of procedures for evaluating the quality of macromolecular structure-factor data and their agreement with the atomic model. *Acta Crystallogr., Sect. D: Biol. Crystallogr.* **1998**, 55: 191-205.

Vinogradov, S. N.; Walz, D. A.; Pohajdak, B.; Moens, L.; Kapp, O. H.; Suzuki, T.; Trotman, C. N. Adventitious variability? The amino acid sequences of nonvertebrate globins. *Comp. Biochem. Physiol. B.* **1993**, 106 (1): 1-26.

Vu, B. C.; Nothnagel, H. J.; Vuletich, D. A.; Falzone, C. J.; Lecomte, J. T. Cyanide Binding to Hexacoordinated Cyanobacterial Hemoglobins: Hydrogen-Bonding Network and Heme Pocket Rearrangement in Ferric H117A *Synechocystis* Hemoglobin. *Biochemistry.* **2004**, 43, 12622-12633.

Weber, R. E.; Vinogradov, S. N. Nonvertebrate hemoglobins: functions and molecular adaptations. *Physiol. Rev.* **2001**, 81 (2): 569-628.

Winn, M. D.; Isupov, M. N.; Murshudov, G. N. Use of TLS parameters to model anisotropic displacements in macromolecular refinement. *Acta Crystallogr., Sect. D: Biol. Crystallogr.* **2001**, 57 (1): 122-133.

Wittenberg, J. B. Facilitated oxygen diffusion. The role of leghemoglobin in nitrogen fixation by bacteroids isolated from soybean root nodules. *J. Biol. Chem.* **1974**, 249 (13): 4057-4066.

Wittenberg, J. B.; Bolognesi, M.; Wittenberg, B. A.; Guertin, M. Truncated Hemoglobins: A New Family of Hemoglobins Widely Distributed in Bacteria, Unicellular Eukaryotes and Plants. *J. Biol. Sci.* **2002**, 277 (2): 871-874.

Wittenberg, J. B. and Kraus, D. W. Hemoglobins of Eukaryote/Prokaryote Symbiosis. *Structure and Function of Invertebrate Oxygen Carriers*. New York, **1991**, Springer Verlag 323-330.

Wittenberg, J. B.; Stein, J. L. Hemoglobin in the symbiont-harboring gill of the marine gastropod *Alviniconcha hessleri*. *Biol. Bull.* **1995**, 188 (1): 5-7.

Wlodawer, A.; Minor, W.; Dauter, Z.; Jaskolski, M. Protein crystallography for non-crystallographers, or how to get the best (but not more) from published macromolecular structures. *FEBS J.* **2008**, 275 (1): 1-21.

Yang, J.; Kloek, A. P.; Goldberg, D. E.; Mathews, F. S. The structure of *Ascaris* hemoglobin domain I at 2.2 Å resolution: Molecular features of oxygen avidity." *Proc. Natl. Acad. Sci. USA* **1995**, 92: 4224-4228.

Yamamoto, Y.; Ōsawa, A; Inoue, Y.; Chûjô, Y.; Suzuki, T. Determination of the functionally important heme peripheral vinyl group orientation in paramagnetic hemoprotein by 2D NMR. *FEBS Lett.* **1989**, 247, 2, 263-267.